A GENERALISED LATTICE-BOLTZMANN MODEL OF FLUID FLOW AND HEAT TRANSFER WITH POROUS MEDIA

XIONG JIE

NATIONAL UNIVERSITY OF SINGAPORE

2007

A GENERALISED LATTICE-BOLTZMANN MODEL OF FLUID FLOW AND HEAT TRANSFER WITH POROUS MEDIA

XIONG JIE

B. Eng. HUST

A THESIS SUBMITTED

FOR THE DEGREE OF MASTER OF ENGINEERING

DEPARTMENT OF MECHANICAL ENGINEERING

NATIONAL UNIVERSITY OF SINGAPORE

October 2007

ACKNOWLEDGEMENTS

I would like to thank my Supervisors A/Prof. Low Hong Tong and A/Prof. Lee Thong See for their direction, assistance, and guidance in this interesting area. In particular, Prof. Low's suggestions and encouragement have been invaluable for the project results and analysis. I would also like to thank Professor Shu Chang who first introduced me to the Lattice Boltzmann Method through his lecture notes, which provided the foundation of my research technique. I am grateful to the National University of Singapore for the award of a Research Scholarship which financed my graduate studies.

I also wish to thank Dr. Shi Xing, Dr. Dou Huashu, Dr. Zheng Hongwei, Mr. Li Jun, Mr. Liu Gang, Mr. Fu Haohuan, Ms. Yu Dan, Ms. Song Ying, Mr. Sui Yi, Mr. Xia Huaming, Mr. Bai Huixing, Mr. Shi Zhanmin, Mr. Daniel Wong, Mr. Darren Tan, Mr. Chen Xiaobing, Mr. Li Qingsen, Mr. Zheng Ye, Mr. Figo Pang, and Mr. Patrick Han from the Computational Bioengineering Lab, who have taught me programming skills, offered useful expertise, and provided friendship. Special thanks should be given to Mr. Peter Liu and Ms. Stephanie Lee, who have helped me in many ways in my life and career path.

Last but not least, I would like to thank my family, Xiong Shilu, Chen Shuying, and Xiong Wei, whose love has always been with me. I would like to thank all my friends, who provided great encouragement and support for all these days.

Thank you all who have helped me in this effort.

TABLE OF CONTENTS

SUMMARY

A numerical model, based on the Lattice Boltzmann Method, is presented for simulating two dimensional flow and heat-transfer in porous media. The drag effect of the porous medium is accounted by an additional force term. To deal with the heat transfer, a temperature distribution function is incorporated, which is additional to the usual density distribution function for velocity. The numerical model was demonstrated on a few simple geometries filled fully or partially with a porous medium: channel with fixed walls, channel with a moving wall, and cavity with a moving wall.

The numerical results confirmed the importance of the nonlinear drag force of the porous media at high Reynolds or Darcy numbers. For flow through a full porous medium, the results shows an increase of velocity with porosity. The velocity profile for the partial porous medium, shows a discontinuity of velocity gradient at the interface when the porosity is very small. At higher Peclet number, the temperature in full and partial porous media is slightly higher, more so for the case of high heat dissipation at the wall.

The good agreement of the GLBM solution with finite difference solutions and experimental results demonstrated the accuracy and reliability of the present model. Previous studies have been mainly focused on the effect of different Reynolds and Darcy numbers. In this thesis, it is extended to investigate the effect of different porosity and Peclet number.

NOMENCLATURE

Δr	discrete displacement
n	occupation number
ν	shear viscosity
ε	porosity for full porous media
K	permeability
ν_{eff}	effective viscosity
Ω	collision operator
c_s	speed of sound
e_i	particle velocity
f_i	density distribution function
λ	expansion parameter
t	time
x	Cartesian coordinate, horizontal
y	Cartesian coordinate, vertical
X	non-dimensional Cartesian coordinate, horizontal
Y	non-dimensional Cartesian coordinate, vertical
η	index of spatial dimension
d	number of spatial dimension
b	number of spatial dimension in Fermi-Dirac distribution
z	number of links
Z	number of discrete particle velocity

N	number of nodes
U	non-dimensional velocity
u_0	characteristic velocity
L	characteristic length
H	characteristic height
h	height
k_m	thermal conductivity
k_e	stagnant thermal conductivity
k_d	dispersion thermal conductivity
m	particle mass
ρ	density
p	pressure
β	thermal expansion coefficient
l	length
α	thermal diffusivity
α_m	effective thermal diffusivity
δ_t	time step
δ_x	lattice space
u	x-direction velocity component
v	y-direction velocity component
F	total body force
G	body force

$\mathbf{g}$	gravitational acceleration
T	temperature
T_0	reference temperature
T_i	temperature distribution function
σ	heat capacity ratio between solid and fluid
w_i	weight coefficient
d_p	diameter of particle
c_p	heat capacity
F_ε	geometric function
τ	relaxation time in LBM for velocity field
τ'	relaxation time in LBM for temperature field
τ_b	relaxation time in LBM with BGK approximation
R	gas constant
D	spatial dimension
B	boundary
Re	Reynolds number
Kn	Knudsen number
Ma	Mach number
Da	Darcy number
Je	viscosity ratio
Pr	Prandtl number
Ra	Rayleigh number

Pe	Peclet Number

Subscripts

i	discrete velocity direction
eff	effective

Superscripts

eq	equilibrium

LIST OF FIGURES

LIST OF TABLES

CHAPTER 1

INTRODUCTION

1.1 Background

Transport phenomena in porous media is a subject of wide interdisciplinary concern. It has various applications in fluid mechanics, condensed matter, and environment sciences (Succi 2001). There are many fluid problems where an external force or internal force should be considered, such as multi-phase or multi-component fluids. To obtain the correct hydrodynamics, the force term in simulation model should be treated appropriately.

Due to many engineering applications such as electronic and transportation cooling, drying process, porous bearing, solar collectors, heat pipes, nuclear reactors, and crude oil extraction, the characteristics of fluid flow and heat transfer at the interface region of mixed system with a porous medium and an adjacent fluid domain have attracted attentions of researchers.

The problems discussed above have been studied both experimentally and theoretically. A generalized model was recently developed in modeling flow transport in porous media. In these models, the drag forces and the fluid forces were considered in the momentum equation (Tien 1990, Hsu and Cheng 1990, and Nithiarasu et al. 1997). The Darcy, Brinkman-extended Darcy, and Forchheimer-extended Darcy models can be taken as the limiting generalized model. Additionally, the generalized models mentioned above can be used to model transient flow in porous media. Since the analytical solutions of the flows in porous media are difficult to obtain, usually only the approximate numerical solutions can be acquired. Besides the experimental and analytical investigations, many

computational methods have been presented to solve the problems of fluid flow and heat transfer in porous media. Most conventional simulations use the standard approaches based on the discretizations of some semi-empirical models, such as the finite-element methods, the finite-difference method, and the finite-volume methods (Nithiarasu et al. 1997, Hickox and Gartling 1985, Nishimura et al. 1986, Gartling et al. 1996, Nithiarasu et al. 1998, and Amiri 2000).

The simulation of physical phenomenon can be described at three levels: macroscopic, mesoscopic and microscopic as shown in Figure 1.1 (Shu 2004). As most numerical approaches, differential equations are used to model the variations such as variations of velocity or temperature. These quantities describe the mean behavior of molecules on discretizations of the domain. In this case, the macroscopic scale is based on discretization of macroscopic continuum equations.

The correspondence scale is microscopic scale or molecular dynamics method. They are based on atomic representation with complicated molecule collision rules and describe the molecular behavior of the phenomena with more accurate results. At this scale, the questions that macroscopic can not solve could be solved by microscopic. Obviously, comparing to the macroscopic scale computation, more computational time is needed for a microscopic computation. Using microscopic scale to simulate some physical processes may take months. Thus, the application size is indeed reduced.

An intermediate scale is the mesoscopic scale which is based both on microscopic models and mesoscopic kinetic equations. It is defined as larger than an atom, but smaller than anything manipulated with human hands (Shu 2004). At mesoscopic scale, pseudo fluid particles are defined as moving and interacting in an imagined world obtained by a

discretization of the real world, according to a set of simplified and relevant rules. Although this representation is far from the reality, it has been shown to be effective to recover complicated physical phenomenon. Informally, it is called Cellular Automata (CA) (Chopard and Droz 1998).

As an alternative computational method, the CA and later developed Lattice Boltzmann Method (LBM) have gained much progress since last decade. Some CA models have been successfully simulated various phenomena, such as diffusion processes (Chopard and Droz 1998). Next, CA models are used to simulate more complicated phenomena such as some fluid flows (Succi 2001). These models are called Lattice Boltzmann Method (LBM), of which details will be introduced in the following chapters.

Both CA and LBM use regular and uniform grids, such as lattices. This particular structure is usually represented as regular arrays which are used for various functions. Because the aim is to build more efficient programs, the reusability or maintenance is ignored in simulation. For instance, a modification of the lattice topology implies many changes traditionally. Hence, an efficient and simulation oriented implementation is a must.

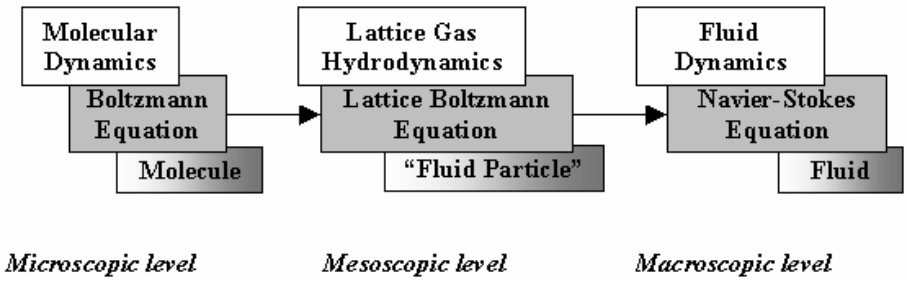

Figure 1.1 Three levels of natural phenomenon description from (Shu 2004)

By tracking the evolution of the distribution functions of the microscopic fluid particles, LBM is different from traditional methods which solve the usual continuum hydrodynamic equations (Dupuis 2002). The kinetic nature of LBM introduces some important and even unique features, such as the easy modeling of interactions among the fluid and porous medium. Originally, in LBM simulations only mass and momentum conservations were considered. However, the thermal effects in fluid flows need to be considered in many applications for its importance and critical ability.

1.2 LITERATURE REVIEW

1.2.1 Flow with Porous Media

The LBM has been applied to the study of flows in porous media since the 1980s (Balasubramanian et al. 1987 and Rothman 1988). Reviews of the subject may be found in Chen and Doolen (1998) and Nield and Bejan (1992). Further development of LBM to simulate flows in porous media have been carried out by many authors (Succi 1989, Adrover and Giona 1996, Koponen et al 1998, Langass and Grubert 1999, Singh and Mohanty 2000, Bernsdorf et al. 2000, and Kim et al. 2001).

There are mainly three scales of simulation involved in flow of porous media: the representative elementary volume (REV) scale, domain scale, and pore scale (Guo and Zhao 2002d). The REV scale is defined as the minimum element which the characteristics of a porous flow present. The REV scale is much smaller than the domain scale but much larger than the pore scale. In conventional methods, due to the complex structure of a porous medium, some semi-empirical models were used in the flow in porous media. They were based on the volume-averaging at the REV scale.

Usually, the LBM with pore scale and REV scale methods have been used in simulating the porous flows (Guo and Zhao 2002d). In the pore scale method, the fluid in the pores of the medium is directly modeled by the standard Lattice Boltzmann Equation (LBE). LBM's kinetic nature makes it very suitable for microscopic interactions in fluid. Additionally, the full bounce back rule for no-slip boundary condition, called the no-slip bounce-back rule, makes simulation of flow in porous media by suitable LBM. The main advantage of this method is that the local information of the flow can be obtained and

used to study macroscopic relations. In fact, the pore-scale method is the most natural way to simulate flows in porous flows by LBM.

However, there are some disadvantages of the pore scale method. One of the main disadvantages is that this scale required the geometric information in detail (Guo and Zhao 2002d). However, the computation domain size has to be limited to reduce usage of the computer resources. This is because each pore should contain several lattice nodes. Therefore the pore scale method is not suitable for a large domain size flow.

Another disadvantage of the pore scale method is that the flow superficial velocity, such as the volume-averaged velocity of the flow, cannot be too high. The volume-averaged velocity is defined as $\bar{u} = \varepsilon u_f$, where u_f is the pure fluid velocity, $\bar{u}$ is the fluid averaged velocity, and ε is the medium porosity. If the aim is to simulate the interstitial fluid in the pores of the system, the volume-averaged velocity cannot be too high for LBM's limit of low Mach number condition. Therefore the pure fluid velocity u_f can not be high.

The other method to simulate the porous fluid flow by LBM is using the REV scale (Guo and Zhao 2002d). This is utilized by revising the standard LBE by adding an additional term to account for the influence of the porous medium (Dardis and McCloskey 1998, Spaid and Phelan 1997, Freed 1998, Kang et al. 2002, Spaid and Phelan 1998, and Martys 2001). In this method, the detailed medium structure and direction are usually ignored, including the statistical properties of the medium into the model. Thus, it is not suitable to obtain detailed pore scale flow information. But the LBM with REV scale could be used for porous medium system of large size. Some examples of the models with REV scales are discussed below.

Dardis and McCloskey (1998) proposed a Lattice Boltzmann scheme for the simulation of flow in porous media by introducing a term describing the no-slip boundary condition. By this approach, the loss of momentum resulting from the solid obstacles is incorporated into the evolution equation. A number ordered parameter of each lattice node related to the density of solid scatters is used to represent the effect of porous medium solid structure on the hydrodynamics. This method removes the need to obtain spatial averaging and temporal averaging, and avoid the microscopic length scales of the porous media.

Spaid and Phelan (1997) proposed a SP model of Lattice Boltzmann Method which is based on the Brinkman equation for single-component flow in heterogeneous porous media. The scheme uses a hybrid method in which the Stokes equation is applied to the free domains; and the Brinkman equations is used to model the flow through the porous structures. The particle equilibrium distribution function was modified to recover the Brinkman equation. In this way, the magnitude of momentum at specified lattice nodes is reduced and the momentum direction is kept.

Freed (1998) proposed a similar approach using an additional force term to simulate flows through a resistance field. An extension term was implemented to modify the standard LBGK model, which results in a local resistance force appropriate for simulating the porous medium region. Simulation results for uniform flow confirmed that the LBGK algorithm yields the satisfied and precise macroscopic behaviors. Also, it was observed that the fluid compressibility simulated by LBM influences its ability to simulate incompressible porous flows.

Later the SP model was combined with a multi-component Lattice Boltzmann algorithm to extend for multi-component system (Spaid and Phelan 1998). The method was developed by introducing a momentum sink to simulate the multi-component fluid flow of a fiber system. It was confirmed that the model is useful to simulate the multi-component fluid flow system. By using the LBM, the complex interface between two immiscible fluids can be easily dealt with those without special treatment of the interface by tracking algorithm.

Shan and Chen (1993) combined the Stokes/Brinkman LBM with the algorithm to model the multi-component infiltration of the fiber microstructure. The developed LBM is suitable to simulate flows containing multiple phases and multi-components immiscible fluids of different masses in constant temperature. One of the main improvements of this model is to include a dynamical temperature. The component equilibrium state can have a non-ideal gas state equation at a given temperature showing phase transitions of thermodynamics.

The SP model was improved to generalize the Lattice Boltzmann Method by introducing an effective viscosity into the Brinkman equation to improve the accuracy and stability (Martys 2001). The approach can describe the general case when fluid viscosity is not the same as the effective viscosity. By implementing the dissipative forcing term into a linear body force term, the validity of the Brinkman equation is extended to a larger range of forcing and effective viscosity. This model eliminates the second order errors in velocity and improves stability over the SP model. It also improves the accuracy of other applications of the model, such as fluid mixtures.

The discussed Brinkman model and improved models have been proved to be an easily implemented and a computationally efficient method to simulate fluid flows in porous media. However, these models are based on some relative simple semi-empirical models such as Darcy or Brinkman models. Therefore they have some intrinsic limitations. Vafai and Kim (1995) pointed out that if there is no convective term, the drive to development of the flow field does not exist. Since Brinkman model does not contain the nonlinear inertial term, it is only suitable for low-speed flows.

Recently, a generalized Lattice Boltzmann Method based on general Lattice Boltzmann Equations (GLBE) called DDF (double density distribution) LBM by Guo and Zhao (2002d) was developed for isothermal incompressible flows. It is used to overcome the limitations of the Darcy or Brinkman model for flows in porous media. This generalized LBM could automatically deal with the interfaces between different media without applying any additional boundary conditions. This enables the DDF LBM suitable to model flows in a medium with a variable porosity. The DDF LBM is based on the general Navier–Stokes model and considered the linear and nonlinear matrix drag components as well as the inertial and viscous forces. The inertial force term of DDF LBM is based on a recently developed method (Guo et al. 2002c), and the newly defined equilibrium distribution function is modified to simulate the porosity of the medium. Because the GLBE is very close to the standard LBE, the DDF LBM solvers for the generalized Navier-Stokes equations are similar to the standard LBM solvers for the Navier-Stokes equations (Nithiarasu et al. 1997 and Vafai and Tien, 1981).

Furthermore, the force term in GLBE was used to simulate the interaction between the fluid and the media. It was equivalent to implement an effective boundary

condition between the fluid and the solid (Guo and Zhao 2002d). The relationship between GLBE with pore scale and GLBE with REV scale could be built through the drag force term derived directly from the boundary rules. The results also showed that the nonlinear drag force due to the porous media is important and could not be neglected for high-speed flows. The numerical results agreed well with the analytical or the finite difference solutions.

1.2.2 Flow with Temperature

The LBM discussed so far did not address the issue of a self-consistent coupling between temperature dynamics and heat transfer within the porous fluid flow. Fully thermo-hydrodynamic LBM scheme is still a challenge to LBM research. A consistent thermodynamic LBM method is needed to simulate over various temperatures, such as investigating convection heat transfer in porous media. The reason is that the heat and temperature dynamics require more kinetic momentum. This is one of the most challenging parts of LBM development.

Usually, there are four ways of applying LBM into heat transfer problems for a fluid flow in a plain medium (Shu 2004), the multi-speed (MS) approach, the passive-scalar approach, the Luo's scheme (1998), and the double distribution function (DDF) models.

The MS method is a straightforward extension of the LBE isothermal models by using only the density distribution function (Shu 2004). To get the macroscopic energy equation, the MS models used a bigger set of discrete velocities and the equilibrium distributions which usually contain higher order velocities. Some limitations in the MS

models severely restrict their applications: the numerical instability, the narrow range of temperature variation, and the fixed Prandtl number. Some previous works for this type of approach can be found as follows.

A Lattice Boltzmann computational scheme was introduced to model viscous, compressible and heat-conducting flows of an ideal monatomic gas (Alexander et al. 1993). The scheme has a small number of discrete velocity states and a linear, single-time relaxation collision operator. Numerical results of adiabatic sound propagation and Couette flow with heat transfer confirmed that the new model agreed well with exact solutions.

Qian (1993) proposed a Lattice BGK models (LBGK) for all dimensional thermohydrodynamics by introducing a proper internal energy and the energy equation. The model can be used to simulate many interesting problems, especially the transonic regimes where the compressibility is important. The systematic thermohydrodynamic equations were derived. And numerical results were used to verify the theoretic values of the sound speed, the shear viscosity and the conductivity. It is also used to solve two-dimensional Rayleigh-Benard convection whose results matched the analytical solutions well.

The second approach of the applying LBM into heat transfer problems is the passive-scalar approach. In the LBM thermal model based on a passive-scalar, the temperature is simulated by a new density distribution function. Compared with the MS approach the main advantage of the passive-scalar approach is the enhancement of the numerical stability.

The third approach is Luo's scheme (1998), by obtaining a systematic derivation of the LBE describing multiphase flow from the discretized Enskog equation (in the presence of an external force) in both phase space and time. It was suggested that the model should go back to the Boltzmann equation for dense gases and the time-honored Enskog equation should be used to overcome the difficulty of solving thermal problems. In this way, the derived LBM helped to obtain not only the equation of state for non-ideal gases, but also the thermodynamic consistency. It was proved to be thermodynamically consistent and free of the previous models' defects. Also, the procedure could be easily extended to other LBMs for complex fluids such as the multi-component fluids.

Pavlo et al. (1998) proposed the non-space filling (high order) isotropic lattices, typically octagonal lattices to uncouple the velocity lattice for solving the thermal problems. The non-space-filling isotropic lattices could greatly enhance the numerical stability, particularly in thermal problems. Another approach of using Luo's scheme is to construct an energy conserved LBM by implementing a hybrid scheme. This model is decoupled from the solution of the temperature equation which is simulated by the conventional energy equation.

The final approach of the applying LBM into heat transfer problems is the thermal model called the internal energy density distribution function (IEDDF) or called double distribution function (DDF) model proposed by He et al. (1998). This scheme is based on the kinetic theory to simulate thermo-hydrodynamics in incompressible flow. It introduces two sets of distributions: the density distribution to simulate hydrodynamics and the internal energy density distribution function to simulate the thermodynamics. In addition, compared with the thermal LBM models based on the passive scalar, the DDF

scheme can incorporate the correct viscous heat dissipation and the compression work done by the pressure. The simulation results and the experiments of Couette flow with a temperature gradient and Rayleigh–B´enard convection showed this scheme has good agreement with analytical solutions and benchmark data. This DDF thermal model has proven to be more stable and simpler than the multi-speed LBM thermal models; therefore it is widely used currently.

The limitations of the MS models could be partly overcome by the DDF models. The DDF models utilize the fact that if the viscous heat dissipation and compression resulted from the pressure could be ignored; a simpler convection-diffusion equation for the temperature could be obtained (He et al. 1998 and Guo and Zhao 2005a). In a DDF LBM model, the temperature equation is modeled by a LBE with an independent temperature distribution function (TDF) proposed by Bartoloni and Battista (1993). Through DDF models, the numerical stability and the range of temperature variation could be improved.

Recently, another thermal lattice BGK with DDF model, a coupled LBGK model called CLBGK was developed by Guo et al. (2002a) for the Boussinesq incompressible fluids. The basic idea is to propose two LBGK equations for the velocity field and temperature field respectively, and then couple them into one composite model based on the Boussinesq approximation for the whole system. Simulation was used to model porous plate problem with temperature gradient and the two-dimensional natural convection flow in a square cavity with Pr =0.71 and different Rayleigh numbers. The numerical results agree well with the analytical solutions and benchmark solutions (Hortmann et al. 1990).

Several benchmark studies of the reliability of the DDF models for fluid flows in a plain medium have been discussed these years (Guo et al. 2002a). Bartoloni and Battista (1993) used the LBM to simulate the fluid flow on the APE100 parallel computer. Shan (1997) used the multiple component LBE model to simulate the Rayleigh-Be´nard convection for fluid system. When simulating the temperature field by using an additional component the numerical instability of the thermal LBMs could be avoid. The algorithm is simple, and the results of studying the Rayleigh-Be´nard convection through this method match very well the theoretical predictions and experimental observations at moderate or even near the critical Rayleigh numbers.

The density of the additional component which evolves from the advection diffusion equation satisfies a passive-scalar equation. In the simulation of the Boussinesq equations except for a slight compressibility, the external force proportional to the temperature is made to be a linear function of the passive scalar. And the passive-scalar can be used to simulate some more complicated fluid equations, such as the dynamic process of phase transition. It was showed that using the multiple component LBE model to simulate of fluid flows with heat and mass transfer was efficient, accurate, and numerically stable.

1.3 Objectives and Scope of Study

In this study, a numerical method based on LBM is implemented to investigate the flow and heat transfer with full and partial porous media. The method is to follow the double distribution function (DDF) approach, DDF LBM. The basic idea is to use Global Lattice Boltzmann Equation (GLBE, proposed by Guo and Zhao, 2005a) to simulate the velocities fields in porous media, and use the GLBE with DDF to derive the temperature fields. Several two dimensional flow problems will be considered: generalized Poiseuille flow with full and partial porous media, Couette flow with full and partial porous media, and lid-driven cavity flow with porous media.

The effects of Reynolds number, Darcy number, Peclet number, and porosity on flow and temperature profiles with full and partial porous media will also investigated. The results of GLBE with DDF method will be compared with previous studies.

CHAPTER 2

STANDARD LATTICE BOLTZMANN METHOD

2.1 The Lattice Gas Cellular Automata

Before going through the Lattice Boltzmann Method (LBM), an overview is given of its ancestors, the Lattice Gas Cellular Automata (LGCA), which was first introduced by Hardy, Pomeau and Pazzis as HPP (1973). There are some LGCA models discussed in Guo and Zhao (2002d). One of them was the HPP model (Vafai and Tien 1981) with a D2Q4 lattice model. HPP model is used to conserve the mass and moment. But it does not yield the macroscopic scale Navier-Stokes equations.

In other discussions, a set of simple rules are used to simulate a gas. It is known that the HPP model with D2Q4 lattice is not isotropic. In 1986, Frisch, Hasslacher and Pomeau (FHP) developed an important class of LGCA model with a higher symmetry lattice. This yields the Navier-Stokes equations and the continuity equation. FHP models are defined with hexagonal symmetry lattices such as D2Q7 and D2Q6, which are isotropic (Doolen 1990). By averaging the dynamics in some conditions, the rules of FHP model reproduce a hydrodynamic fluid (i.e. the Navier-Stokes equations and the continuity equation) as developed by Chopard and Droz (1998), Zanetti (1989) and Succi (2001). LGCA became popular after the discovery of the symmetry lattice. Wolfram (1986) and Frisch et al. (1986) worked out the LGCA's theory foundations. They showed that in the LGCA with collisions, the mass and momentum are conserved and yields the macroscopic scale Navier-Stokes equations when the isotropy is guaranteed. This makes the LGCA a new numerical scheme in CFD. There are many studies on LGCA, for example Chopard and Droz (1998) and Rothman and Zaleski (1994). In fact, the LGCA

method was already applied to the study of flows in porous media early in the 1980s. And the LBM was applied to porous flows successfully soon after its emergence.

Informally, LGCA implements the particles colliding in a fully discrete dimension. For example, an FHP model with D2Q6 lattice is listed in Figure 2.1. First, Lattice implies that it is working on a d - dimensional regular lattice. Second, Gas suggests that a gas represented by Boolean particles, which is moving along the link of the lattice. Then, Cellular means the particles are in a full discretization of the real world. Finally, Automata indicates that the gas evolves according to a particular rule. These are mainly defined to confirm mass conservation (number of particles) and momentum conservation (product of particle mass by particle velocity). These rules are imposed to yield a hydrodynamical flow, i.e. the Navier-Stokes equation and continuity equation.

Formally, the LGCA is constructed as a simplified and imagined molecular dynamics model, where the time, space, temperature and particle velocities are discrete (Dupuis 2002). Here an FHP model is considered on a D2Q6 regular lattice with hexagonal symmetry. Then each lattice node is surrounded by six neighbors identified by six connecting vectors $c_i = c_{i\eta}$, $i = 1,...,6$, the index $\eta = 1,2$ meaning the spatial dimensions. It is regular arrangement of cells with the same kind. The cells are positioned at nodes of the lattice and hold a finite number of discrete states. Each lattice node is indistinguishable and hosts up to six cells which occupies with at most one particle. The particles can move only along one of the six directions defined by the discrete displacements $\Delta \mathbf{r} = \mathbf{c}_i \delta_t$, and $\sqrt{2}\Delta \mathbf{r}$ or $\sqrt{3}\Delta \mathbf{r}$ for diagonal or longer links, and ruled by the exclusion principle. That means a lattice is a set of nodes which link to its nearest neighbor, where empty or there is a cell occupied by at most one particle. In a

lattice time δ_t, the particles hop to the nearest neighbor with discrete vector $\mathbf{c}_i$. All particles have the same mass m = 1. A lattice forms a discrete and regular space. The states are updated simultaneously at discrete time level by the particle evolutions. The fictitious particles occupation is defined by an occupation number $n_i(\mathbf{r},t)$, which are a set of Boolean variables. It is populated by fictitious particles

$$n_i^{in,out}(\mathbf{r},t) \in \{0;1\} \tag{2.1}$$

where the subscript in, out indicates going in or going out at node **r** and time t; and $n_i(\mathbf{r},t)=0$ means particle absence at node **r** and time t ; while $n_i(\mathbf{r},t)=1$ particle presence at node r and time t. Usually, i runs between 0 and z, where z is the number of links, and z is assumed to be 6. Figure 2.2 presents the most common lattices.

A lattice topology is denoted by $DdQ(N+1)$ where d is the spatial dimension with N nodes. Over the entire lattice with N nodes the occupation numbers defines 6N-dimensional time-dependent Boolean field (Shu 2004). And the Boolean phase-space requires 2^{6N} discrete states.

The evolution of an LGCA consists of a collision and a streaming step (Succi 2001). In the collision step, each cell is assigned new values based on the values of the cells in their neighborhood. In the streaming step, the state of each cell is propagated by the particle to its local neighboring. Applying the automata rules for the collision step:

$$n_i^{out}(\mathbf{r},t) = n_i^{in}(\mathbf{r},t) + \Omega_i(n_i^{in}(\mathbf{r},t),...n_z^{in}(\mathbf{r},t)) \tag{2.2}$$

where $\Omega_i(n_i^{in}(\mathbf{r},t),...n_z^{in}(\mathbf{r},t))$ is the collision operator which depends on the model. $\Omega_i(n_i^{in}(\mathbf{r},t),...n_z^{in}(\mathbf{r},t))$ means that once the particles arriving at the same node, they interact with each other and reshuffle their momentums to exchange mass and momentum

among the different directions allowed by the lattice. Note that the collision process is local to a node.

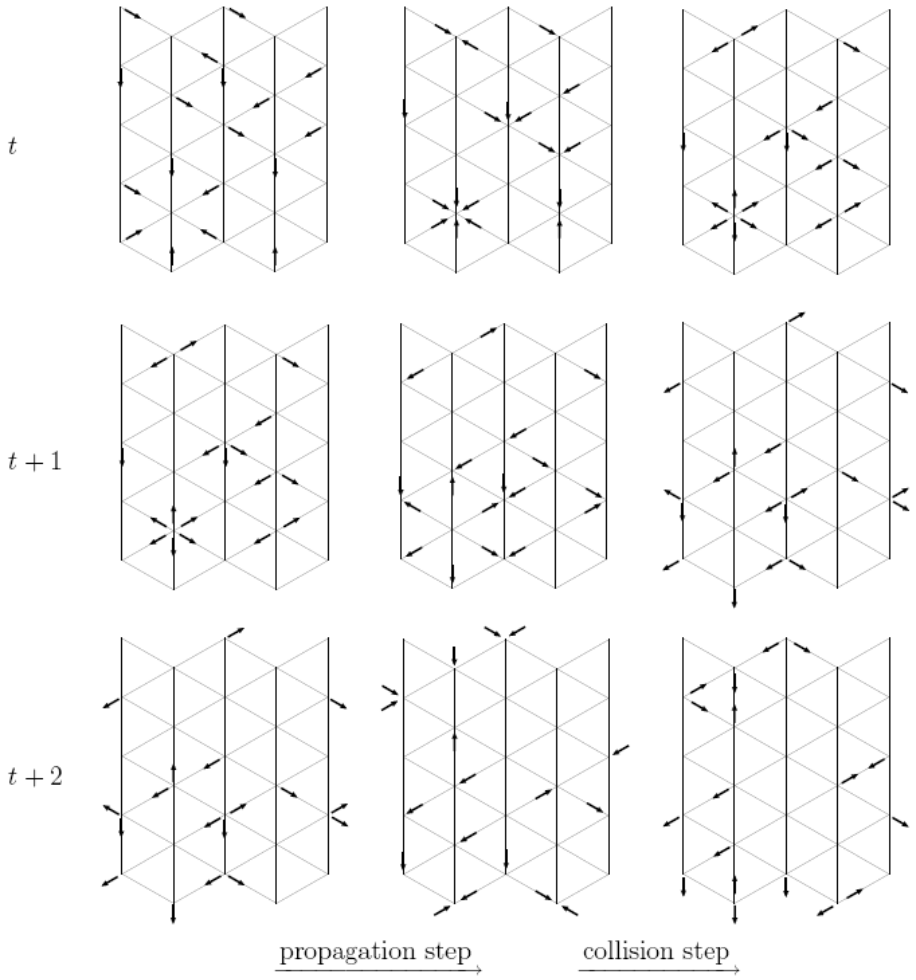

Figure 2.1 The domain geometry is a 5 x 5 torus of the FHP with D2Q6 model from (Dupuis 2002). Due to mass conservation law and momentum conservation law, there are only two non-trivial collision rules (Frisch et al. 1986).

The $\Omega_i(n_i^{in}(\mathbf{r},t),...n_z^{in}(\mathbf{r},t))$ is a long arithmetic Boolean expression if Z is huge. Computation at each step and each direction represents an important amount of time. Hence, it is a usual recourse to use a look-up table for storing all possible configurations and collisions. The table only needs to be computed once before the simulation.

The previous FHP D2Q6 model requires $2^6 = 64$ entries; however its collision expression yields 27 multiplications and 23 additions at each time step and for every direction (Chopard and Droz 1998). Naturally it is efficient to use a look-up table coding the LGCA. The evolution rules are uniform in space and time. Figure 2.1 shows the collision rules and some typical iterations of FHP.

The streaming step aims to let the particles stream from one site to the other. It can be written as $n_i^{in}\left(\mathbf{r}+\Delta\mathbf{r},t+\delta_t\right)=n_i^{out}(\mathbf{r},t)$ .Therefore the evolution equation of FHP model can be written as:

$$n_i^{in}(\mathbf{r}+\Delta\mathbf{r},t+\delta_t)=n_i^{in}(\mathbf{r},t)+\Omega_i(n_i(\mathbf{r},t),n_i^{eq}(\mathbf{r},t))i=1,...,6 \qquad (2.3)$$

For simplicity, the subscript in will be omitted in the following, and n_i is used to replace n_i^{in} . $n_{in}^{eq}(\mathbf{r},t)$ is the local equilibrium distribution and expressed by a Fermi-Dirac distribution (Frisch et al. 1987):

$$n_i^{eq}(\mathbf{r},t)=\frac{\rho/b}{1+e^{\Phi_i}} \qquad (2.4)$$

where ρ is the density, b is the number of the discrete speeds, and Φ_i is a linear expression of the mass, momentum and energy and for isothermal ideal fluids:

$$\Phi_i = A+Bc_{i\alpha}u_\alpha \qquad (2.5)$$

where A and B are free Lagrange parameters to guarantee mass and momentum conservation; u_α is the macroscopic velocity vector.

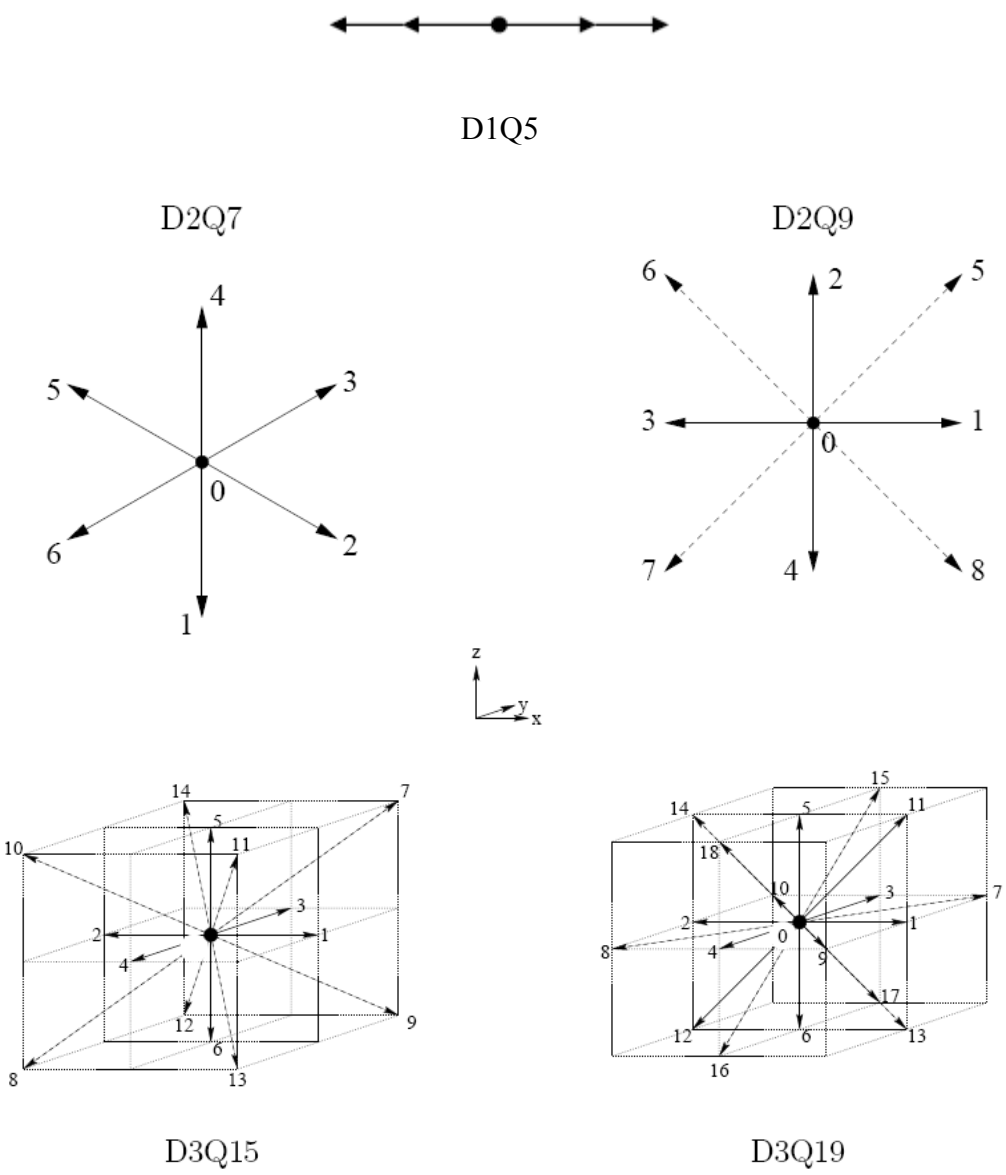

Figure 2.2 Sketches of the some common $DdQ(N+1)$ lattice models from (Shu 2004 and Dupuis 2002). The direction i is numbered and correspond to the velocity vector e_i. The D2Q5 model is the D2Q9 model without the diagonals. Links of size Δr are drawn as a solid line while the others as a dashed line.

A and B can be calculated by an expansion of Equation (2.4) for small Mach numbers which is defined as $Ma = U / c_s$, where $U = |u|$ is the characteristic flow velocity and c_s is the sound speed. The Mach numbers here are usually smaller than 0.3 when considering fluid flow simulations (Dupuis 2002).

So the equilibrium distributions without truncation (Shu 2004) can be expressed as follows:

$$n_i^{eq}(\mathbf{r},t) = \frac{\rho}{b} + \frac{\rho}{b}\frac{c_{i\alpha}u_\alpha}{{c_s}^2} + \frac{\rho}{b}G(\rho)\frac{Q_{i\alpha\beta}u_\alpha u_\beta}{2{c_s}^4} + O(u^3) \tag{2.6}$$

with

$$G(\rho) = \frac{b-2\rho}{b-\rho} \tag{2.7}$$

$$Q_{i\alpha\beta} = c_{i\alpha}c_{i\beta} - {c_s}^2\delta_{\alpha\beta} \tag{2.8}$$

$$c_s = \frac{c}{\sqrt{d}} \tag{2.9}$$

where d is the space dimension number. The density $\rho(\mathbf{r},t)$ and velocity $u_\gamma(\mathbf{r},t)$ are defined as:

$$\rho(\mathbf{r},t) = \sum_i n_i(\mathbf{r},t) \tag{2.10}$$

$$\rho(\mathbf{r},t)u_\gamma(\mathbf{r},t) = \sum_i c_{i\gamma}n_i(\mathbf{r},t) \tag{2.11}$$

where $c_{i\alpha}u_\beta$ and $Q_{i\alpha\beta}u_\alpha u_\beta$ are tensor operations, and when 2 indices are identical they mean summation.

It was known that the LGCA models deal with Boolean particles. Hence, to obtain a macroscopic value, such as the velocity or density, the average quantities are needed to

guarantee the accuracy. The average quantities are taken over time and over the spatial neighborhood. This is time consuming and causes the statistical noises. Also, due to the unsuitable collision model, LGCA suffered lack of Galilean invariance (Shu 2004).

Moreover, since the viscosity of the LGCA models is rather large, the valid Reynolds numbers are quite low. Thus, to acquire higher Reynolds numbers model, the lattice distance needs to be enlarged. However, this is much more time and resources consuming.

Further discussion will be presented in the next chapter about how to implement this idea. And the results are confirmed to be important, accurate and efficient. Thus the models with higher Reynolds numbers could be simulated.

2.2 Basic Idea of LBM

As the Boolean particle distribution and the Fermi-Dirac equilibrium distribution are used in the LGCA, the LGCA has major drawbacks such as suffering some drawbacks of large statistical noise, non-Galilean invariance, an unphysical velocity-dependent pressure and large numerical viscosities, which hampered the developments of LGCA (Shu 2004). On the other hand, the collision term in the LGCA is also complicated and any efforts to seek the numerical solutions of the LGCA are difficult to obtain. To overcome the LGCA's shortcomings, several Lattice Boltzmann Method (LBM) models had been developed.

Historically, four models are the most important. Frisch et al. (1987) used LBE at the basic level of LGCA to calculate the viscosity. In 1988 McNamara and Zanetti introduced a LBE model by using a single particle distribution function instead of the Boolean function to eliminate the statistical noise and using Fermi-Dirac distributions as the equilibrium functions (Shu 2004). Higuera et al. (1989a) developed a LBE with a linearized collision operator, which improved the LBE numerical efficiency. The Bhatnagar-Gross-Krook (BGK) relaxation was developed as an approximation to further simplify the collision operator in the classic kinetic theory (Koelman 1991, Qian et al. 1992, and Bhatnagar et al. 1954). The BGK Lattice Boltzmann Method eliminates the Galilean invariance and pressure problem of the LGCA (Shu 2004). Moreover, it also allows the easy tuning of numerical viscosities by the relaxation parameters to make high Reynolds number simulations possible.

The basic idea of LBM is to construct simplified kinetic models which consist of mesoscopic processes so that the macroscopic properties of the LBM obey the desired

macroscopic hydrodynamics (Shu 2004). The basic premise of using the simplified kinetic-type methods is that the macroscopic flow property is the collection behaviors of many microscopic flow particles and the details in microscopic fluid particles have little or no influence on the macroscopic dynamics (Shu 2004).

There are three key features that make LBM different from other numerical methods (Shu 2004). First, the LBM convection operator is linear in velocity space instead of the nonlinear effects in macroscopic level. Comparing to the Navier-Stokes equation solvers, the computational efforts of LBM are greatly reduced because of no nonlinear terms. Second, the pressure of the LBM could be directly derived from a state equation. In contrast, the direct numerical simulation of the incompressible Navier-Stokes equations involves the Poisson equation to obtain pressure. And this approach often causes numerical difficulties because some cases need special treatments. Third, the LBM facilitates a minimal set of velocities in phase space. In comparison, the phase space of the traditional Maxwell Boltzmann equation uses a complete functional space and the average process involves information from the whole velocity space. It implies that the density and the velocity are computed more quickly and then more efficiently by LBM. Thus the transformation from the microscopic distribution function to macroscopic quantities is greatly simplified.

The LBGK models are based on kinetic theory representations of fluid flow in a highly reduced "particle" velocity space. In the reduced space, flow is described through the evolution of the discrete particle distribution functions on uniform lattices. With second-order of accuracy for the low Knudsen number in space and time the incompressible unsteady Navier-Stokes equations can be recovered through Chapman-

Enskog expansions (Chapman and Cowling 1990). Because the kinetic form of the LBM is the same as the LGCA's, the locality in the kinetic approach of LGCA is retained. Thus, the LBM still keeps the LGCA's advantages such as easy implementation of boundary conditions, full parallelism, and clear physical pictures.

2.3 BGK Approximation

The classic kinetic theory is a branch of statistic physics which deal with the dynamics of non-equilibrium processes and their relaxation to thermodynamic equilibrium.

From Figure 2.1, it is noted that the continuum Boltzmann equation describes the fluid phenomena at a microscopic level. The classic expression of continuum Boltzmann equation is an intergro-differential equation for a single particle density distribution function (Maxwell distribution function) or so called the particle density $f(\mathbf{r},\mathbf{c},t)$ (Shu 2004). f is the probability to have a fictitious particle with velocity **c** entering lattice site **r** at discrete time t and it can be written as

$$\frac{\partial f}{\partial t}+\mathbf{c}\frac{\partial f}{\partial \mathbf{r}}+\mathbf{F}\frac{\partial f}{\partial \mathbf{c}}=Q(f) \tag{2.12}$$

where $f_i^{in}=\langle n_i^{in}\rangle \in [0;1]$, **c** is the particle velocity and **F** is the body force. $Q(f)$ is the collision integral (Shu 2004) which describes the two-particle collision as

$$Q(f(f_1,f_2))=\int d\mathbf{c}_2\int \sigma(\Omega)\,|\mathbf{c}_1-\mathbf{c}_2|\,[f_1' f_2'-f_1 f_2]\,d\Omega \tag{2.13}$$

where $\sigma(\Omega)$ is the differential collision for the two particle collision which exchanges the velocities from incoming ($\{\mathbf{c}_1,\mathbf{c}_2\}$) into outgoing ($\{\mathbf{c}_1',\mathbf{c}_2'\}$).

The local equilibrium is used to obtain the hydrodynamic fluid from the continuum Boltzmann equation. Mathematically, it requires the collision term to be removed (i.e. $Q(f)=0$) and yields the balance condition (Shu 2004):

$$f_1' f_2' = f_1 f_2 \tag{2.14}$$

which means that any collision is dynamically balanced by a corresponding partner. Taking logarithms of Equation (2.14), it is seen that the microscopic property of a system does not change due to the effect of collision:

$$ln f_1^{'} + \ln f_2^{'} = \ln f_1 + \ln f_2 \tag{2.15}$$

To guarantee momentum and energy conserved, $\ln f$ must be merely a function of dynamic collision invariants $\psi(\mathbf{c}) \equiv [1, \mathbf{c}, \mathbf{c}^2/2]$ at the thermodynamic equilibrium (Shu 2004). $\psi(\mathbf{c})$ is proportional to mass, momentum and kinetic energy, thus the equilibrium distribution functions can be expressed as the form:

$$f^{eq}(\mathbf{c}) = \exp(A + B \cdot \mathbf{c} + \frac{1}{2} C\mathbf{c}^2) \tag{2.16}$$

where A, B and C are Lagrangian parameters for hydrodynamic fluid fields for the function which depends on ρ , $\mathbf{u}$ and the internal energy e. The Maxwell distribution function (Shu 2004) can be written as:

$$f^{eq}(\mathbf{r}, \mathbf{c}, t) = \rho(2\pi RT)^{-D/2} \exp[-\frac{(\mathbf{c}-\mathbf{u})^2}{2RT}] \tag{2.17}$$

where R is the gas constant, T is the temperature and D is spatial dimension.

In the small Mach number condition the Maxwell distribution function can be expanded by using Taylor series expansion by Shu (2004) as

$$
\begin{aligned}
f^{eq}(\mathbf{r},\mathbf{c},t) &= \rho(2\pi RT)^{-D/2}\exp[-\frac{(\mathbf{c}-\mathbf{u})^2}{2RT}] \\
&= \rho(2\pi RT)^{-D/2}\exp[-\frac{\mathbf{c}^2-2\mathbf{cu}+\mathbf{u}^2}{2RT}] \\
&= \rho(2\pi RT)^{-D/2}\exp[-\frac{\mathbf{c}^2}{2RT}]\exp[\frac{2\mathbf{c}\cdot\mathbf{u}-\mathbf{u}^2}{2RT}] \\
&= \rho(2\pi RT)^{-D/2}\exp[-\frac{\mathbf{c}^2}{2RT}]\left(1+\frac{\mathbf{c}\cdot\mathbf{u}}{RT}+\frac{(\mathbf{c}\cdot\mathbf{u})^2}{2(RT)^2}-\frac{\mathbf{u}^2}{2RT}\right)+O(\mathbf{u}^3) \\
&= \mathrm{w(c)}\rho\left(1+\frac{\mathbf{c}\cdot\mathbf{u}}{RT}+\frac{(\mathbf{c}\cdot\mathbf{u})^2}{2(RT)^2}-\frac{\mathbf{u}^2}{2RT}\right)+O(\mathbf{u}^3)
\end{aligned}
\tag{2.18}
$$

where w(c) is constant.

One of the main problems that need to be considered when dealing with the Boltzmann Equation is the complicated nature of the collision integral $Q(f)$. To acquire the numerical solutions of the Boltzmann equation $Q(f)$ is often replaced by a simplified term. The basic idea of this replacement is that the interactions of detailed two-body almost have no influence on the physical quantities (Shu 2004). One of the most widely used replacements is the so called BGK approximation, which was proposed by Bathnagar et al. (1954), can be written as:

$$
Q_{BGK}(f) = -\frac{f-f^{eq}}{\tau} \tag{2.19}
$$

In above equation, τ is a typical single time relaxation parameter associated with collision relaxation to the local equilibrium. In principle, τ is a complicated function of the density distribution function *f*. The simplification with BGK approximation is the assumption that the relaxation scale is a constant value, which is equivalent to sum the whole spectrum of relaxation scales into a single value.

To overcome the LGCA drawbacks, the LBM is introduced by replacing the Boolean particle distribution n_i by the continuum particle distribution function f_i and the collision term by the BGK approximation. Indeed, a formal averaging of Equation (2.3) gives

$$f_i^{in}(\mathbf{r}+\Delta\mathbf{r}, t+\delta_t) = f_i^{in}(\mathbf{r},t) + \left\langle \Omega_i(n_i(\mathbf{r},t), n_i^{eq}(\mathbf{r},t)) \right\rangle i = 1,...,6 \qquad (2.20)$$

where the term $\left\langle \Omega_i(n_i(\mathbf{r},t), n_i^{eq}(\mathbf{r},t)) \right\rangle$ still needs to be expressed as the distribution function f_i s. In order to do this, the Boltzmann chaos hypothesis (Dupuis 2002) is used to neglect particle correlations which is assumed that the Boltzmann hypothesis is valid for LGCA models, i.e. $\langle \Omega(\cdots) \rangle = \Omega(\langle \cdots \rangle)$ (Chopard and Droz 1998). Hence, the evolution of a LBM can be written as

$$f_i^{in}\left(r+\Delta\mathbf{r}, t+\delta_t\right) = f_i^{in}(\mathbf{r},t) + \Omega_i(f_0^{in},..., f_z^{in}) \qquad (2.21)$$

The collision operator Ω_i is real-valued variables instead of a Boolean function.

Due to the change, the LBM possible states and collisions are much more numerous compared to the ones of an LGCA. It is noted that because of the finite aspect of the real number representation on a computer, the states of an LBM are not infinite. Thus a look-up table is no longer suitable now (Dupuis 2002). On the other hand, the collision operator is generally consisted of hundreds of floating point operations which needs a large amount of time in computer running. Therefore, another way to determine the post-collision state is needed.

A way to linearize the collision operator around the local equilibrium solution was proposed by Higuera et al. (1989a and 1989b). This considerably reduces the complexity of the collision operator. Focusing on the microdynamics, the LBE can be written as a

relaxation equation (Chen et al. 1994). Here the Lattice Boltzmann Equation with BGK models could be written as:

$$f_i(\mathbf{r}+\Delta\mathbf{r}, t+\delta_t) = f_i(\mathbf{r},t) - \frac{1}{\tau}(f_i(\mathbf{r},t) - f_i^{eq}(\mathbf{r},t)) \quad \text{(i=0,1,...,Z)} \qquad (2.22)$$

or equivalently as:

$$f_i(\mathbf{r}+\mathbf{e}_i\delta_t,\ t+\delta_t) = f_i(\mathbf{r},t) - \frac{1}{\tau}(f_i(\mathbf{r},t) - f_i^{eq}(\mathbf{r},t)) \quad \text{(i=0,1,...,Z)} \qquad (2.23)$$

where f_i is the density distribution function, which depends on position $\mathbf{r}$ in the physical space, the particle discrete velocity $\mathbf{e}_i$ and time t; f_i^{eq} is its local equilibrium state, which is a function of the local macroscopic variables, ρ and $\mathbf{u}$; τ is the single relaxation parameter related to the hydrodynamic viscosity ($\tau > 0.5$); δ_t is the time step; and Z is the number of discrete particle velocity.

Here, the aim is to derive LBE from the discrete Boltzmann equation. Without considering the external force **F** (Shu 2004), the Boltzmann equation with BGK approximation (the single relaxation model) can be written as

$$\frac{\partial f(\mathbf{c},\mathbf{r},t)}{\partial t} + \mathbf{c}\cdot\nabla f(\mathbf{c},\mathbf{r},t) = -\frac{1}{\tau_b}[f(\mathbf{c},\mathbf{r},t) - f^{eq}(\mathbf{c},\mathbf{r},t)] \qquad (2.24)$$

It can be shown that the velocity space of **c** can be discretized into a finite set of velocities $\{\mathbf{e}_i\}$ without affecting the conservation laws (Shu 2004). In the discrete velocity space, the Boltzmann equation becomes

$$\frac{\partial f_i(\mathbf{r},t)}{\partial t} + \mathbf{e}_i\cdot\nabla f_i(\mathbf{r},t) = -\frac{1}{\tau_b}[f_i(\mathbf{r},t) - f_i^{eq}(\mathbf{r},t)] \qquad (2.25)$$

where *i* indicates the different velocity directions. In the lattice context, *i* is equivalent to the lattice direction, which is a form of hexagonal or rectangular shapes. Integrating Equation (2.25) from *t* to $t + \delta_t$ with the second order of accuracy gives

$$f_i(\mathbf{r}+\mathbf{e}_i\delta_i, t+\delta_t) - f_i(\mathbf{r},t) = -\frac{\delta_t}{\tau_b}(f_i(\mathbf{r},t) - f_i^{eq}(\mathbf{r},t)) \quad (i = 0,1,...,Z) \tag{2.26}$$

where $\frac{\delta_t}{\tau_b}$ here is the same as τ (Shu 2004).

Note that in the following, the reference to time and space for the local density and velocity will be omitted usually. The macroscopic density ρ is defined as a function of the density distribution f_i:

$$\rho(\mathbf{r},t) = \sum_{i=1}^{Z} f_i(\mathbf{r},t) \tag{2.27}$$

and momentum density $\rho\mathbf{u}$ are defined as particle moments relation of the distribution function f_i :

$$\rho(\mathbf{r},t)\mathbf{u}(\mathbf{r},t) = \sum_{i=1}^{Z} f_i(\mathbf{r},t)\mathbf{e}_i(\mathbf{r},t) \tag{2.28}$$

The equation of the state and kinematic viscosity (Wolf-Gladrow et al. 2000) are defined as:

$$P = \rho c_s^2 \tag{2.29}$$

$$\nu = c_s^2(\tau - \frac{1}{2})\delta_t \tag{2.30}$$

where ν is the kinematic viscosity and c_s is the sound speed. Note that sound speed is a free parameter. The Einstein convention is used for repeated spatial indices (Dupuis 2002). Equation (2.30) indicates that the relaxation time τ has to be greater or equal to

0.5. Otherwise the viscosity would be negative. The viscosity is low when τ is close to 0.5. Note that a dedicated initialization makes it possible to simulate a periodic fluid considering a relaxation time very close to 0.5 (Succi 2001).

A recent proposition of Pierre and Luo (2000) suggests working on a momentum space rather than in a discrete velocity space. The numerical stability seems to be improved (Dupuis 2002).

A lot of benchmarking has been carried out (Chopard et al. 1998 and Filippova et al. 1997) in order to show that the LBM with second order accuracy provides a reliable, accurate and efficient algorithm for simulating low Reynolds number incompressible flows with complex boundaries. There are several different Lattice-Boltzmann Models for incompressible Newtonian fluids (Chen et al.1991, He and Luo 1997b, Qian et al. 1995, Benzi et al. 1992, and Krafczyk et al. 2003).The LBM is just one of the methods that are based on solving a discretized form of the Boltzmann equation.

2.4 Determination of Lattice Weights

Through the Chapman-Enskog expansion, the LBGK microdynamics (Equation 2.23) can recover the governing fluid equations, such as Navier-Stokes equations (Chopard et al. 1998, Chen et al. 1992 and Qian et al. 1996). The assumptions of above derivations are that Δr and Δt are small enough and the local equilibrium functions are chosen properly. It is known that discretization error $O(\varepsilon^2)$ is attached to the macroscopic continuity equation and $O(\varepsilon^2)+O(Ma^3)$ to the Navier-Stokes equation where $O(Ma^3)$ is called the compressibility error (Sterling and Chen 1994). Among others, it is shown that a small Δr leads to a small $O(\varepsilon^2)$ and that a small Δt, which implies the sound speed c_s is high, ensures a small Ma (Dupuis 2002).

From the states equation, Equation (2.27), it is known that $c_s^2 = RT$. Thus, along the discrete velocity direction e_i it yields:

$$f_i^{eq} = w_i \rho \left(1 + \frac{\mathbf{e}_i \cdot \mathbf{u}}{c_s^2} + \frac{(\mathbf{e}_i \cdot \mathbf{u})^2 - c_s^2 |\mathbf{u}|^2}{2c_s^4} \right) \tag{2.31}$$

where w_i are the weight constants. The values of w_i and c_s are up to the choice of the discrete velocities $\mathbf{e}_i$. Equation (2.31) can also be expressed as its tensor form

$$f_i^{eq} = w_i \rho \left(1 + \frac{e_{i\alpha} u_\alpha}{c_s^2} + \frac{e_{i\alpha} e_{i\beta} u_\alpha u_\beta - c_s^2 u^2}{2c_s^4} \right) \tag{2.32}$$

where indexes α , β mean summation over the space when they are identical (Shu 2004).

The constants w_i which are chosen to ensure the lattice isotropy can be derived through mass conservation and momentum conservation. The lattice isotropy is defined

as no physical quantity is dependent of a specific lattice orientation (Shu 2004). The lattice isotropy is related to its tensors isotropy (Wolf-Gladrow 2000). In the Lattice Boltzmann hydrodynamics context, the lattice velocity can form lattice tensor with several ranks. A n th rank tensor is defined as

$$T_{\alpha_1\alpha_2\cdots\alpha_n} = \sum_{i=1}^{Z} e_{i\alpha_1} e_{i\alpha_2} \ldots e_{i\alpha_n} \tag{2.33}$$

If the tensor is invariant with the arbitrary orthogonal transformations such as rotations and reflections, then it is isotropic. A sufficient condition for reasonable accuracy is to make sure the isotropy of lattice tensors up to the fourth order (Chopard and Droz 1998), which is provided by Jeffreys (1965).

$$\begin{aligned} T_{\alpha} &= \sum_{i=1}^{Z} e_{i\alpha} \\ T_{\alpha\beta} &= \sum_{i=1}^{Z} e_{i\alpha} e_{i\beta} \\ T_{\alpha\beta\gamma} &= \sum_{i=1}^{Z} e_{i\alpha} e_{i\beta} e_{i\gamma} \\ T_{\alpha\beta\gamma\zeta} &= \sum_{i=1}^{Z} e_{i\alpha} e_{i\beta} e_{i\gamma} e_{i\zeta} \end{aligned} \tag{2.34}$$

The Jeffreys' theorem argues that there are no isotropic tensors T_{α} of rank 1; and a tensor $T_{\alpha\beta}$ of rank 2 is isotropic if it is proportional to the Kronecker function $\delta_{\alpha\beta}$. An isotropic tensor of rank 3 is proportional to $\varepsilon_{\alpha\beta\gamma}$ with $\varepsilon_{123} = \varepsilon_{231} = \varepsilon_{312} = 1$, $\varepsilon_{132} = \varepsilon_{213} = \varepsilon_{321} = -1$, and zero others. There are three different tensors $T_{\alpha\beta\gamma\zeta}$ of rank 4, $\delta_{\alpha\beta}\delta_{\gamma\zeta}$, $\delta_{\alpha\gamma}\delta_{\beta\zeta}$, and $\delta_{\alpha\zeta}\delta_{\beta\gamma}$, which are linear independent. It is isotropic if it is in the form of

$$T_{\alpha\beta\gamma\zeta} = a\delta_{\alpha\beta}\delta_{\gamma\zeta} + b\delta_{\alpha\gamma}\delta_{\beta\zeta} + c\delta_{\alpha\zeta}\delta_{\beta\gamma} \tag{2.35}$$

where a, b and c are arbitrary constants. Recall that if $\alpha = \beta$, the Kronecker function $\delta_{\alpha\beta}$ is equal to 1 and 0 otherwise. The lattice tensors with odd rank vanish because of the symmetry of the lattice.

To find the weight constants w_i through the first five lattice tensors relations (Shu 2004):

$$\sum_{i=1}^{Z} w_i = 1$$

$$\sum_{i=1}^{Z} w_i e_i = 1 \rightarrow \sum_{i=1}^{Z} w_i e_{i\alpha} = 0$$

$$\sum_{i=1}^{Z} w_i((e_i \cdot u)^2 - c_s^2 \mid u \mid^2) = 0 \quad \rightarrow \quad \sum_{i=1}^{Z} w_i e_{i\alpha} u_\beta e_{i\beta} u_\beta = c_s^2 u^2 \tag{2.36}$$

$$\sum_{i=1}^{Z} w_i e_i \cdot e_j = c_s^2 \delta_{ij}$$

$$\sum_{i=1}^{Z} w_i e_i((e_j \cdot u)^2 - c_s^2 \left|u\right|^2) = 0$$

One can compute the tensor of D2Q5 lattice model as (Wolf-Gladrow 2000) and a hexagonal lattice D2Q7, which is isotropic. In D2Q5, the second order tensor $T_{\alpha\beta}$ is equal to $2\delta_{\alpha\beta}$ and the fourth order tensor $T_{\alpha\beta\gamma\zeta}$ is equal to $2\delta_{\alpha\beta\gamma\zeta}$ .And the other isotropic lattices could be obtained by using the Face Centered Hyper Cubic (FCHC) four dimensional lattice onto a subspace (D'Humieres and Lallemand 1986).

The weight constants w_i could be derived through Equation (2.36) and the Chapman-Enskog expansion to recover the Navier-Stokes (N-S) equation. In the following, the particle discrete velocity (DV) model is written as $DdQ(Z+1)$, where Z is

the number of discrete speeds and *d* is the space dimension. The classic models are listed such as: D1Q5, D2Q7, D2Q9, D3Q15 and D3Q19 and their main parameters in Table 2.1 (Shu 2004).

From the results listed, the similarities of the D2Q7 lattice model and D2Q9 lattice model are seen. The D2Q7 lattice model requires less memory to store its states while the D2Q9 lattice model uses a Cartesian grid for simpler data structure. Note that a checkerboard invariant is presented in the D3Q15 lattice model (Drona et al. 1999). Because the fluid momentum may form unphysical patterns, the D3Q19 lattice is usually preferred when using a three dimensional simulation.

Models	$\mathbf{e}_i$	w_i	c_s^2
D1Q5	(0) ($\pm$ 1) ($\pm$ 2)	6/12 (i =0) 2/12 (i =1,2) 1/12 (i =3,4)	1
D2Q7	(0,0) ($\pm$ 1, 0), ($\pm$ 1/2, $\pm$ $\sqrt{3}$ /2)	6/12 (i =0) 1/12 (i =1,6)	1/4
D2Q9	(0,0) ($\pm$ 1,0),(0, $\pm$ 1) ($\pm$ 1, $\pm$ 1)	16/36 (i =0) 4/36 (i =2l +1, l =0,…3,) 1/36 (i =2l , l =1,…,4)	1/3
D3Q15	(0,0,0) ($\pm$ 1,0,0), (0, $\pm$ 1,0), (0,$\pm$ 1,0) ($\pm$ 1, $\pm$ 1, $\pm$ 1)	16/72 (i =0) 8/72 (i =1,…,6) 1/72 (i =7,…,14)	1/3
D3Q19	(0,0,0) (($\pm$ 1,0,0), (0, $\pm$ 1,0), (0,$\pm$ 1,0) ($\pm$ 1, $\pm$ 1,0), ($\pm$ 1, 0, $\pm$ 1), (0, $\pm$ 1, $\pm$ 1)	12/36 (i =0) 2/36 (i =1,…,6) 1/36 (i =7,…,18)	1/3

Table 2.1 Main parameters of the most common $DdQ(Z+1)$ lattices from Shu (2004), where *d* is the spatial dimension and z is the number of link, e_i is the velocity on link i, w_i are the weights coefficients associated with each link.

2.5 Chapman-Enskog Expansion

The macroscopic fluid properties can be considered as the collective behaviors of microscopic particles in the lattice system. And they are well described by the Navier-Stokes equation and the continuity equation. The derivation from the LBEs to the macroscopic Navier-Stokes equations is under the Chapman-Enskog expansion, a multi-scale analysis developed by Chapman and Enskog between 1910 and 1920.

The first order solution $O(\tau^{-1})$ of the LBE by the Chapman-Enskog expansion yields the Euler equation (Chapman et al. 1970), which is by substituting the Maxwell-Boltzmann particle distribution in the steady state and neglecting the disturbances. The Navier-Stokes equation is a second-order solution $O(\tau^{0})$ of LBE by the Chapman-Enskog expansion (Chapman et al. 1970). Thus the continuum description of fluid with second order accuracy in space and time is given by the continuity and Navier-Stokes (momentum) equations (Landau and Lifshitz 1963).

The expansion parameter used in Chapman-Enskog expansion is the Knudsen number Kn = λ/L (Shu 2004), where λ is the molecular mean free path and L the characteristic length of the system.

Here, the incompressible Navier-Stokes equation based on the D2Q9 model is derived through the Chapman-Enskog expansion (Shu 2004). Since the spatial density variation is not zero in LBE simulations, the compressible Navier-Stokes equation is simulated instead of incompressible one. To simulate incompressible Navier-Stokes equation accurately, it must be ensured that the Mach number is low (usually less than 0.3) and the density fluctuation ($\delta\rho$) is of the order $O(Ma^2)$ (Dupuis 2002).

In the macroscopic level, the flow has three basic time scales: collision, convection and diffusion. The diffusion happens very slowly; the convection happens faster in the scale of ε; and the collision happens very much faster in the scale of ε^2. In the space, the collision happens in the scale of λ, while the convection and diffusion happen in the scale of L, where $L = \frac{\lambda}{\varepsilon}$. In the Chapman-Enskog expansion, the multi-scale expansion is introduced by Shu (2004) as:

$$f_i = \sum_{j=0}^{2} \varepsilon^j f_i^{(j)} \tag{2.37}$$

$$\partial_t = \sum_{j=0}^{1} \varepsilon^{j+1} \partial_{t_j} \tag{2.38}$$

$$\nabla_r = \varepsilon^1 \nabla_{r1} \tag{2.39}$$

where ε is a small number, and δ_t is in the same order of ε.

Using the second order Taylor series expansion on the left hand side of the Equation (2.10):

$$(\frac{\partial}{\partial t} + \mathbf{e}_i.\nabla) f_i + \frac{\delta_t}{2}(\frac{\partial}{\partial t} + \mathbf{e}_i \nabla)^2 f_i + \frac{1}{\tau \delta_t}(f_i - f_i^{eq}) + O(\delta_t^3) = 0 \tag{2.40}$$

Then using the Equation (2.37), (2.38) and (2.39):

$$E_i^{(0)} + \varepsilon E_i^{(1)} + \varepsilon^2 E_i^{(2)} = 0 \tag{2.41}$$

where

$$E_i^{(0)} = (f_i^{(0)} - f_i^{(eq)})/(\tau \delta_t) \tag{2.42}$$

$$E_i^{(1)} = (\partial_{t_0} + \mathbf{e}_i \cdot \nabla_1) f_i^{(0)} + \frac{1}{\tau \delta_t} f_i^{(1)} \tag{2.43}$$

$$E_i^{(2)} = \partial_{t_1} f_i^{(0)} + (\partial_{t_0} + \mathbf{e}_i \cdot \nabla_1) f_i^{(1)} + \frac{\delta_t}{2}(\partial_{t_0} + \mathbf{e}_i \cdot \nabla_1)(\partial_{t_0} + \mathbf{e}_i \cdot \nabla_1) f_i^{(0)} + \frac{1}{\tau\delta_t} f_i^{(2)}$$

$$= \partial_{t1} f_i^{(0)} + (\partial_{t_0} + \mathbf{e}_i \cdot \nabla_1)(1 - \frac{1}{2\tau}) f_i^{(1)} + \frac{1}{\tau\delta_t} f_i^{(2)} \tag{2.44}$$

The distribution function f_i is constrained by the following relationships

$$\sum_{i=0}^{Z} f_i^{(0)} = \rho, \sum_{i=0}^{Z} f_i^{(0)} \mathbf{e}_i = \rho\mathbf{u} \tag{2.45}$$

$$\sum_{i=0}^{Z} f_i^{(j)} = 0, \sum_{i=0}^{Z} f_i^{(j)} \mathbf{e}_i = 0, \sum_{i=0}^{Z} f_i^{(2)} = 0, \sum_{i=0}^{Z} f_i^{(2)} \mathbf{e}_i = 0 \tag{2.46}$$

In the following section, the mass conservation law and the momentum conservation law are shown to be obeyed. For the mass conservation, first to get the summation of the Equation (2.43) over i, which leads to:

$$\sum_{i=0}^{Z} E_i^{(1)} = \frac{\partial}{\partial t_0} \sum_{i=0}^{Z} f_i^{(0)} + \nabla_1 \cdot \sum_{i=0}^{Z} \mathbf{e}_i f_i^{(0)} + \frac{1}{\tau\delta_t} \sum_{i=0}^{Z} f_i^{(1)} \tag{2.47}$$

which could reduce to

$$\frac{\partial}{\partial t_0} \rho + \nabla_1 \cdot \rho\mathbf{u} = 0 \tag{2.48}$$

where $t_0 = \lambda t$ is the macroscopic time scale.

Similarly, to get the summation of Equation (2.44) over i, that is

$$\sum_{i=0}^{Z} E_i^{(2)} = \frac{\partial}{\partial t_1} \sum_{i=0}^{Z} f_i^{(0)} + \sum_{i=0}^{Z} (\partial_{t_0} + \mathbf{e}_i \cdot \nabla_1) f_i^{(1)} [1 - \frac{1}{2\tau}] + \frac{1}{\tau\delta_t} \sum_{i=0}^{Z} f_i^{(2)} \tag{2.49}$$

Then using Equation (2.45) and Equation (2.46), which have

$$\frac{\partial}{\partial t_1} \rho = 0 \tag{2.50}$$

where $t_1 = \lambda^2 t$ is also the macroscopic time scale.

Combining the Equation (2.48) and Equation (2.50) yields the continuum equation as follows:

$$\frac{\partial}{\partial t}\rho + \nabla \rho \mathbf{u} = 0 \tag{2.51}$$

For the momentum conservation, it is needed to consider the second moment of Equation (2.43), which leads to

$$\sum_{i=0}^{Z} E_i^{(1)} \mathbf{e}_i = \sum_{i=0}^{Z} \frac{\partial}{\partial t_0} f_i^{(0)} \mathbf{e}_i + \sum_{i=0}^{Z} (\mathbf{e}_i \cdot \nabla) f_i^{(0)} \mathbf{e}_i + \frac{1}{\tau \delta_t} \sum_{i=0}^{Z} f_i^{(1)} \mathbf{e}_i \tag{2.52}$$

Through Equation (2.45) and Equation (2.46):

$$\frac{\partial}{\partial t_0}\rho \mathbf{u} + \nabla \cdot \sum_{i=0}^{Z} \mathbf{e}_i \mathbf{e}_i f_i^{(0)} = 0 \tag{2.53}$$

or in its equivalent form as

$$\frac{\partial}{\partial t_0}\rho \mathbf{u} + \nabla \cdot \underline{\underline{\prod}}^{(0)} = 0 \tag{2.54}$$

where $t_0 = \lambda t$ is the macroscopic time scale , and $\underline{\underline{\prod}}^{(0)}$ is the zeroth-order momentum flux tensor, where

$$\underline{\underline{\prod}}_{\alpha\beta}^{(0)} = \sum_{i=0}^{Z} e_{i,\alpha} e_{i,\beta} f_i^{(0)} \tag{2.55}$$

Using Equation (2.43) for the second moment of Equation (2.44):

$$\sum_{i=0}^{Z} E_i^{(2)} \mathbf{e}_i = \sum_{i=0}^{Z} \frac{\partial}{\partial t_1} f_i^{(0)} \mathbf{e}_i + (1 - \frac{1}{2\tau})[\sum_{i=0}^{M} \frac{\partial}{\partial t_0} f_i^{(1)} \mathbf{e}_i + \sum_{i=0}^{Z} (\mathbf{e}_i \cdot \nabla) f_i^{(1)} \mathbf{e}_i] + \frac{1}{\tau \delta_t} \sum_{i=0}^{Z} f_i^{(2)} \mathbf{e}_i \tag{2.56}$$

where $t_1 = \lambda^2 t$ is also the macroscopic time scale.

Then using Equation (2.45) and Equation (2.46):

$$\frac{\partial}{\partial t_1}\rho\mathbf{u}+(1-\frac{1}{2\tau})\nabla\cdot\sum_{i=0}^{Z}\mathbf{e}_i\mathbf{e}_i f_i^{(1)}=0 \tag{2.57}$$

or in the form of

$$\frac{\partial}{\partial t_1}\rho\mathbf{u}+(1-\frac{1}{2\tau})\nabla\cdot\underline{\underline{\prod}}^{(1)}=0 \tag{2.58}$$

where $\underline{\underline{\prod}}^{(1)}$ is the first-order momentum flux tensor,

$$\underline{\underline{\prod}}_{\alpha,\beta}^{(1)}=\sum_{i=0}^{Z}e_{i,\alpha}e_{i,\beta}f_i^{(1)} \tag{2.59}$$

The tensor $E^{(q)}$ of order q is defined as follows:

$$E_{jk\ldots q}^{(q)}=\sum_{i=0}^{Z}w_i e_{i,j}e_{i,k}\ldots e_{i,q},\ j,k,\ldots q=1\ldots 3 \tag{2.60}$$

Equation (2.60) is used to evaluate $\underline{\underline{\prod}}^{(0)}$ and $\underline{\underline{\prod}}^{(1)}$, where $e_{i,j}$ is the projection of $\mathbf{e}_i$ on j-axis ($j=x_1,x_2$ or x_3). In the D2Q9 model $\underline{\underline{E}}^{(q)}$ can be written as:

$$E_j^{(1)}=\sum_{i=0}^{Z}w_i e_{i,j}=0 \tag{2.61}$$

$$E_{jk}^{(2)}=\sum_{i=0}^{Z}w_i e_{i,j}e_{i,k}=c_s^2\delta_{jk} \tag{2.62}$$

$$E_{jkl}^{(3)}=\sum_{i=0}^{Z}w_i e_{i,j}e_{i,k}e_{i,l}=0 \tag{2.63}$$

$$E_{jklm}^{(4)}=\sum_{i=0}^{Z}w_i e_{i,j}e_{i,k}e_{i,l}e_{i,m}=c_s^4\Delta_{jklm} \tag{2.64}$$

where δ_{jk} and δ_{jklm} are Kronecker delta with two and four indices respectively:

$$\Delta_{jklm}=\delta_{jk}\delta_{lm}+\delta_{jl}\delta_{km}+\delta_{jm}\delta_{kl} \tag{2.65}$$

Using tensor $\underset{=}{E}^{(q)}$ properties and Equation (2.32), it follows for the zeroth order momentum flux tensor as follows:

$$\Pi_{jk}^{(0)} = \sum_{i=0}^{Z} e_{i,j} e_{i,k} f_i^{(0)} = c_s^2 \rho \delta_{jk} + \rho u_j u_k \tag{2.66}$$

since

$$f_j^0 = f_i^{eq} = w_i \rho \left(1 + \frac{e_{i\alpha} u_\alpha}{c_s^2} + \frac{e_{i\alpha} e_{i\beta} u_\alpha u_\beta - c_s^2 u^2}{2 c_s^4} \right)$$

$$\Delta_{jklm} = \delta_{jk}\delta_{lm} + \delta_{jl}\delta_{km} + \delta_{jm}\delta_{kl}$$

$$\Delta_{jklm} u_l u_m = (\delta_{jk}\delta_{lm} + \delta_{jl}\delta_{km} + \delta_{jm}\delta_{kl}) u_l u_m = \delta_{jk} u^2 + 2 u_j u_k$$

and first order momentum flux tensor

$$\begin{aligned} \Pi_{jk}^{(1)} &= \sum_{i=0}^{Z} e_{i,j} e_{i,k} f_i^{(1)} = -\tau \delta_t \sum_{i=0}^{Z} e_{i,j} e_{i,k} D_{t_0} f_i^{(0)} \\ &= -\tau \delta_t \left[\frac{\partial}{\partial t_0} \Pi_{jk}^{(0)} + \nabla_1 \cdot \sum_{i=0}^{Z} e_{i,j} e_{i,k} f_i^{(0)} \right] \end{aligned} \tag{2.67}$$

since

$$\begin{aligned} \nabla_1 \cdot \sum_{i=0}^{Z} e_{i,j} e_{i,k} f_i^{(0)} &= \frac{1}{c_s^2} \nabla_1 \cdot \rho \sum_{i=0}^{Z} w_i e_{i,j} e_{i,k} e_{i,l} e_{i,m} u_m \\ &= c_s^2 \nabla_1 \cdot \rho \Delta_{jklm} u_m = c_s^2 \partial_{x_l} (\rho \delta_{jk}\delta_{lm} + \rho \delta_{jl}\delta_{km} + \rho \delta_{jm}\delta_{kl}) u_m \\ &= \rho c_s^2 (\delta_{jk} \nabla_1 \cdot u + \frac{\partial u_j}{\partial x_k} + \frac{\partial u_k}{\partial x_j}) + c_s^2 \delta_{jk} u_m \frac{\partial \rho}{\partial x_m} + c_s^2 (u_j \frac{\partial \rho}{\partial x_k} + u_k \frac{\partial \rho}{\partial x_j}) \end{aligned}$$

$$\frac{\partial}{\partial t_0}\Pi_{jk}^{(0)} = \frac{\partial}{\partial t_0}(\rho c_s^2 \delta_{jk} + \rho u_j u_k)$$

$$= c_s^2 \delta_{jk} \frac{\partial}{\partial t_0}\rho + u_j \frac{\partial}{\partial t_0}(\rho u_k) + u_k \frac{\partial}{\partial t_0}(\rho u_j) - u_j u_k \frac{\partial}{\partial t_0}\rho$$

$$= (c_s^2 \delta_{jk} - u_j u_k)\frac{\partial}{\partial t_0}\rho + u_j[-\frac{\partial}{\partial x_k}(\rho c_s^2) - \frac{\partial}{\partial x_m}(\rho u_k u_m)] + u_k[-\frac{\partial}{\partial x_j}(\rho c_s^2) - \frac{\partial}{\partial x_m}(\rho u_j u_m)]$$

$$= c_s^2 \delta_{jk} \frac{\partial}{\partial t_0}\rho - c_s^2(u_j \frac{\partial \rho}{\partial x_k} + u_k \frac{\partial \rho}{\partial x_j}) - \frac{\partial}{\partial x_m}(\rho u_j u_k u_m) - u_j u_k[\frac{\partial}{\partial t_0}\rho + \frac{\partial}{\partial x_m}(\rho u_m)]$$

$$= c_s^2 \delta_{jk} \frac{\partial}{\partial t_0}\rho - c_s^2(u_j \frac{\partial \rho}{\partial x_k} + u_k \frac{\partial \rho}{\partial x_j}) - \frac{\partial}{\partial x_m}(\rho u_j u_k u_m)$$

$$= -c_s^2 \delta_{jk} \frac{\partial}{\partial x_m}(\rho u_m) - c_s^2(u_j \frac{\partial \rho}{\partial x_k} + u_k \frac{\partial \rho}{\partial x_j}) - \frac{\partial}{\partial x_m}(\rho u_j u_k u_m)$$

$$= -\rho c_s^2 \delta_{jk} \nabla_1 \cdot u - c_s^2 \delta_{jk} u_m \frac{\partial}{\partial x_m}\rho - c_s^2(u_j \frac{\partial \rho}{\partial x_k} + u_k \frac{\partial \rho}{\partial x_j}) - \frac{\partial}{\partial x_m}(\rho u_j u_k u_m)$$

Therefore:

$$(1-\frac{1}{2\tau})\prod_{jk}^{(1)} = \sum_{i=0}^{Z} e_{i,j} e_{i,k} f_i^{(0)} = -\tau \delta_t \sum_{i=0}^{Z} e_{i,j} e_{i,k} D_{t_0} f_i^{(0)}$$

$$= -\tau \delta_t (1-\frac{1}{2\tau})\left[\rho c_s^2 \left(\frac{\partial u_j}{\partial x_k} + \frac{\partial u_k}{\partial x_j}\right) - \frac{\partial}{\partial x_m}(\rho u_j u_k u_m)\right] + O(Ma^2) \qquad (2.68)$$

$$\approx -c_s^2 \rho \tau \delta_t (1-\frac{1}{2\tau})\left(\frac{\partial u_j}{\partial x_k} + \frac{\partial u_k}{\partial x_j}\right) + O(Ma^2)$$

where the term $\frac{\partial(\rho u_j u_k u_m)}{\partial x_m}$ is ignored, which is very small. Combining the Equation (2.53), (2.54), (2.57) and (2.58) to obtain the momentum equation as follows:

$$\frac{\partial \rho \mathbf{u}}{\partial t} + \nabla(\rho \mathbf{u}\mathbf{u}) = -\nabla P + \rho \nu \nabla^2 \mathbf{u} \qquad (2.69)$$

where ν is kinematic viscosity given by Shu (2004) as:

$$\nu = \frac{2\tau - 1}{6}\delta_t$$

In the small Mach number limit, we could ignore variation of the density. Thus the incompressible Navier-Stokes equations can be obtained

$$\nabla \cdot \mathbf{u} = 0 \tag{2.70}$$

$$\frac{\partial \mathbf{u}}{\partial t} + \mathbf{u} \cdot \nabla \mathbf{u} = -\frac{1}{\partial \rho}\nabla \rho + \nu \nabla^2 \mathbf{u} \tag{2.71}$$

CHAPTER 3

A GENERALIZED LATTICE BOLTZMANN METHOD

3.1 Porous Flow Model

Many authors have presented the generalized model for isothermal incompressible fluid flow in porous media recent years. In this thesis the form proposed by Nithiarasu et al. (1997) is used, which is applicable for a porous medium with both a constant and a variable porosity. Assuming in the Boussinesq limit that the local thermal equilibrium exists between the fluid and the solid, the generalized model for incompressible fluid flow and convection heat transfer in porous media (Guo and Zhao 2005a) can be expressed by the generalized Navier-Stokes equation as:

$$\nabla \cdot \mathbf{u} = 0 \tag{3.1}$$

$$\frac{\partial \mathbf{u}}{\partial t} + (u \cdot \nabla)\left(\frac{\mathbf{u}}{\varepsilon}\right) = -\frac{1}{\rho}\nabla(\varepsilon p) + \nu_e \nabla^2 \mathbf{u} + \mathbf{F} \tag{3.2}$$

$$\sigma \frac{\partial T}{\partial t} + \mathbf{u} \cdot \nabla T = \nabla \cdot (\alpha_m \nabla T) \tag{3.3}$$

where $\mathbf{u}$ is the volume averaged velocity; ρ is the fluid density; p is the volume averaged pressure; T is the volume-averaged temperature of the fluid; ε is the porosity of the porous medium and ν_e is an effective viscosity parameter.

The coefficient σ represents the ratio between the heat capacities of the solid and fluid phases:

$$\sigma = \varepsilon + (1-\varepsilon)\rho_s c_{ps} / \rho_f c_{pf} \tag{3.4}$$

where ρ_f is the fluid density; ρ_s is the solid density; c_{pf} is the fluid specific heats at a constant pressure; and c_{ps} is the solid specific heats at constant pressure.

The effective thermal diffusivity α_m is defined as $\alpha_m = k_m / \rho_f c_{pf}$, where k_m is the effective thermal conductivity, which is $k_m = k_e + k_d$, with k_e representing the stagnant thermal conductivity and k_d the thermal conductivity due to thermal dispersion.

The last term **F** on the right-hand side of Equation (3.2) represents the total body force due to the presence of a porous medium and other external force fields and is given by Guo and Zhao (2002d)

$$\mathbf{F} = -\frac{\varepsilon \nu}{K}\mathbf{u} - \frac{\varepsilon \mathrm{F}_\varepsilon}{\sqrt{K}}|\mathbf{u}|\mathbf{u} + \varepsilon \mathbf{G} \tag{3.5}$$

where ε is the porosity of the porous medium; ν is the fluid viscosity which is not necessarily the same as the effective viscosity ν_e ; and **G** is the body force induced by an external force, which is given by

$$\mathbf{G} = -\mathbf{g}\beta(T - T_0) + \mathbf{a} \tag{3.6}$$

where **g** is the gravitational acceleration; β is the thermal expansion coefficient; T is the fluid temperature; and T_0 is the reference temperature. The first term of Equation (3.6) represents the buoyancy force due to the temperature effects and the second term **a** is the acceleration due to other external force fields (Guo and Zhao 2005a).

The geometric function F_ε and the porous medium permeability K are related to the porosity ε based on Ergun's experimental investigations (Ergun 1952), which can be expressed by Vafai et al. (1984) as

$$F_\varepsilon = \frac{1.75}{\sqrt{150\varepsilon^3}} \tag{3.7}$$

$$K = \frac{\varepsilon^3 d_p^2}{150(1-\varepsilon)^2} \tag{3.8}$$

where d_p is the diameter of the solid particle.

It is known that when the porosity ε gets very close to 1 in the absence of porous medium and no external force exists, the generalized momentum Equation (3.2) reduces to the Navier-Stokes equation, Equation (2.71), for free fluid flows (Guo and Zhao 2005a). The second term ($\nu_e \nabla^2 \mathbf{u}$) on the right side of Equation (3.2) is the Brinkman term due to the presence of a solid boundary. Although the boundary layer of some cases may be very thin, its inclusion, especially for flow involving heat transfer, is very important (Guo and Zhao 2005a). The first term ($\frac{\varepsilon \nu}{K}\mathbf{u}$) of the right side of Equation (3.5) is the linear drag, the Darcy term due to the porous medium. And the second term ($\frac{\varepsilon \mathbf{F}_\varepsilon}{\sqrt{K}}|\mathbf{u}|\mathbf{u}$) of the right side of Equation (3.5) is the nonlinear drag, the Forchheimer term due to the porous medium. In low speed limit flow, the quadratic nature of the nonlinear resistance is always negligible, but it is very important for fluid of high-speed flows. Without the nonlinear term of Forchheimer, Equation (3.2) becomes the Brinkman-extended Darcy equation (Guo and Zhao 2005a).

The fluid flow governed by Equation (3.1-3.3) is characterized by the porosity ε, the heat capacity ratio σ, and some non-dimensional parameters: the Darcy number Da, the viscosity radio Je (between the effective viscosity and the shear viscosity), the Prandtl number Pr, the Rayleigh number Ra (for natural convection), the Reynolds number Re (for forced or mixed convection), and the Peclect number Pe respectively, defined as:

$$\mathbf{Re} = \frac{LU}{\nu} \quad \mathbf{Da} = \frac{K}{L^2} \quad \mathbf{Je} = \frac{\nu_e}{\nu} \quad \mathbf{Pr} = \frac{\nu}{\alpha} \quad \mathbf{Ra} = \frac{g\beta \Delta T L^3}{\nu\alpha} \quad \mathbf{Pe} = \frac{LU}{\alpha} \tag{3.9}$$

where L is the characteristic length of the system, and U is the characteristic velocity of the fluid, respectively. Here, the relationship between the linear drag and the nonlinear drag for a given medium by a ratio (Guo and Zhao 2002d) is as follows:

$$\frac{F_\varepsilon \left|\mathbf{u}\right| / \sqrt{K}}{\nu / K} \sim \sqrt{Da}\,\mathrm{Re} \tag{3.10}$$

Therefore, the nonlinear drag term, $\frac{\varepsilon \mathrm{F}_\varepsilon}{\sqrt{K}}\left|\mathbf{u}\right|\mathbf{u}$, could be ignored for the cases with small Reynolds number or small Darcy number, and the above mentioned general model reduces to the Brinkman-extended Darcy model. But if the Reynolds number or the Darcy number is huge, the nonlinear drag needs to be considered.

3.2 Velocity Field

In this section, the Lattice Boltzmann Method with Double Distribution Function (DDF LBM) approach proposed by Guo and Zhao (2002d) is used to model the fluid flow and convection heat transfer in porous media. In this method, the evolution of the velocity field is derived by the density distribution function of DDF LBM. The fluid is modeled by a single-particle distribution function (DF). The evolution of the DF is governed by a lattice Boltzmann equation as Equation (2.23):

$$f_i(\mathbf{x}+\mathbf{e}_i\delta_t, t+\delta_t) - f_i(\mathbf{x},t) = -\frac{\left[f_i(\mathbf{x},t) - f_i^{eq}(\mathbf{x},t) \right]}{\tau}$$

And the equilibrium distribution function (EDF) of the DnQb (Qian et al. 1992) models is defined as the Equation (2.31)

$$f_i^{eq} = w_i \rho \left(1 + \frac{\mathbf{e}_i \cdot \mathbf{u}}{c_s^2} + \frac{(\mathbf{e}_i \cdot \mathbf{u})^2 - c_s^2 \,|\, \mathbf{u} \,|^2}{2c_s^4} \right)$$

or its equivalent form as

$$f_i^{(eq)} = w_i \rho \left[1 + \frac{\mathbf{e} \cdot \mathbf{u}}{c_s^2} + \frac{\mathbf{uu} : (\mathbf{e}_i \mathbf{e}_i - c_s^2 \mathrm{I})}{2c_s^4} \right] \qquad (3.11)$$

In Chapter 2, it is shown that the Navier-Stokes equations without external force and no porous medium effect can be derived from the lattice Boltzmann Equation (2.31) through a Chapman-Enskog expansion procedure in the incompressible limit. The main parameters of the above Equation (2.23) and Equation (3.11) are the same as the parameters discussed in Chapter 2.

Here, the above generalized equations in the LBM framework is taken to model incompressible fluid flow in a porous medium. Firstly a LBE is proposed for a porous

medium with porosity ε, when the linear ($\frac{\varepsilon\nu}{K}\mathbf{u}$) and nonlinear ($\frac{\varepsilon\mathbf{F}_\varepsilon}{\sqrt{K}}|\mathbf{u}|\mathbf{u}$) drag effects of the medium, and the external force (F) is temporally ignored. Therefore the LBE is obtained as follows:

$$\overline{f_i}(\mathbf{x}+\mathbf{e}_i\delta_t, t+\delta_t) - \overline{f_i}(\mathbf{x},t) = -\frac{\overline{f_i}(\mathbf{x},t) - \overline{f_i^{(eq)}}(\mathbf{x},t)}{\tau} \tag{3.12}$$

where $\overline{f_i}(\mathbf{x},t)$ and $\overline{f_i^{(eq)}}(\mathbf{x},t)$ are the volume-averaged DF and EDF at the REV scale, respectively (Guo and Zhao 2002d). Here, the averaging is only conceptual. It is the same as the averaged particle number (or the distribution function) in the standard LBE, and used to replace the Boolean number in LGCA. Thus, in practical problems it is unnecessary to obtain averaging. In following chapters, the over bars will omitted for the sake of convenience. To include the effect of the porous medium, the EDF from Equation (3.11) could be defined as follows:

$$f_i^{(eq)} = w_i\rho\left[1 + \frac{\mathbf{e}\cdot\mathbf{u}}{c_s^2} + \frac{\mathbf{uu}:(\mathbf{e}_i\mathbf{e}_i - c_s^2\mathrm{I})}{2\varepsilon c_s^4}\right] \tag{3.13}$$

The volume averaged fluids density ρ and velocity $\mathbf{u}$ are defined the same as Equation (2.27) and Equation (2.28) by the averaged DFs, which are

$$\rho(\mathbf{r},t) = \sum_{i=1}^{Z} f_i(\mathbf{r},t), \qquad \rho(\mathbf{r},t)\mathbf{u}(\mathbf{r},t) = \sum_{i=1}^{Z} f_i(\mathbf{r},t)\mathbf{e}_i(\mathbf{r},t)$$

Similar to the process in Chapter 2, the following macroscopic equations can be obtained from the Equation (3.12) by the Chapman-Enskog procedure in the limit of small Mach number:

$$\frac{\partial\rho}{\partial t} + \nabla\cdot(\rho\mathbf{u}) = 0 \tag{3.14}$$

$$\frac{\partial(\rho\mathbf{u})}{\partial t}+\nabla\cdot\left(\frac{\rho\mathbf{u}\mathbf{u}}{\varepsilon}\right)=-\nabla(\varepsilon \mathrm{p})+\nabla\cdot[\rho\nu_e(\nabla\mathbf{u}+\mathbf{u}\nabla)] \tag{3.15}$$

where

$$p=c_s^2\rho/\varepsilon$$

$$\nu_e=c_s^2\left(\tau-0.5\right)\delta_t$$

If the density is nearly a constant, which means $\rho\approx\rho_0=const$, the Equation (3.14) and Equation (3.15) could be reduced to:

$$\nabla\cdot\mathbf{u}=0$$

$$\frac{\partial\mathbf{u}}{\partial t}+(\mathbf{u}\cdot\nabla)\left(\frac{\mathbf{u}}{\varepsilon}\right)=-\frac{1}{\rho}\nabla(\varepsilon p)+\nu_e\nabla^2\mathbf{u}$$

which are the generalized Navier-Stokes equations when the external force $F=0$. Furthermore, in the case of no effect of the porous medium, the above mentioned equations could be reduced to:

$$\nabla\cdot\mathbf{u}=0$$

$$\frac{\partial\mathbf{u}}{\partial t}+\mathbf{u}\cdot\nabla\mathbf{u}=-\frac{1}{\rho}\nabla p+\nu_e\nabla^2\mathbf{u}$$

which are the incompressible Navier-Stokes equations of Equation (2.70) and (2.71).

However, most of the time, the problems are the general cases where $F\neq0$. Therefore, the LBE has to be modified to account for effect of the total force. This is done by adding a force term into the LBE of Equation (3.12) (Guo and Zhao 2002d) as follow:

$$f_i(\mathbf{x}+\mathbf{e}_i\delta_t,t+\delta_t)-f_i(\mathbf{x},t)=-\frac{f_i(\mathbf{x},t)-f_i^{eq}(\mathbf{x},t)}{\tau}+\delta_t F_i \tag{3.16}$$

The last term on the right-hand side of above equation, $\delta_t F_i$, is accounted for by the total force due to the presence of the porous medium and other external force fields. Recently it is shown that the force term F_i has to be chosen appropriately and the fluid velocity $\mathbf{u}$ has to be refined to obtain correct flow equations (Guo et al. 2002c). In this thesis a suitable choice for flow in porous media is proposed, which is governed by Equation (3.1) and Equation (3.2) for the total force F_i (Guo and Zhao 2002d) as

$$F_i = w_i \rho (1 - \frac{1}{2\tau}) \left[1 + \frac{\mathbf{e}_i \cdot \mathbf{F}}{c_s^2} + \frac{\mathbf{uF} : (\mathbf{e}_i \mathbf{e}_i - c_s^2 \mathbf{I})}{\varepsilon c_s^4} \right] \tag{3.17}$$

Accordingly, the fluid density ρ and fluid velocity $\mathbf{u}$ can be defined by

$$\rho(\mathbf{r}, t) = \sum_{i=1} f_i(\mathbf{r}, t) \tag{3.18}$$

$$\rho \mathbf{u} = \sum_i \mathbf{e}_i f_i + \frac{\delta_t}{2} \rho \mathbf{F} \tag{3.19}$$

It is noted that the force term $\mathbf{F}$ of Equation (3.19) also contains the velocity $\mathbf{u}$. That means Equation (3.19) is a nonlinear equation for the velocity $\mathbf{u}$.

However, the velocity $\mathbf{u}$ could be obtained explicitly due to its quadratic nature of the Equation (3.19) itself as

$$\mathbf{u} = \frac{\mathbf{v}}{c_0 + \sqrt{c_0^2 + c_1 |\mathbf{v}|}} \tag{3.20}$$

where $\mathbf{v}$ is a auxiliary velocity defined as

$$\rho \mathbf{v} = \sum_i \mathbf{e}_i f_i + \frac{\delta_t}{2} \varepsilon \rho \mathbf{G} \tag{3.21}$$

The two parameters c_0 and c_1 in Equation (3.20) can be obtained by

$$c_0 = \frac{1}{2}\left(1 + \varepsilon \frac{\delta_t}{2} \frac{\nu}{K}\right) \tag{3.22}$$

$$c_1 = \varepsilon \frac{\delta_t}{2} \frac{F_\varepsilon}{\sqrt{K}} \tag{3.23}$$

Through the Chapman-Enskog expansion (Guo et al. 2002c), the macroscopic equations can be obtained from the Equation (3.16) as:

$$\frac{\partial \rho}{\partial t} + \nabla \cdot (\rho \mathbf{u}) = 0 \tag{3.24}$$

$$\frac{\partial (\rho \mathbf{u})}{\partial t} + \nabla \cdot \left(\frac{\rho \mathbf{u}\mathbf{u}}{\varepsilon}\right) = -\nabla(\varepsilon p) + \nabla \cdot [\rho \nu_e (\nabla \mathbf{u} + \mathbf{u} \nabla)] + \rho \mathbf{F} \tag{3.25}$$

where the velocity $\mathbf{u}$ is given by Equation (3.20) and pressure p is defined as

$$p = c_s^2 \rho / \varepsilon \tag{3.26}$$

and the effective viscosity is defined as

$$\nu_e = c_s^2 \left(\tau - 0.5\right) \delta_t \tag{3.27}$$

Equations (3.24) and (3.25) are the generalized lattice Boltzmann Equation (GLBE) proposed by Guo and Zhao (2002d) for fluid flows in porous media. The equations can reduce to the generalized Navier–Stokes Equations (3.1) and (3.2) in the incompressible limit, i.e., $\rho \approx \rho_0 = const$. When the porosity of the porous medium close to unity i.e. ε = 1, the GLBE reduces to the standard LBE for fluid flows in case of no porous medium.

Also, if $F_\varepsilon = 0$ in GLBE, then it reduces to the Simplified Lattice Boltzmann Equation (SLBE) for the Brinkman-extended Darcy model (Guo and Zhao 2002d). However, it is indicated that the simplified model, SLBE is different from the SP model proposed by Spaid and Phelan (1997) and also different from the improved version developed by Martys (2001) in several aspects, although all of these models implement a

force term to account for the effect of the porous medium. Firstly, the force term of the present SLBE model is based on the method proposed by Guo et al. (2002c), which can produce correct hydrodynamics. However, the force term of the SP model is based on the method of Shan (1993), which produces errors of order $\tau^2 |\mathbf{F}|^2$ (Martys et al. 1998). Later in an improved SP model by Martys (2001), the force term is based on their previous method (Martys et al. 1998), which was observed to have undesirable errors (Guo et al. 2002c). Another obvious difference between the SLBE and the improved SP model is the different definitions of the equilibrium distribution functions (EDF). The EDF of improved SP model is the same as that of the standard LBM. However, EDF of includes explicitly the porosity of the porous medium. From the discussion above, it is concluded that the DDF LBM is superior to the original and improved SP models, which were proved to be not suitable for flows with high Reynolds numbers and Darcy numbers.

3.3 Temperature Field

In the original Double Distribution Function Lattice Boltzmann Methods (DDF LBM) for convection heat transfer in a fluid medium, the evolution of the temperature field is described by another LBE of a temperature distribution function (TDF) (Guo and Zhao 2005a). Both the Equilibrium Distribution Function (EDF) and the TDF can be obtained directly from density distribution function (DF) of the Boltzmann equation (He et al. 1998).

However, for convection heat transfer in a porous medium, the TDF has to be modified due to the effect of the presence of the solid matrix. Thus the following LBE is used to describe the evolution of the temperature field (Guo and Zhao 2005a), which accounts for this influence:

$$T_i(\mathbf{x}+\mathbf{e}_i\delta_t, t+\delta_t) - T_i(\mathbf{x},t) = -\frac{1}{\tau'}\left[T_i(\mathbf{x},t) - T_i^{eq}(\mathbf{x},t)\right] \tag{3.28}$$

where T_i is the temperature distribution function, τ' is the dimensionless relaxation time and T_i^{eq} is the equilibrium temperature distribution function which is defined as:

$$T_i^{eq} = w_i T\left(1+\frac{\mathbf{e}_i\cdot\mathbf{u}}{c_s^2}\right) \tag{3.29}$$

where w_i is the weights coefficient parameter and c_s is the sound speed. The values of these parameters are the same as those of GLBE for the velocity field. Through the TDF, the temperature T of the system is defined as

$$\sigma T = \sum_i T_i \tag{3.30}$$

where σ is the heat capacity ratio.

Apparently, both the EDF of the present model and definition of temperature depends on the heat capacity ratio σ. σ accounts for the influence of the presence of porous medium on the temperature field. It is known that, the presence of the medium also affects the relaxation time parameter τ', which relates to the effective thermal diffusivity α_m.

Here, similarly, the Chapman-Enskog expansion is used to derive the temperature equation of Equation (3.3) from the new LBE of Equation (3.28) by Guo and Zhao (2005a). Before starting the derivation, the multi-scaling expansions are first introduced as:

$$T_i = T_i^{(0)} + \lambda' T_i^{(1)} + \lambda'^2 T_i^{(2)} + \cdots \tag{3.31}$$

$$\frac{\partial}{\partial t} = \lambda' \frac{\partial}{\partial t_1} + \lambda'^2 \frac{\partial}{\partial t_2} \quad \nabla = \lambda' \nabla_1 \tag{3.32}$$

where λ' here is a small expansion parameter proportional to the Knudsen number $Kn = \frac{\lambda'}{L}$, where λ' is the molecular mean free path and L the characteristic length of the fluid system.

The equations in the consecutive order of the parameter λ' is obtained by expanding the temperature term after collision, $T_i(\mathbf{x} + \mathbf{e}_i \delta_t, t + \delta_t)$ of Equation (3.28) about $\mathbf{x}$ and t; and applying the multi-scaling expansions of Equation (3.31) and Equation (3.32) to obtain the resulting equation as follows:

$$O\left(\lambda'^0\right): T_i^{(0)} = T_i^{(eq)} \tag{3.33}$$

$$O\left(\lambda'^1\right): D_{1i} T_i^{(0)} = \frac{1}{\tau' \delta_t} T_i^{(1)} \tag{3.34}$$

$$O\left(\lambda'^{2}\right):\frac{\partial T_i^{(0)}}{\partial t_2}+D_{1i}\left[\left(1-\frac{1}{2\tau}\right)T_i^{(1)}\right]=\frac{1}{\tau'\delta_t}T_i^{(2)} \tag{3.35}$$

where $D_{1i}=\dfrac{\partial}{\partial t_1}+\mathbf{e}_i\cdot\nabla_1$

From Equation (3.29) and Equation (3.30):

$$\sum_i T_i^{(m')}=0 \quad \text{for } m'>0 \tag{3.36}$$

Therefore, through moments of Equation (3.34) and Equation (3.35), the macroscopic equations at two different time scales, t_1 and t_2, could be derived where $t_1=\lambda' t$ and $t_2=\lambda'^{2}t$:

$$\frac{\partial(\sigma T)}{\partial t_1}+\nabla\cdot(\mathbf{u}T)=0 \tag{3.37}$$

$$\frac{\partial(\sigma T)}{\partial t_2}+\nabla_1\cdot\left[\left(1-\frac{1}{2\tau'}\right)\mathbf{q_1}\right]=0 \tag{3.38}$$

where $\mathbf{q_1}=\sum_i \mathbf{e_i}T_i^{(1)}$.

Use some standard algebraic manipulations to $\mathbf{q_1}$ (Guo and Zhao 2005a):

$$\mathbf{q_1}=-\tau'\delta_t\left[\frac{\partial(\mathbf{u}T)}{\partial t_1}+c_s^2\nabla_1(\sigma T)\right] \tag{3.39}$$

And the non- dimensional form of the terms in the brackets of Equation (3.39) can be written as:

$$\frac{UT_0}{t_0}\frac{\partial \mathbf{u}'T'}{\partial t_1'}+\frac{c_s^2T_0}{L}\nabla_1'(\sigma T') \tag{3.40}$$

where U, T_0, t_0, and L are the characteristic velocity, temperature, time, and length of the fluid flow system, respectively. For incompressible flows in the model, the Mach

number Ma is less than 1.0 (Guo and Zhao 2005a). Therefore, when the flow varies slowly (i.e. $t_0 = \frac{L}{c_s}$), the first term the term $\frac{\partial(\mathbf{u}T)}{\partial t_1}$ must be very small compared with $c_s^2 \nabla_1 (\sigma T)$ of Equation (3.39) and thus it is negligible. In this case, when

$$\frac{U}{c_s}\frac{L}{c_s t_0} = Ma\frac{L/c_s}{t_0} << 1.0 \tag{3.41}$$

the term $\frac{\partial(\mathbf{u}T)}{\partial t_1}$ and its non-dimensional form $\frac{UT_0}{t_0}\frac{\partial \mathbf{u}'T'}{\partial t_1'}$ will be negligible.

Consider the conditions when σ varies slowly in space, the equation at the t_2 time scale ($t_2 = \lambda'^2 t$) can be rewritten as

$$\frac{\partial(\sigma T)}{\partial t_2} = \nabla_1 \cdot (\alpha_m \nabla_1 T) \tag{3.42}$$

where

$$\alpha_m = \sigma c_s^2 \left(\tau' - \frac{1}{2}\right)\delta_t \tag{3.43}$$

Combining the equations at the time scales of t_1 and t_2, the temperature equation can finally be obtained as follow:

$$\frac{\partial(\sigma T)}{\partial t} + \nabla \cdot (\mathbf{u}T) = \nabla \cdot (\alpha_m T) \tag{3.44}$$

In the incompressible limit, Equation (3.44) could reduce to the temperature Equation, Equation (3.3), with further assumption that σ does not vary with time.

In DDF LBM, the velocity field and the temperature field of the fluid system are coupled by using two Lattice Boltzmann Equations (LBE) for the velocity and temperature fields. The effect of temperature to the fluid flow not only lies in the forcing

term F_i which is defined by Equation (3.17), but also in the fluid velocity **u** and **v** in Equation (3.20) and Equation (3.21), respectively (Guo and Zhao 2005a). Meanwhile, the velocity field affects the temperature field obviously through the equilibrium temperature distribution function T_i^{eq} defined by Equation (3.29).

As discussed before, the DDF LBM is supposed to have better numerical stability than the MS model. This is because Multispeed (MS) model uses a single density distribution function and a larger set of discrete velocities in its model (Guo and Zhao 2005a). In fact, in a LBE for fluid flow in a plain medium as discussed by Lallemand et al. (2003), a single density distribution function and a larger set of discrete velocities will suffer from serious numerical instability. This is due to the algebraic coupling between the viscous mode and the energy mode of the evolution operator of the system.

When simulating the temperature field with an isothermal LBE, and dealing with the macroscopic energy equation with other numerical techniques; the drawbacks of algebraic coupling may be avoided. In the DDF LBM, this idea is totally reflected as simulating the flow field by the GLBE for isothermal flow through porous media, and dealing with the temperature field by another LBM which serves as an independent numerical solver. Thus the DDF LBM is supposed to be more stable numerically.

Like standard LBMs, the stability of the DDF LBM also depends on other factors, such as the viscosity, diffusivity, and boundary conditions. Particularly, when the effective viscosity ν_{eff} is too small (i.e. $\tau \to 0.5$ as $\nu_e = c_s^2 (\tau - 0.5)\delta_t$), the numerical instability of the LBE of the velocity field, Equation (3.16), will happen. Similarly for the LBE of the temperature field, Equation (3.28), will suffer from numerical instability (Guo and Zhao 2005a) when the effective diffusivity α_m is too small (i.e. $\tau' \to 0.5$ as

$\alpha_m = \sigma c_s^2\left(\tau' - \frac{1}{2}\right)\delta_t$). Additionally, for the temperature field, when the Prandtl numbers are too large or too small, the instability for heat transfer problems may also occur.

The accuracy and efficiency of the DDF LBM can also be evaluated. The LBEs of the velocity field, Equation (3.16), can be considered as a special finite-difference scheme of one continuous Boltzmann equation. It is a first-order upwind finite difference scheme along the characteristic line of the fluid system. As discussed by Guo and Zhao (2002d), the LBE Equation (3.16) of the velocity field has second order accuracy in both space and time by including the first order numerical error into the physical viscosity. Similarly, the spatial temporal accuracy of the Lattice Boltzmann Equation (3.28) of the temperature field also has second order by including the first order numerical error into the physical thermal diffusivity. Thus, the overall accuracy of the DDF LBM should have second order spatial and temporal accuracy.

Besides the truncated errors of the DDF LBM, there is a compressible error between the GLBE and the generalized Navier-Stokes equations given by Equation (3.1-3.3). The compressible error is just like the one in the standard LBE for fluid flows in a plain medium which is due to replacing the LBM solvers Equations (3.24), (3.25) and (3.44), instead of the true governing Equations (3.1-3.3) respectively. However, some ‘‘incompressible’’ GLBEs can be used to reduce compressible error partially, as done by Guo et al. (2002a).

Finally, the efficiency of the DDF LBM is considered. For an isothermal fluid flow in a plain medium, the efficiency of the GLBE in DDF LBM has been proved to be the same as the standard LBE’s (Guo and Zhao 2005a). The above argument is based on

the fact that all the evolution equations, the EDFs, and the definitions of macroscopic variables are very similar to those of the standard LBE.

3.4 Boundary Conditions

3.4.1 General

For concept understanding, the infinite domains are introduced in the previous chapters; however, special treatments should be paid for the dynamics on boundaries by defining boundary conditions for physical experiments of finite domains. Numerically, appropriate treatments of boundaries are able to accommodate not only the Dirichlet and Neumann boundary conditions, but also accommodate some complicated boundaries.

There are many boundary conditions discussed by Chen and Doolen (1998). The most widely used and simple one is the bounce-back boundary condition. An alternative scheme is proposed by Skordos (1993), and is implemented initial and boundary conditions of LBM to include velocity gradients in the equilibrium distribution function at a wall boundary node from the fluid variables there. The bounce-back boundary condition is extended by He and Zou (1995) for the non-equilibrium distribution to the two dimensional LBGK model simulation by analytically modeling a simple flow in a two dimensional channel. Takaji et al. (1995) suggested using a counter slip velocity instead of a slip velocity in the lattice Boltzmann simulations. A simple extrapolation scheme was proposed by Chen et al. (1996) with a dynamical evolution of the LBGK on boundary nodes for simulating a lattice Boltzmann boundary condition.

All the boundary conditions mentioned above are used to deal with the flat walls, by defining the unknown conditions which come from the solid boundaries. Recently, some treatments of curved boundaries and off lattice boundaries have been discussed. Depending on the simulation of curved boundaries, the approximation by series of stairs reduces its numerical accuracy. Detailed discussions of the curved boundary condition

are given by Filippova and Hänel (1998b), Mei et al. (1999) and Filippova and Succi (2001).

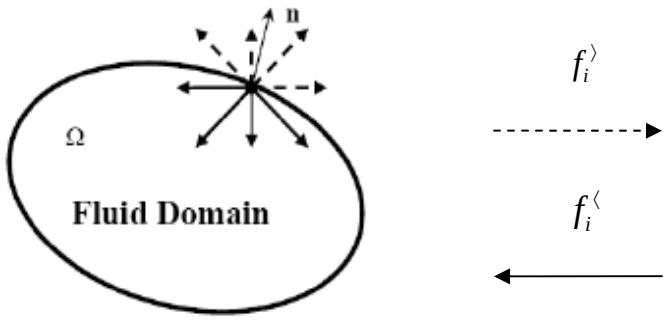

Figure 3.1 Sketch of the boundary conditions from Shu (2004)

Generally speaking, the task of boundary conditions on the LBM models is finding an appropriate relation between the incoming distribution functions $f_i^{\langle}$ which is unknown and the outgoing distribution functions $f_i^{\rangle}$ which is already known (Shu 2004). From Figure 3.1, a fluid flow is considered in closed domain Ω confined by a surrounding boundary ∂Ω. The outgoing $f_i^{\rangle}$ and incoming $f_i^{\langle}$ functions are defined at a boundary site **x** at time **t** as

$$\mathbf{e}_i \cdot \mathbf{n} > 0 \text{ and } \mathbf{e}_i \cdot \mathbf{n} < 0 \tag{3.45}$$

where **n** means the outward vector of the boundary element normal to the boundary wall centered in **x**. The expression of Equation (3.45) can be expressed as a linear integral equation mathematically (Shu 2004) as follows

$$f_i^{\langle}(\mathbf{x}) = \sum_y \sum_j \Pi_{ij}(\mathbf{x}-\mathbf{y}) f_j^{\rangle}(\mathbf{y}) \tag{3.46}$$

where $\prod_{ij}(\mathbf{x}-\mathbf{y})$ is the kernel of the boundary operator extending over a finite of values **y** inside the computation domain. The boundary operator of Equation (3.46) stands for the relationship between the fluid particles and the boundary. Consistent with Figure 3.1, the boundary conditions could be taken as special collisions between the fluid particles and the boundaries.

3.4.2 Bounce-Back Condition

The bounce back boundary condition is the simplest boundary condition. It means that a fluid particle streams to a boundary site and simply reverses the direction of its velocity to the point it comes from (Shu 2004). The bounce-back rule is widely used because of its simple implementation and its generality, since any wall orientation and border shape could be treated in the same way. Hence:

$$f_i^{\langle}(B) = f_i^{\rangle}\left(\overline{B}\right) \tag{3.47}$$

where $f_i^{\rangle}$ is a fluid particle streaming to the boundary and $f_i^{\langle}$ is a fluid particle scattering back from the boundary site; B and $\overline{B}$ denote directions opposite to each other. Note that the collision process does not occur at the boundary with this boundary condition.

In the D2Q9 LBM, considering the direction along the vertical axis, on the bottom wall as shown in Figure 3.2, Equation (3.47) can be written in terms of the boundary kernel (Shu 2004), Equation (3.46), as follows:

$$\begin{bmatrix} f_2^{\langle} \\ f_3^{\langle} \\ f_4^{\langle} \end{bmatrix} = \begin{pmatrix} 1 & 0 & 0 \\ 0 & 1 & 0 \\ 0 & 0 & 1 \end{pmatrix} \begin{bmatrix} f_6^{\rangle} \\ f_7^{\rangle} \\ f_8^{\rangle} \end{bmatrix} \tag{3.47}$$

The complete reflection guarantees that both tangential and normal components of the wall fluid speed vanish identically, as any fluid particle streaming to the nodes of the boundary with a given velocity scatters back with the opposite velocity. Thus, the balance is null and the mass and momentum conservation on the boundary can be obtained.

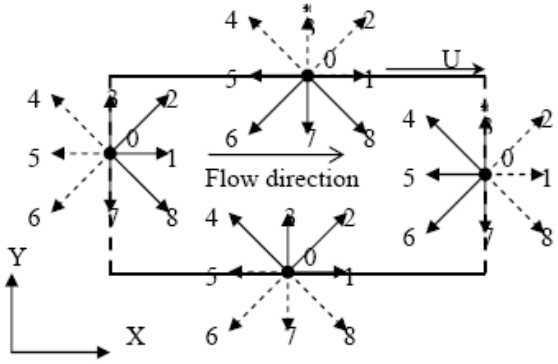

Figure 3.2 Sketch of wall boundary conditions for D2Q9 Model from Shu (2004)

Here, it is better to indicate how and when the velocity at the boundary is measured. Usually the velocity is measured at the boundary before the streaming process, which is the velocity at the boundary after the application of the boundary condition and the collision rules.

In LBM, the operations of bounce back yield the mass conservation and zero velocity condition on the wall boundaries. It is very simple compared with other numerical approaches. This is one of the reasons why the LBM is one of the ideal models to simulate fluid flows in fluid flows through porous media.

3.4.3 Periodic Condition

The periodic boundary condition is an important technique in a molecular dynamics simulation. This boundary condition is suitable for a simulation consisting of only a few hundred particles which behave as if the size is infinite. It is used to remove the effects of the surface which determines the internal structure of the computation domain, such as the surface tension.

Thus the practical implementation of the periodic boundary conditions for LBM simulation would be written as:

$$f_i^{<}(B_1) = f_j^{>}(B_2) \tag{3.48}$$

$$f_i^{<}(B_2) = f_j^{>}(B_1) \tag{3.49}$$

where B_1 and B_2 means the left and right boundaries. In this case, an example is the LBM with D2Q9 model. Then consider the direction along the x axis in Figure 3.2. Thus the i and j can be obtained as follows

$$i(<, B_1) = \{1, 2, 8\} \qquad i(>, B_1) = \{5, 4, 6\} \tag{3.50}$$

$$j(<, B_2) = \{5, 4, 6\} \qquad j(>, B_2) = \{1, 2, 8\} \tag{3.51}$$

3.4.4 Non-equilibrium Extrapolation

A nonequilibrium extrapolation method was developed to implement the boundary conditions for the standard LBM (Guo et al. 2002b). The numerical results have shown good numerical stability. In this thesis, the explored boundary conditions are based on the previous non-equilibrium extrapolation method to the LBM for thermal fluid flows in porous media.

In this thesis, it is assumed that x_b is a lattice node on the boundary and $\mathbf{x}_f$ is its nearest neighboring node in the fluid flow domain through the lattice link $\mathbf{e}_i$, where $\mathbf{x}_f = \mathbf{x}_b + \mathbf{e}_i\delta_t$. Thus the non-equilibrium expression of the density distribution function $f_i(\mathbf{x}_b)$ could be derived for the velocity boundary condition in case of the velocity $\mathbf{u}(\mathbf{x}_b)$ is known, while the density $\rho(\mathbf{x}_b)$ is unknown:

$$f_i(\mathbf{x}_b) - \overline{f}_i^{(eq)}(\mathbf{x}_b) = f_i(\mathbf{x}_f) - \overline{f}_i^{(eq)}(\mathbf{x}_f) \tag{3.52}$$

where the nonequilibrium distribution function of density at $\mathbf{x}_b$, $\overline{f}_i^{(eq)}(\mathbf{x}_b)$, could be specified by

$$\overline{f}_i^{(eq)}(\mathbf{x}_b) = \omega_i \rho(\mathbf{x}_f)\left[1 + \frac{\mathbf{e}_i \cdot \mathbf{u}(\mathbf{x}_b)}{c_s^2} + \frac{\mathbf{u}(\mathbf{x}_b)\mathbf{u}(\mathbf{x}_b) : (\mathbf{e}_i\mathbf{e}_i - c_s^2\mathrm{I})}{2\varepsilon c_s^4}\right] \tag{3.53}$$

where Equation (3.52) has second-order accuracy in both space and time in limit of low Mach number (Guo et al. 2002b).

Similarly, the thermal boundary conditions could be obtained through the procedures for velocities discussed above. Firstly, when the temperature on the boundary node x_b is known, the temperature distribution $T_i(\mathbf{x}_b)$ is given by

$$T_i(\mathbf{x}_b, t) - T_i^{(eq)}(\mathbf{x}_b, t) = T_i(\mathbf{x}_f, t) - T_i^{(eq)}(\mathbf{x}_f, t) \tag{3.54}$$

where $T_i^{(eq)}(\mathbf{x}_b, t)$ is defined as $T_i^{(eq)}(\mathbf{x}_b, t) = \omega_i T\left(1 + \frac{\mathbf{e}_i \cdot \mathbf{u}}{c_s^2}\right)$.

Another case is when the temperature on the boundary node $\mathbf{x}_b$ at time t, $T_i(\mathbf{x}_b, t)$ is unknown but the temperature gradient on the boundary node x_b is known. Then the temperature distribution $T_i(\mathbf{x}_b, t)$ is given by

$$T_i\left(\mathbf{x}_b,t\right)=\overline{T}_i^{(eq)}\left(\mathbf{x}_b,t\right)+T_i\left(\mathbf{x}_f,t\right)-T_i^{(eq)}\left(\mathbf{x}_f,t\right) \tag{3.55}$$

where the nonequilibrium distribution function of temperature on the boundary node $\mathbf{x}_b$, $\overline{T}_i^{(eq)}\left(\mathbf{x}_b,t\right)$ could be approximated through the expression of the equilibrium distribution function of temperature on the boundary node $\mathbf{x}_b$, $T_i^{(eq)}\left(\mathbf{x}_b,t\right)$ as following:

$$\overline{T}_i^{(eq)}\left(\mathbf{x}_b,t\right)=\omega_i\left[T_i\left(\mathbf{x}_f,t\right)-\left(\mathbf{x}_f-\mathbf{x}_b\right)\cdot\nabla T_i\left(\mathbf{x}_b,t\right)\right]\left[\sigma+\frac{\mathbf{e}_i\cdot\mathbf{u}\left(\mathbf{x}_b,t\right)}{c_s^2}\right] \tag{3.56}$$

Through the approach proposed by Guo et al. (2002b), it was shown that the temperature boundary conditions, Equation (3.54) and Equation (3.55), both have second-order accuracy in space and time. This procedure can be used in other boundary conditions.

CHAPTER 4

RESULTS AND DISCUSSION

The GLBE proposed by Guo and Zhao (2002d) is used to simulate three cases of two-dimensional problems: channel with fixed walls, channel with a moving wall, and cavity with a moving wall. These problems are studied with full and partial porous media, first without the effect of temperature. Subsequently temperature was included by using DDF LBM. This was applied to forced convection in channel with a fixed wall and then with a moving wall. Full and partial porous media are considered in the last case involving forced convection in channel with heat dissipation.

The analytical solutions are difficult to obtain for these problems, therefore in most of the cases the numerical results are compared with finite-difference solutions.

4.1 Flow in Porous Media

4.1.1 Channel with Fixed Walls

a. Full Porous Medium

The Poiseuille flow is investigated with a two-dimensional channel of length L and width H filled with a porous medium of porosity ε. The GLBE (Guo and Zhao 2002d) is implemented to simulate this problem. A constant force G along the channel direction drives the fluid, which is fully developed along the channel. Thus the stream-wise velocity in the x direction (along the channel) could be expressed as:

$$\frac{\nu_e}{\varepsilon}\frac{\partial^2 u}{\partial y^2} + G - \frac{\nu}{K}u - \frac{F_\varepsilon}{\sqrt{K}}u^2 = 0 \qquad (4.1)$$

where the boundary conditions are u(x, 0) = u(x, H) = 0. The lateral velocity component **v** is zero in the whole domain. The above equation is a nonlinear equation which is difficult to solve analytically.

In Poiseuille flow, the Reynolds number is defined as $\mathrm{Re} = \frac{Hu_0}{\nu}$ (Guo and Zhao 2002d), where the peak velocity of the flow along the centerline in the Brinkman model u_0 is defined as:

$$u_0 = \frac{GK}{\nu}\left[1 - \cosh^{-1}\left(\frac{rH}{2}\right)\right] \qquad (4.2)$$

where $r = \sqrt{\frac{\nu\varepsilon}{K\nu_e}}$

The periodic boundary conditions are implemented at the inlet and outlet boundaries of the channel. And the bounce back boundary conditions are applied to the top and bottom boundary walls. For initial conditions, the velocity field is set to be zero

at each lattice node. And the fluid flow density is set as a constant $\rho = 1.0$ at the beginning. The density distribution function f_i is set to be equal to its equilibrium $f^{(eq)}$ at t =0.

In this problem, the porosity ε is set as 0.1; Re changes from 0.01 to 100; Da varies from 10^{-6} to 10^{-2}; viscosity ratio Je is 1.0; and the relaxation time τ is set to be 0.8 in the simulation with 64 x 64 lattice nodes. Then the results are investigated with different porosity ε from 10^{-3} to 1.0. To solve Equation (4.1), a second-order finite difference scheme is used with a uniform mesh of size 1000 in the y direction (along height of the channel), 1000 mesh size in the x direction and the boundary condition is implemented as u(x,0) = u(x,H) = 0. And the top channel and bottom channel boundaries are input as u(0,y)=u(L,y)=0. Because there is the external force to drive the flow in the channel, it is proper to input the inlet and outlet velocity as 0. For vertical velocity **v**, all the velocity is input as 0. All results are benchmarked with Guo and Zhao (2002d) with the same parameters initially. The comparison results agree well with their results.

The results of velocity fields with different values of Re, Da, and ε are considered and discussed. For convenience, all variables used in this section are dimensionless and they are defined as $Y = \frac{y}{H}$ and $U = \frac{u(x,y)}{u_0}$. Non-dimensional results of the GLBE are compared with the finite difference results in Figure 4.1-4.4. It is confirmed that the horizontal velocity component **u** is uniform along the channel as the flow reaches its steady state, while the vertical velocity component v is much smaller with magnitude of order $O(10^{-12})$ in the whole domain (Guo and Zhao 2002d).

In Figure 4.1, the results of mesh size 256 x 256 are compared with the results of mesh size 64 x 64, when Da = 10^{-5} and ε = 0.1 and Re = 10.0. And it is shown that the results are very close and agree well when the convergence criteria are set to be 10^{-6} .Therefore, it is used mesh size of 64 x 64 with the same accuracy as 256 x 256.

The CPU time of LBM comparing with the FD method is confirmed that the CPU time of LBM will improve 1.87 times without the parallelized computation when Da = 10^{-5} and ε = 0.1 and Re = 10.0, mesh size is 256 x 256. With the computer IBM T43, Intel Pentium M processor 1.86 GHz, 782 MHz, 512 MB of RAM. If future optimization of the LBM program taken, the efficiency will be improved further. Some articles show that the efficiency of CPU time could be improved to 2.17 times than that of the finite difference method. (Satofuka and Nishioka, 1999)

In Figure 4.2, the reference velocity of non-dimensional results is the peak velocity u_0 of different Re, obtained from Equation (4.2). It is seen that for Curve F (Re = 0.01), the maximum velocity from the GLBE is equal to u_0 (Equation 4.2 from Brinkman model). When Re increases, the velocity profile is similar but its magnitude increases because u_0 is higher. However the non-dimensional peak-velocity from GLBE is less than unity (for example, curve A for Re = 100 in Figure 4.1), because u_0 from Brinkman model is higher for high Re, i.e. Re > 0.1, due to neglect of the non linear effects (Guo and Zhao 2002d). The discrepancies are higher when Re is large. The results confirmed that the nonlinear drag force due to the porous medium is significant in GLBE simulation in flows of high Re. The results also show that when Re or Da is very large, the non-linear effect will become more significant. In this case, if using the Brinkman

model, the results of velocities **u** will be larger than the actual velocities. Brinkman model can be used when Da and Re are not big.

Figure 4.3 indicates that Darcy number Da affects the curve shape as well as the magnitude. When Da increases, the curve shape becomes more parabolic. This is due to the effect of permeability K. From the definition of Darcy number $Da = \frac{K}{L^2}$, when it increases, the permeability is high, and thus the porous medium behaves more like a free domain with the velocity profile becoming more parabolic. However, curves A and B show that the peak velocity does not reach unity. This is because the peak velocity from GLBE is lower than the reference velocity u_0. The results confirmed that when Da is high, the effect of nonlinear drag due to the porous medium is still important (Guo and Zhao 2002d). Even though the permeability K is higher when Da increases, the velocity is also higher making the non-linear term (second term of Equation 3.5) higher.

From Figure 4.4, it is shown that the porosity ε also affects the peak velocity and the curve shape. When ε decreases, the curve shape is close to parabolic and the peak velocity decreases too. When ε is very small (i.e. 10^{-2}), the non-linear drag effect is higher, which makes the peak velocity from GLBE less than the reference velocity u_0 from Brinkman model without the Forchheimer term. The influence of porosity ε was not investigated by Guo and Zhao (2002d).

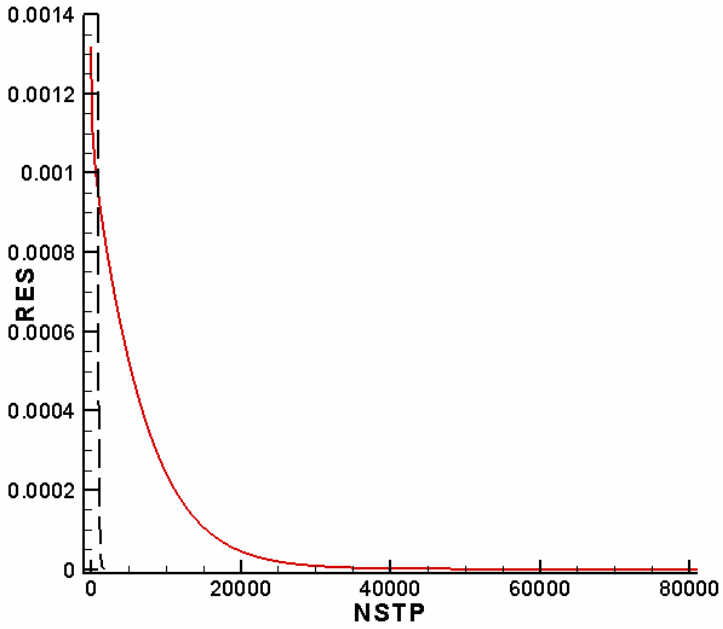

Figure 4.1 Grid independence study of velocity in channel with full porous medium for Da = 10^{-5} and ε = 0.1 and Re = 10.0 with different mesh size. Dashed lines: 64 x 64. Solid line: 256 x 256.

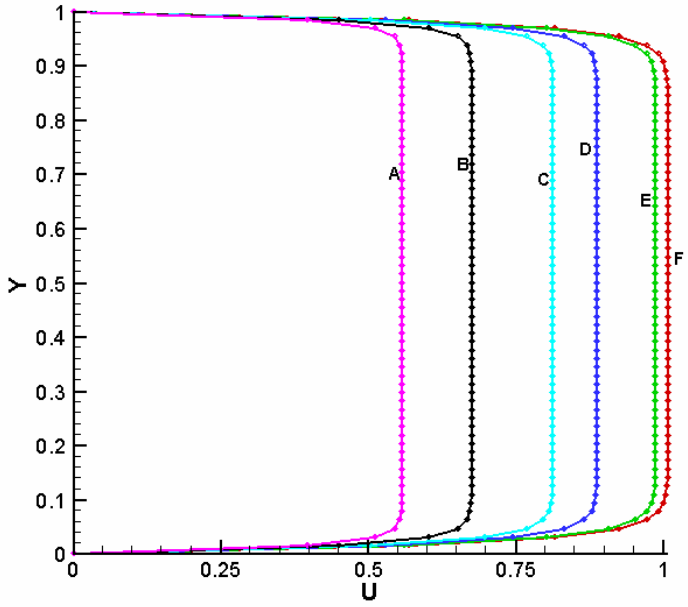

Figure 4.2 Velocity profile in channel with full porous medium for Da = 10^{-5} and ε = 0.1 at different Re. Solid lines: GLBE. Symbols: finite difference. A: Re = 10^{2}, B: Re = 50.0, C: Re = 20.0, D: Re = 10.0, E: Re = 1.0 and F: Re = 10^{-2}.

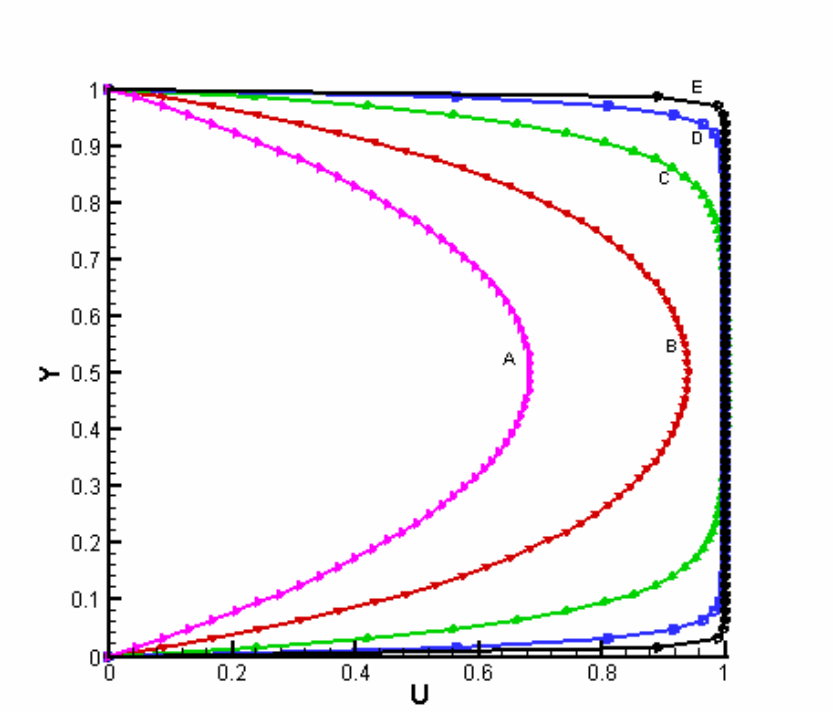

Figure 4.3 Velocity profile in channel with full porous medium for Re = 0.1 and ε = 0.1 at different Da. Solid lines: GLBE. Symbols: finite difference. A: Da = 10^{-2}, B: Da = 10^{-3}, C: Da = 10^{-4}, D: Da = 10^{-5} and E: Da = 10^{-6}.

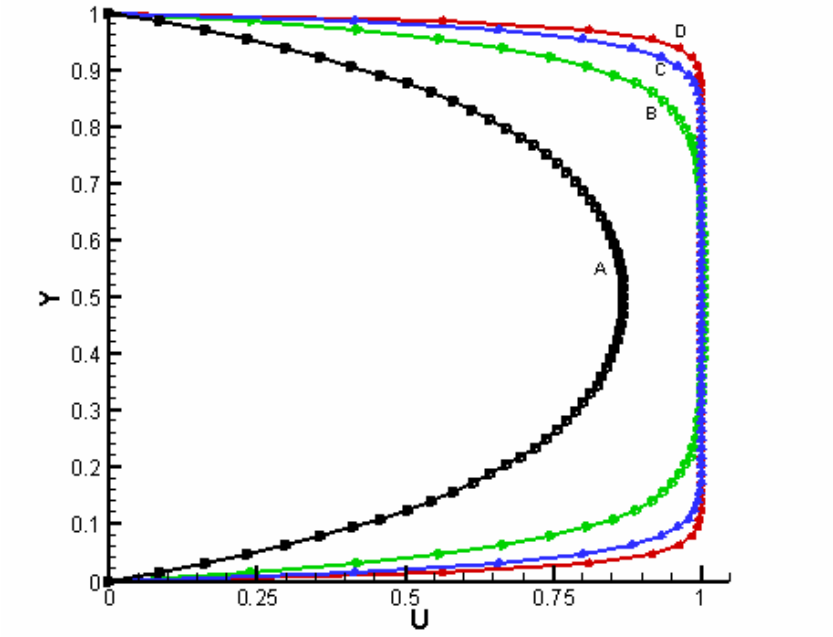

Figure 4.4 Velocity profile in channel with full porous medium for Da = 10^{-4} and Re = 0.1 at different ε. Solid lines: GLBE. Symbols: finite difference. A: ε = 10^{-2}, B: ε = 0.1, C: ε = 0.4 and D: ε = 0.99.

b. Partial Porous Medium

The GLBE is also applied to a channel of length L and width H, partially filled with porous medium. That means there is a porous layer for $0 \le y < \frac{H}{2}$, and an adjacent fluid region for $\frac{H}{2} \le y \le H$. The traditional modeling approach is to treat it as a two domains problem with appropriate boundary conditions at the fluid and porous interface. The interface problem has been reviewed in the field of transport in porous media (Kaviany 1995 and Nield et al. 1998).

The two domain approach was proposed to solve this problem with the assumption that the saturated porous region is homogeneous, the flow is steady and incompressible, and inertia effects in all domains are neglected (Goyeau et al. 2003). In this model the Brinkman equation is applied in the porous layer, and the Stokes equation in the fluid region. If the shear stress and velocity at the interface of fluid and porous medium are continuous (Neale et al. 1974), the analytical solution of the two-domain model is determined by

$$u(y) = U(-y)\left\{ \frac{\left(1+2Je\sqrt{Da}\right)}{2\left(Da+Je\sqrt{Da}\right)} + \frac{\sqrt{Je}}{Da}\frac{\left(1-2Da\right)}{2\left(\sqrt{Da}+\sqrt{Je}\right)}y - \frac{y^2}{2Da} \right\} \quad (4.3)$$

$$u(y) = U(-y)\left\{ 1 + \frac{1-2Da}{2\left(Da+\sqrt{DaJe}\right)} \exp\left(\frac{y}{\sqrt{DaJe}} \right) \right\} \quad (4.4)$$

where Equation (4.3) is for fluid region and Equation (4.4) is for porous medium.

When using GLBE to solve this problem, the periodic boundary conditions are implemented into the inlet and outlet of the channel, Equation (3.52) is applied the upper and bottom plates. For initial conditions, the velocity field is set to be zero at each lattice.

The fluid flow density is set to be a constant $\rho = 1.0$ at the beginning. The density distribution function f_i is set to equal to its equilibrium $f^{(eq)}$ at t = 0. The porosity ε is set as 10^{-3} at first; Re changes from 1.0 to 50; Da varies from 10^{-5} to 10^{2}; Je is 1.0; and the relaxation time τ is set to be 0.8 in the whole procedure of simulation with 64 x 64 lattice nodes. Then the results with different porosity ε from 10^{-4} to 0.1 are investigated. The numerical results of the GLBE are compared with the analytical solution of the two-domain model results in Figure 4.5 to 4.7. For convenience, all variables used in this section are dimensionless and they are defined as $Y = \frac{y}{H}$ and $U = \frac{u(x,y)}{u_{\max}}$, where $u_{\max}$ is the peak velocity of the flow. It is shown that the results of GLBE agree well with the analytical solution. This verifies the GLBE which deals with the interface between different media without any special treatments for the boundary conditions at the interface (Guo and Zhao 2002d).

Figure 4.5 shows that when Da varies, the curve shape changes very much. As Da increases, there is less flow in the fluid medium region, and the velocity at the interface increases. This is because when Da is large, according to the definition of Darcy number, the permeability K is large; therefore the velocities in porous medium and at interface both increases. Different Da have been investigated by another method, the two domain approach by Goyeau et al. (2003), in which porous medium flow is solved using the Brinkman Equation and the free domain using Stokes Equation. The analytical solutions were compared by Goyeau et al. (2003) with experiment results, but in these studies there is little discussion on the influence of Re and ε. In this thesis, GLBE is used as another method to simulate the problem and discuss the influence of different Re and ε.

In Figure 4.6a the reference velocity is the velocity u_0 obtained from the definition of $\mathrm{Re} = \frac{Hu_0}{\nu}$. The non dimensional results show that when Re increase, the magnitude of velocity increases in both porous and fluid media. The ratio of peak velocity to reference velocity u_0 is higher when Re is larger because more flow passes through the fluid medium. In Figure 4.6b the reference velocity is the maximum velocity which is different for different Re. It shows that a higher proportion of the flow goes to the fluid medium.

Figure 4.7 indicates the effect of porosity ε on the flow velocity. When ε is near to 1.0, the result behaves like generalized Poiseuille flow without porous media effect. In limit of high porosity ε, the velocity profile in the fluid region seems close to a parabolic curve, but velocity-gradient in the porous medium changes greatly to match that of the fluid medium. The results of other methods, single and two domain approaches, also confirmed a change of shear gradient at the interface which is more obvious when ε is small (Goyeau et al. 2003). Also the interface velocity is smaller at smaller porosity. This is because when ε is large, more flow will pass through the porous medium because of less drag in the porous medium. Therefore, with a larger porosity ε , the velocity at interface is larger and the change in velocity gradient is less abrupt.

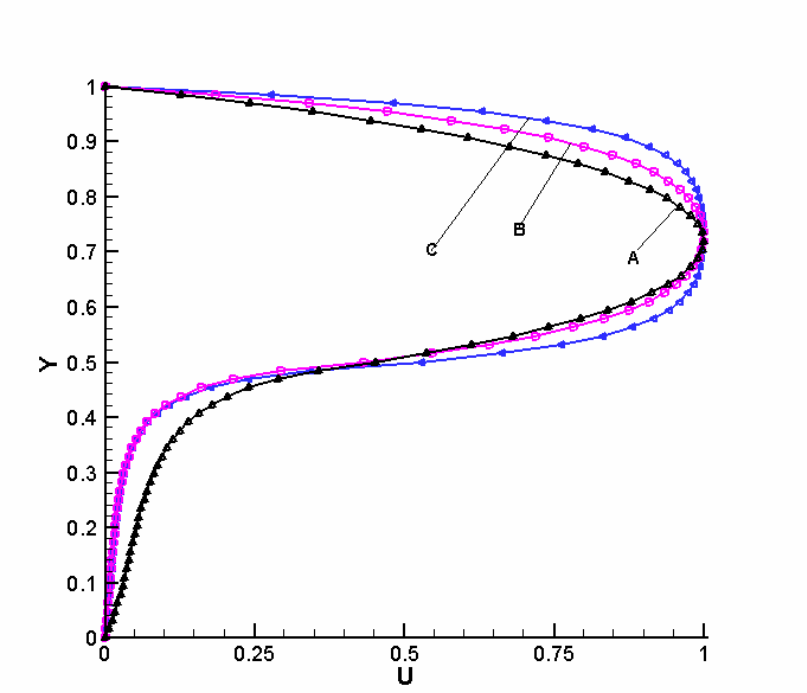

Figure 4.5 Velocity profile in channel with partial porous medium for Re = 10.0 and ε = 10^{-3} at different Da. Solid lines: GLBE. Symbols: analytical solution. A: Da = 1.0, B: Da = 10^{-2}, and C: Da = 10^{-3}.

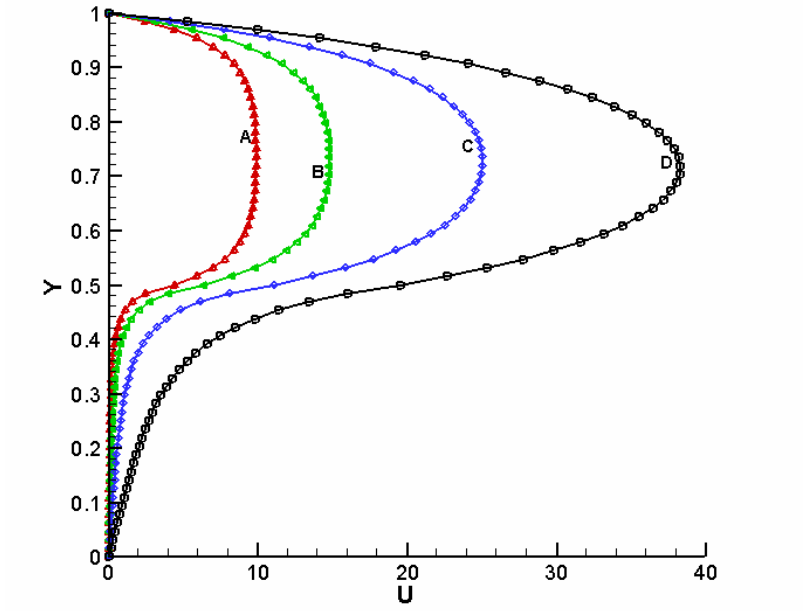

Figure 4.6a Velocity profile in channel with partial porous medium for Da = 10^{-2} and ε = 10^{-3} at different Re. Solid lines: GLBE. Symbols: analytical solution. A: Re = 1.0, B: Re = 5.0, C: Re = 20.0, D: RE = 50.0.

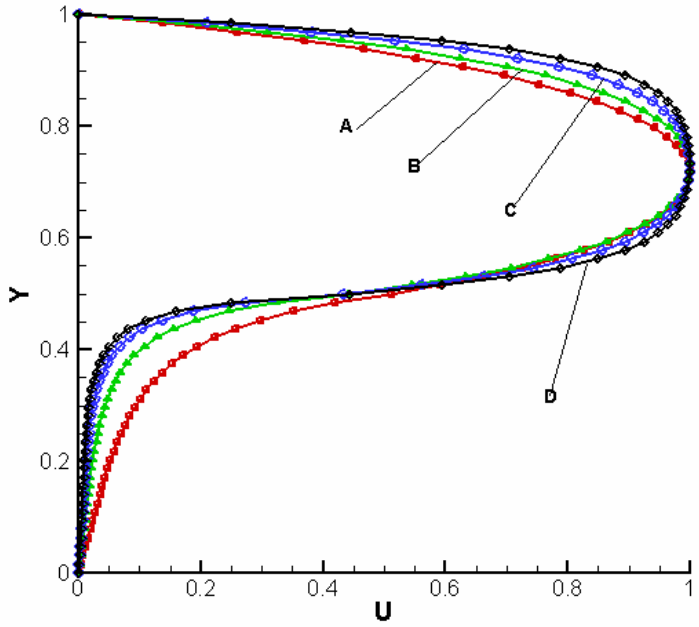

Figure 4.6b Velocity profile in channel with partial porous medium for Da = 10^{-2} and ε = 10^{-3} at different Re. Solid lines: GLBE. Symbols: analytical simulations. A: Re = 1.0, B: Re = 5.0, C: Re = 20.0, and D: RE = 50.0.

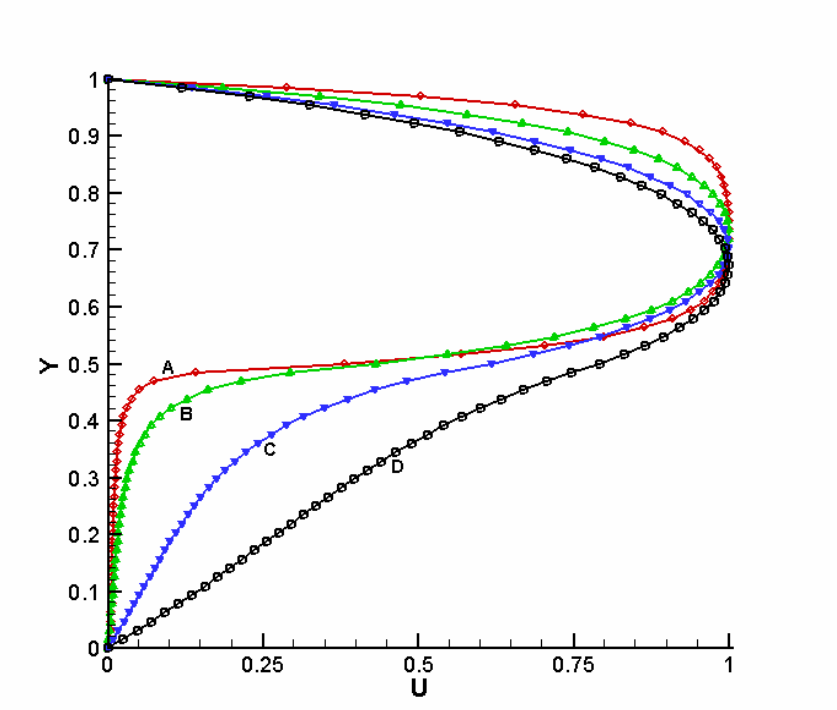

Figure 4.7 Velocity profile in channel with partial porous medium for Da = 10^{-2}, and Re = 10.0 at different ε. Solid lines: GLBE. Symbols: analytical simulations. A: ε = 10^{-4}, B: ε = 10^{-3}, C: ε = 10^{-2}, and D: ε = 5.0x10^{-2}.

4.1.2 Channel with a Moving Wall

a. Full Porous Medium

The GLBE is also implemented to simulate the Couette flow, consisting of a channel flow of length L and width H, which is driven by the upper plate moving along the x direction (along the channel direction) with a constant velocity u_0 . The Reynolds number is defined as $\mathrm{Re} = \frac{Hu_0}{\nu}$. In steady state, the flow still follows Equation (4.1), with the boundary conditions of u(x, 0) = 0, u(x, H) = u_0.

The periodic boundary conditions are implemented into the inlet and outlet of the channel, and the non-equilibrium extrapolation boundary condition (Equation 3.52) is applied to upper and bottom plates. For initial conditions, the velocity field is set to be zero at each lattice. The fluid flow density is set as a constant, $\rho = 1.0$ in the beginning. The density distribution function f_i is set to be its equilibrium $f^{(eq)}$ at t =0.

In this problem, the porosity ε is first set as 10^{-2}; Re changes from 10^1 to 10^3; Da varies from 10^{-6} to 10^{-2}; viscosity ratio Je is 1.0; and the relaxation time τ is set to be 0.8 in the simulation with 64 x 64 lattice nodes. Then the results are investigated with different porosity ε from 0.01 to 0.99. A second-order finite difference results of Brinkman Equation (4.1) is used for comparison with GLBE solution. It is used with a uniform mesh of size 1000 in the y direction (along height of the channel), and the boundary condition is implemented as u(x,0) = u(x, H) = u_0.

The numerical results of the GLBE are shown in Figure 4.8 to 4.10. All variables used in this section are dimensionless, and they are defined as $Y = \frac{y}{H}$ and $U = \frac{u(x,y)}{u_0}$.

The results of velocity fields are presented at different values of Re, Da, and ε. It is seen that in Figure 4.8 to 4.10 the results of GLBE agree well with the analytical solutions of the finite-difference methods.

Figure 4.8 shows results of different Re from 10^1 to10^3. It is seen that when Re increases, the fluid layer near the moving plate becomes thinner. This is because when Re is large, there is more resistance to flow from the porous medium. It is also noted that the curve A of high Re seems to have lower magnitude than curve D of low Re. But the actual velocity of curve A, because of its large reference velocity, is actually much larger than curve D.

Figure 4.9 shows the numerical results when Da varies from 10^{-6} to 10^{-2}. It could be seen that, the flow layer near the moving plate becomes thicker as Da increases. Because when Da is large, the permeability of the porous medium K is large, and thus the porous-medium flow-behavior tends towards that of a free domain with the velocity profile becoming more linear. Therefore the flow layer will increase with larger Da.

Guo and Zhao (2002d) compared GLBE with simplified LBM to emphasize the importance of nonlinear effect. However, Guo and Zhao did not discuss the influence of different porosity ε, which is also very important in GLBE simulations. Figure 4.10 shows results at different porosity ε from 0.01 to 0.99. When ε is close to 1.0 (i.e. curve D), the results are like generalized Couette flow without porous medium effect. It is seen that when ε increases, the flow layer near the moving plate becomes thicker. This is because when ε is large, flow will pass through the porous medium more readily; the drag of porous medium will decrease, which leads to porous medium flow becoming

faster. Therefore, with a larger porosity ε, the velocity is larger, and the layer near the moving plate is thicker.

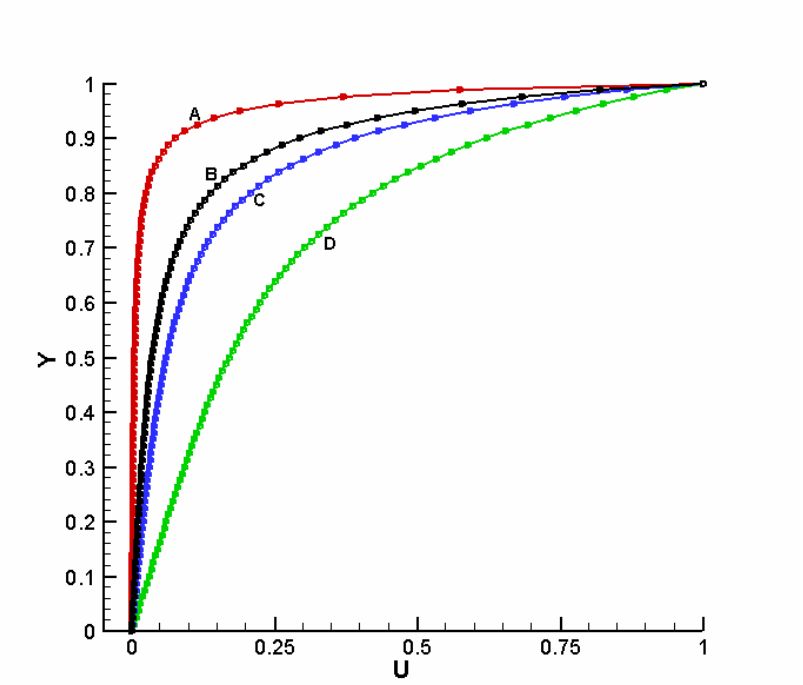

Figure 4.8 Velocity profile in channel with full porous medium for Da = 10^{-2} and ε = 10^{-2} at different Re. Solid lines: GLBE. Symbols: finite difference. A: Re = 10^3, B: Re = 10^2, C: Re = 50, and D: Re = 10.

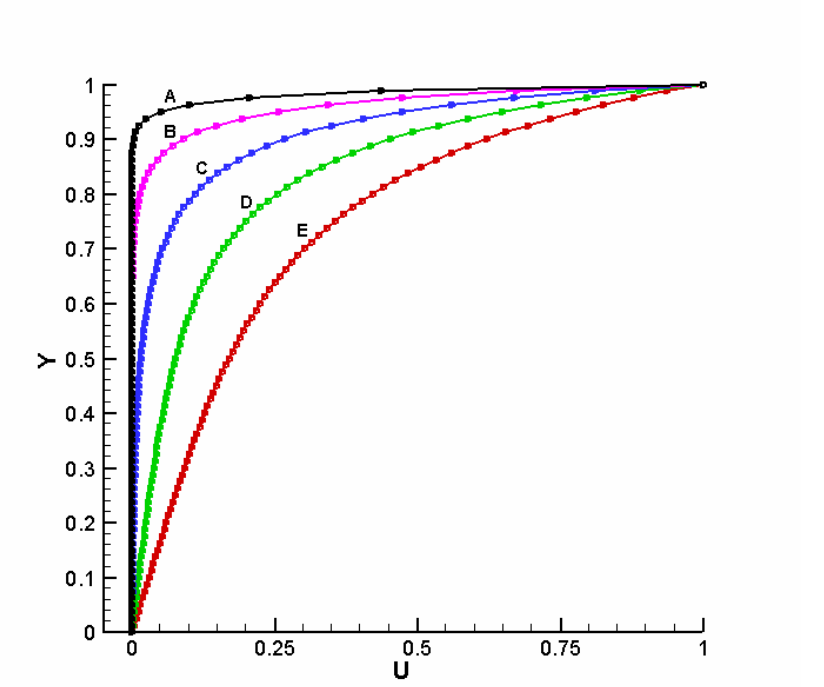

Figure 4.9 Velocity profile in channel with full porous medium for Re = 10.0 and ε = 10^{-2} at different Da. Solid lines: GLBE. Symbols: finite difference. A: Da = 10^{-6}, B: Da = 10^{-5}, C: Da = 10^{-4}, D: Da = 10^{-3}, and E: Da = 10^{-2}.

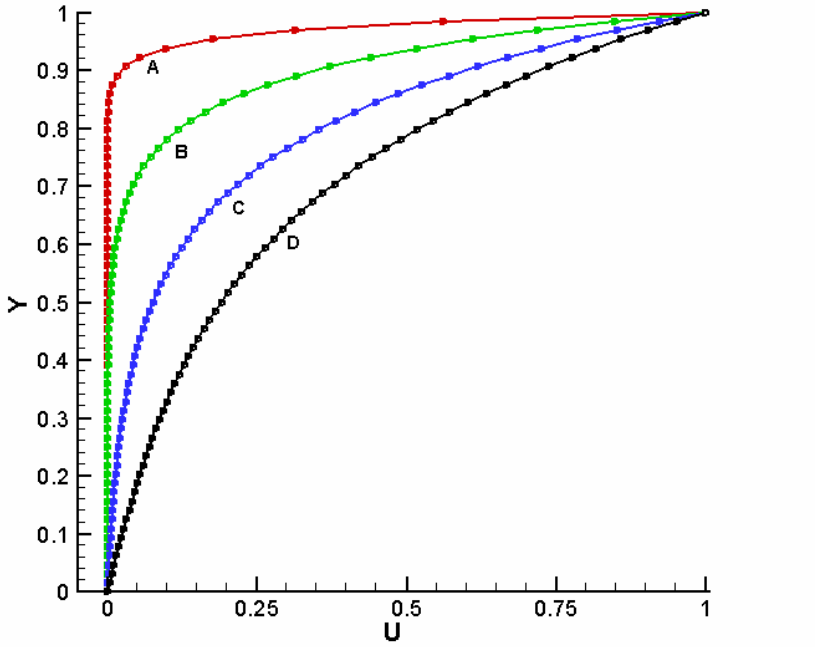

Figure 4.10 Velocity profile in channel with full porous medium for Da = 0.1and Re = 0.1at different ε. Solid lines: GLBE. Symbols: finite difference. A: ε = 0.01, B: ε = 0.1, C: ε = 0.4, and D: ε = 0.99.

b. Partial Porous Medium

Here the GLBE is applied to simulate a channel partially filled with a porous medium. It is a channel of length L and width H where the porous medium for $\frac{H}{2} < y \le H$ and an adjacent fluid region for $0 \le y \le \frac{H}{2}$. The top plate moves with a constant velocity u_0. The porosity of the porous medium in the channel is ε.

In GLBE simulation, the periodic boundary conditions are implemented into the inlet and outlet of the channel and the non-equilibrium extrapolation boundary condition of Equation (3.52) is applied to top and bottom plates. For initial conditions, the velocity field is set to be zero at each lattice. The fluid flow density is set as a constant, $\rho = 1.0$ at the beginning. Density distribution function f_i is set to equal to its equilibrium $f^{(eq)}$ at t =0. The Re is set as 10; Da is 10^{-2}; Je is 1.0, and ε is 10^{-6}. The relaxation time τ is set to be 0.8 in the simulation with 80 x 80 lattice nodes, which is recommended by Guo and Zhao (2002d). When the value of τ ranges from 0.6 to 0.8, the accuracy is approximately of second accuracy (Zhou and He 1997).

By comparison of two different Je at 1.0 and 4.0, it was confirmed the validity of GLBE in simulation of different porosity flow (Guo and Zhao 2002d). However, Guo and Zhao did not discuss the effect of different porosity. Figure 4.11 shows the results at different porosity ε from 10^{-5} to 10^{-1}. All variables used in this section are dimensionless and they are defined as $Y = \frac{y}{H}$ and $U = \frac{u(x,y)}{u_0}$. The velocity profile in fluid region in Figure 4.11 confirmed that for channel with partial porous medium, the velocity profile is linear in the fluid region (Martys et al. 1994). When the porosity ε

increases, the velocity magnitudes of both fluid region and interface increase. This is because when ε is large, more flow will pass through the porous medium; and the drag of porous medium will decrease, which leads to flow velocity in the porous medium becoming faster. Therefore, with a larger porosity ε , the velocity at interface is larger, and the velocity change is less abrupt. There is a discontinuity of velocity-gradients between interface at very small porosity (curve A in Fig 4.11).

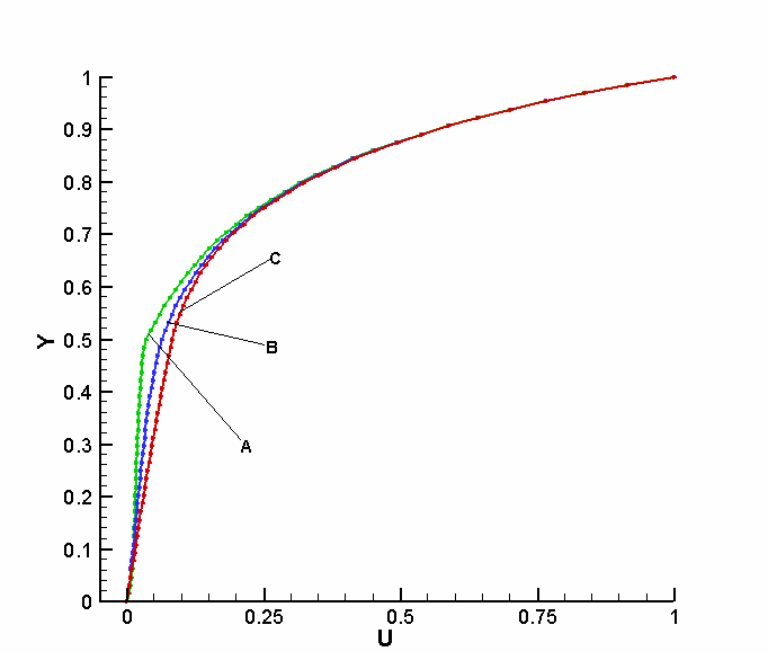

Figure 4.11 Velocity profile in channel with partial porous medium for Da = 10^{-2}, and Re = 10.0 at different ε. Solid lines: GLBE. Symbols: finite difference. A: $\varepsilon = 10^{-5}$, B: $\varepsilon = 10^{-3}$, and C: $\varepsilon = 10^{-1}$.

4.1.3 Cavity with a Moving Wall

a. Full Porous Medium

A two dimensional steady flow in a lid-driven cavity of length L and width H without porous medium is used as a benchmarking problem for many numerical schemes due to the simple geometry and interesting flow behavior (Shu 2004). In this section the GLBE is applied to the fluid flow in a square cavity with porous medium whose upper wall moves along x direction (horizontal, from left to right) with a constant velocity u_0, while the other boundaries are fixed.

The non-equilibrium extrapolation boundary condition of Equation (3.52) is implemented for velocity boundary condition to all walls. For initial conditions, the velocity field is set to be zero at each lattice. The fluid flow density is set as a constant $\rho = 1.0$ at the beginning and density distribution function f_i is set to be equal to its equilibrium at t = 0. The parameter ε is set as 0.1; Je is 1.0; Da varies from 10^{-4} to 10^{-2}; and Re changes from 5.0 x 10^{-3} to 10. The relaxation time τ is set to be 0.65 in the procedure of simulation with 64 x 64 lattice nodes.

The GLBE is applied to simulate the cavity with small viscosity and small Reynolds number. The results of GLBE are compared with the analytical results of finite difference solutions for different Da and Re in Figure 4.12 to 4.15. For convenience, all variables used in this section are dimensionless and they are defined as $X = \frac{x}{L}$, $Y = \frac{y}{H}$, $U = \frac{u(x,y)}{u_0}$ and $V = \frac{v(x,y)}{u_0}$. It is seen that the results of GLBE agree well with the solutions of the finite difference outcomes.

Figure 4.12 shows when Da increases, the flow layer near the moving lid becomes thicker, and velocity magnitudes increases. Figure 4.13 confirms that when Da increases, the recirculation velocity the cavity becomes larger. When Da is large, according to the definition of Darcy number, the permeability K is huge; therefore the velocities in porous medium increase. This result is consistent with that of Guo and Zhao (2005a) who confirmed, using different parameters, that when Da increases, the flow layer near the moving lid becomes thicker, and the recirculation flow becomes stronger.

Figure 4.14 shows when Re increases, the layer near the top moving wall becomes slightly thinner. Figure 4.15 shows that when Re increases, the recirculation flow does not change much. The flow seems to be developed at these Reynolds number range. It is also noted that the magnitude of curve A (high Re) is slightly less than that of curve C (low Re). But the actual velocity of curve A, because of its large reference velocity, is larger than curve C. Results of Figure 4.14 and Figure 4.15 indicate the similarity of velocity profile of lid-driven cavity with porous medium at different Re. The present results could not be compared with previous studies as Guo and Zhao (2002d) did not investigate the effect of Re for the lid-driven cavity with porous medium.

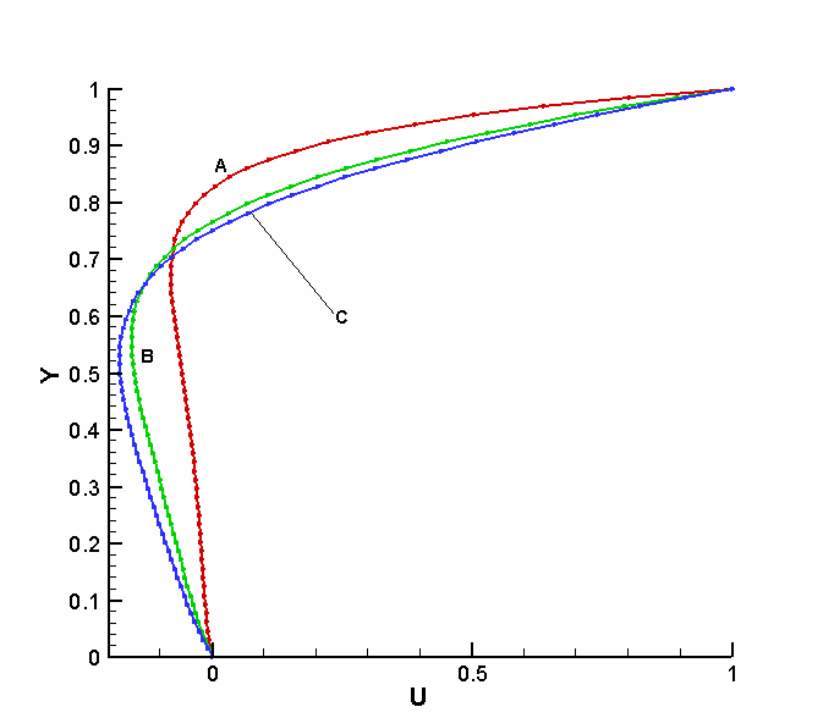

Figure 4.12 Horizontal velocity profile in cavity with full porous medium for Re=0.1, ε=0.1, and x = L/2, at different Da. Solid lines: GLBE. Symbols: finite difference. A: Da=10^{-4}, B: Da=10^{-3}, and C: Da=10^{-2}.

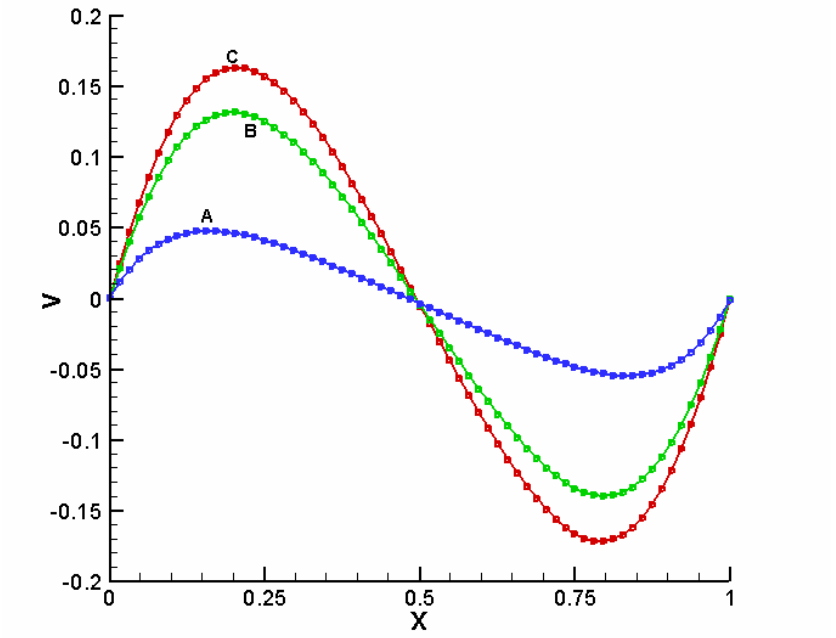

Figure 4.13 Vertical velocity profile in cavity with full porous medium for Re=0.1, ε=0.1, and y = H/2 at different Da. Solid lines: GLBE. Symbols: finite difference. A: Da=10^{-4}, B: Da=10^{-3}, and C: Da=10^{-2}.

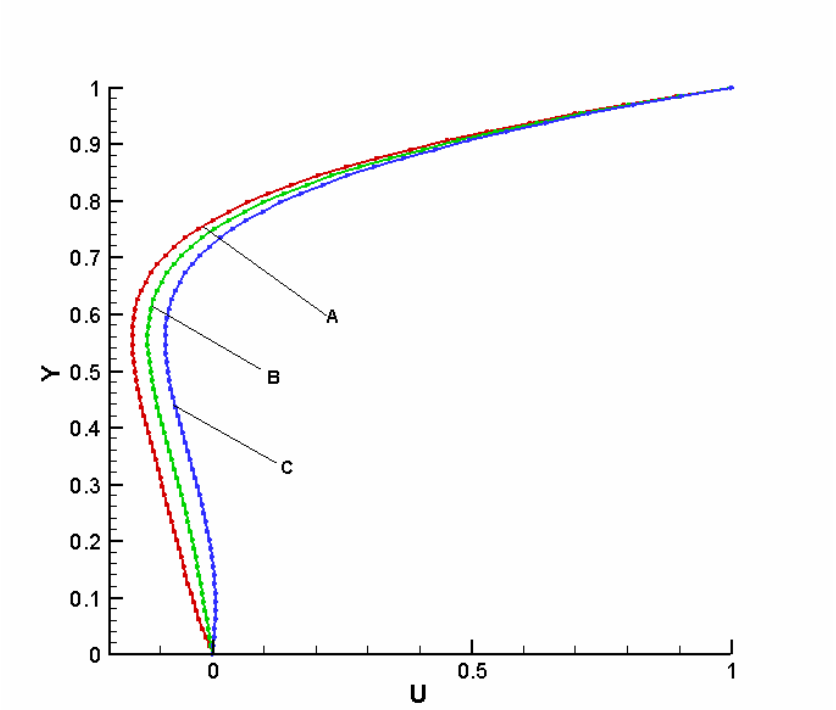

Figure 4.14 Horizontal velocity profile in cavity with full porous medium for Da=10^{-3}, ε=0.1, and x = L/2 at different Re. Solid lines: GLBE. Symbols: finite difference. A: Re=10^{-1} B: Re=10^{-2}, and C: Re=5.0x10^{-3}.

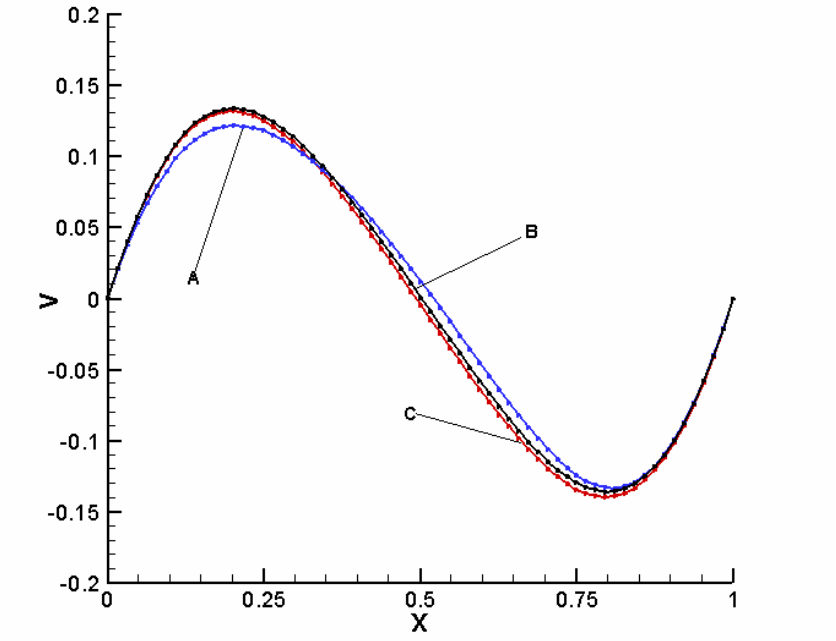

Figure 4.15 Vertical velocity profile in cavity with full porous medium for Da=10^{-3}, ε=0.1, and y = H/2 at different Re. Solid lines: GLBE. Symbols: finite difference. A: Re=10.0, B: Re=1.0, and C: Re=0.1.

b. Partial Porous Medium

The application of the GLBE is also investigated in the lid-driven cavity of length L and width H partially filled with porous medium. The fluid flow in a square cavity with porous medium whose upper wall moves from along x direction (from left to right) with a constant velocity u_0, while the rest boundaries are fixed. The porous medium lies in the cavity such that there is fluid region domain ($\frac{H}{2} < y \le H$) between the porous medium (with porosity ε for $0 \le y \le \frac{H}{2}$) and the top lid boundary.

The non-equilibrium extrapolation boundary condition of Equation (3.52) is implemented for velocity boundary conditions to all walls. For initial conditions, the velocity field is set to be zero at each lattice. The fluid flow density is set as a constant $\rho = 1.0$ at the beginning. Density distribution function f_i is set to be equal to its equilibrium at t = 0. Da is set to be 10^{-2}, Re is 10.0, and Je is 1.0. The simulation is with the relaxation time τ is set to be 0.8 in the simulation with 64 x 64 lattice nodes.

For convenience, dimensionless results used in this section are defined as $X = \frac{x}{L}, Y = \frac{y}{H}$, $U = \frac{u(x,y)}{u_0}$ and $V = \frac{v(x,y)}{u_0}$. Results of GLBE at different ε are listed in Figure 4.16, which agree well with the solutions of finite difference. It shows that the discontinuity of velocities at the interface is less obvious when ε is large. It is seen that when ε increases, the flow layer near the moving lid does not change much. This is because the porosity range is not large, and less flow pass through the porous medium.

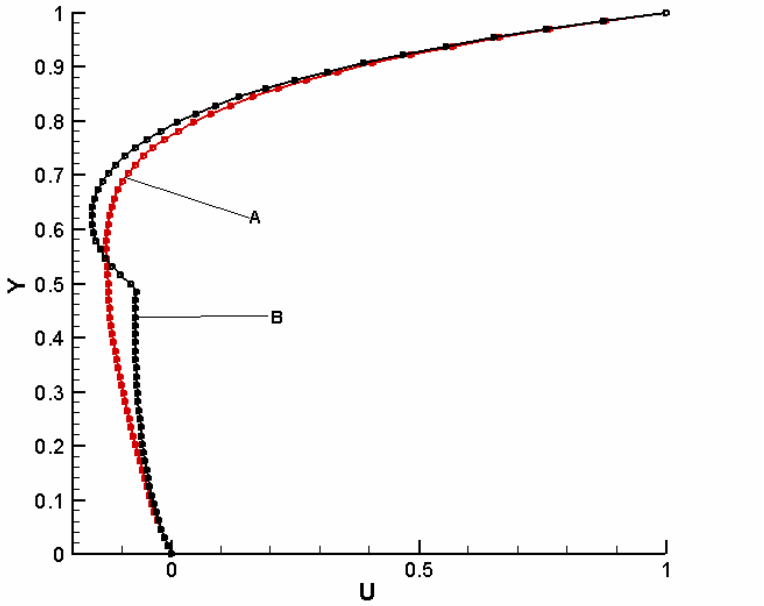

Figure 4.16 Horizontal velocity profile in cavity with full porous medium for Da = 10^{-2}, Re = 10.0, and x = L/2 at different ε. Solid lines: GLBE. Symbols: finite difference. A: ε = 0.1 and B: ε = 10^{-2}.

4.2 Forced Convection in Porous Media

4.2.1 Channel with a Moving Wall

The DDF LBM is used to simulate the channel of length L and width H which is filled with porous medium. The upper plate is cold (with temperature T_0) and moves with a constant velocity u_0. And the bottom plate is hot (with temperature T_1) with a constant normal flow of fluid injected (with velocity v_0) through the bottom. If the Forchheimer term is neglected (Guo and Zhao 2005a), the governing equations at steady state are:

$$\frac{\nu}{\varepsilon}\frac{\partial u}{\partial y} = \nu_e \frac{\partial^2 u}{\partial y^2} - \frac{\varepsilon \nu}{K} u \tag{4.5}$$

$$\frac{\partial p}{\partial y} = g\beta\left(T - T_m\right) - \frac{\nu}{K} v + a_y \tag{4.6}$$

$$v\frac{\partial T}{\partial y} = \nabla \cdot \left(\alpha_m \nabla T\right) \tag{4.7}$$

where T_m is the average temperature which is defined as $T_m = \frac{T_0 + T_1}{2}$ and a_y represents the external force in y direction (along the height of the channel) which is defined as follows:

$$a_y = \frac{\nu}{K} v_0 - g\beta\Delta T \left[\frac{\exp\left(\frac{y v_0}{\alpha_m}\right) - 1}{\exp\left(\frac{H v_0}{\alpha_m}\right) - 1} \right] \tag{4.8}$$

The governing equation of Equations (4.5 to 4.7) has analytical solution which can be expressed as

$$u = u_0 \exp\left[r\left(\frac{y}{H} - 1\right)\right] \frac{\sinh\left(\frac{\zeta \cdot y}{H}\right)}{\sinh\left(\zeta\right)} \tag{4.9}$$

$$v = v_0 \tag{4.10}$$

$$T = T_0 + \Delta T \frac{\exp\left(\frac{\mathrm{Pr}_m \,\mathrm{Re}\cdot y}{H}\right) - 1}{\exp\left(\mathrm{Pr}_m \,\mathrm{Re}\right) - 1} \tag{4.11}$$

where u_0 is the velocity of the upper moving plate; Re is the Reynolds number defined as $\mathrm{Re} = \frac{Hv_0}{\nu}$; v_0 is the velocity of the injected flow; and ΔT is the temperature difference of the system as $\Delta T = T_1 - T_0$. ζ and **r** are the parameters given respectively by Guo and Zhao (2005a) as

$$r = \frac{\mathrm{Re}}{2\varepsilon Je} \tag{4.12}$$

$$\zeta = \frac{1}{2\varepsilon Je}\sqrt{\mathrm{Re}^2 + \frac{4\varepsilon Je}{Da}} \tag{4.13}$$

The periodic boundary conditions are implemented at the inlet and outlet of the channel. The non-equilibrium extrapolation boundary conditions of Equation (3.52) and Equation (3.54) are applied for velocity and temperature boundary conditions of the upper and bottom plates. For initial conditions, the velocity field is set to be zero at each lattice. The fluid flow density is set to be a constant $\rho = 1.0$ at the beginning. The density distribution function f_i is set to be equal to its equilibrium $f^{(eq)}$. And the temperature distribution T_i is set to be equal to the equilibrium $T^{(eq)}$ at t =0.

The DDF LBM without the Forchheimer term is implemented to predict the velocity field and temperature field of the problem. The parameters σ is set as 1.0; ε is 0.7; Pr_m is 1.0; Ra is 100; Je is 1.0; τ' is set as $\tau' = 1.5 + \frac{Je(\tau - 0.5)}{\mathrm{Pr}_m \sigma}$; Re changes from

0.1 to 20; and Da varies from 10^{-3} to 1.0 and the relaxation time τ is set to be 1.25 in the simulation with 64 x 64 lattice nodes. Then the results are investigated with different porosity ε from 0.1 to 0.99.

The results of DDF LBM are also compared with the analytical results at different Re, Da, and porosity ε in Figure 4.17 to 4.20. All variables used in this section are dimensionless and they are defined as $Y = \frac{y}{H}$, $U = \frac{u(x,y)}{u_0}$ and $T = \frac{T(x,y) - T_0}{\Delta T}$. It is seen that the results of DDF LBM agree well with the solutions of the analytical solutions.

Figure 4.17 shows when Re increases, flow temperature decreases, and the thermal boundary-layer near the moving plate decreases as well. This is because when Re is large; the convection in the channel is stronger, and more heat will be taken away by the flow. Therefore, the temperature is low when Re is large.

Figure 4.18 shows the velocity layer near the moving plate becomes thinner when Re increases. This is because when Re is large, there is more resistance to flow from the porous medium. Results at different Re were discussed in Guo and Zhao (2005a), but their Da was not varied and is very small (i.e. 0.01); therefore their permeability is very small.

Figure 4.19 shows the results of temperature at different Da; it shows that there is little difference of the temperature profile when Da changes. This is because the heat transfer is vertical from bottom to top walls, at which the temperatures of both walls are fixed, and thus there is less effect from the horizontal flow.

Figure 4.20 shows the results of velocity filed at different Da, which agree well with the analytical solution. When Da increases, the flow layer near the moving plate becomes thicker and the flow velocity increases as well. Because when Da is large, the

permeability of the porous medium K is large, and thus the porous-medium flow-behavior tends towards that of a free domain with the velocity profile becoming more linear. Therefore the flow layer will increase with larger Da. The effect of Da or ε were not investigated by Guo and Zhao (2005a)

Figure 4.21 shows the results of temperature at different ε and it shows that there is little difference of the temperature profile when ε varies. This is the vertical heat transfer is little affected by the horizontal flow.

Figure 4.22 shows that the flow layer near the moving plate is thicker when ε increases. This is because when ε is large, flow will pass through the porous medium more readily; the drag of porous medium will decrease, which leads to porous medium flow becoming faster. Therefore, with a larger porosity ε, the velocity is larger, and the layer near the moving plate is thicker.

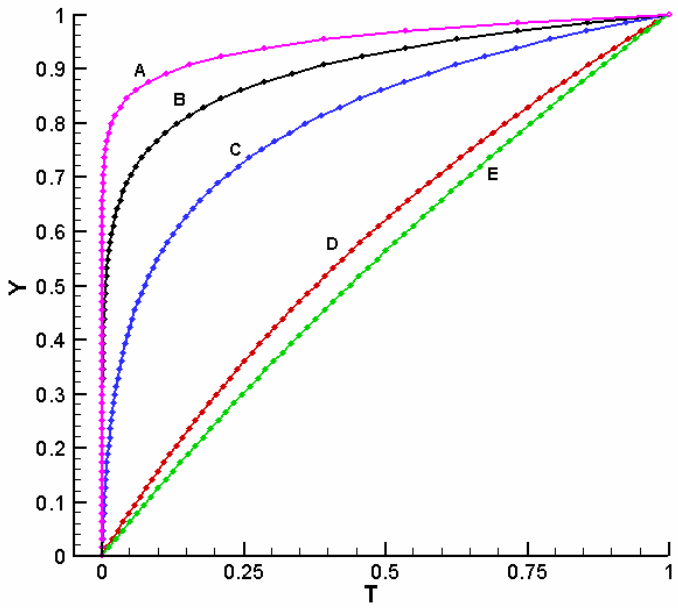

Figure 4.17 Temperature profile in channel with porous medium for Da = 0.1, ε = 0.7 and Ra = 100.0 at different Re. Solid lines: DDF LBM. Symbols: analytical simulations. A: Re = 20.0, B: Re = 10.0, C: Re = 5.0, D: Re = 1.0, and E: Re = 0.5.

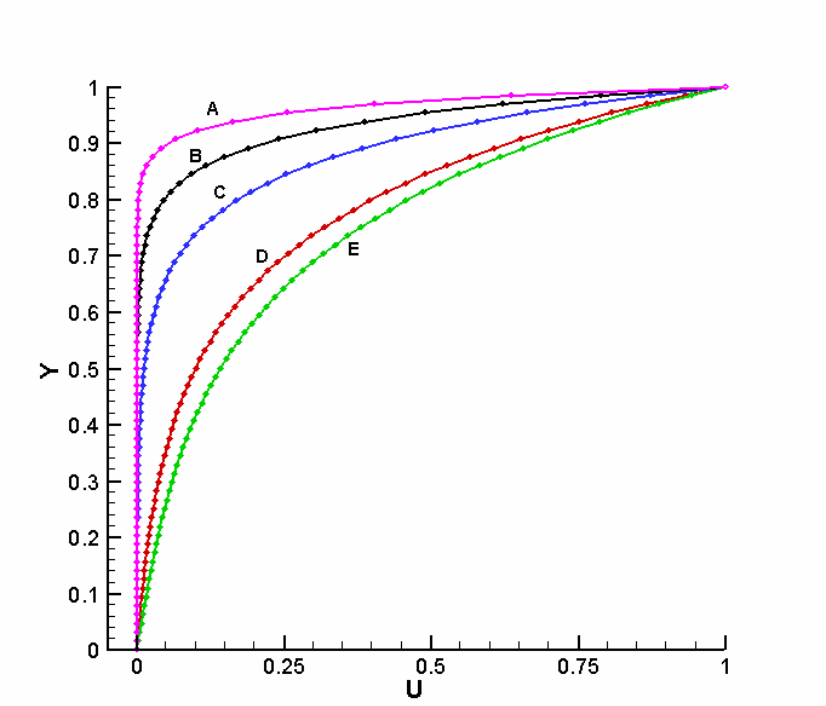

Figure 4.18 Velocity profile in channel with porous medium for Da = 0.1, ε = 0.7 and Ra = 100.0 at different Re. Solid lines: DDF LBM . Symbols: analytical simulations. A: Re = 20.0, B: Re = 10.0, C: Re = 5, D: Re = 1.0, and E: Re = 0.1.

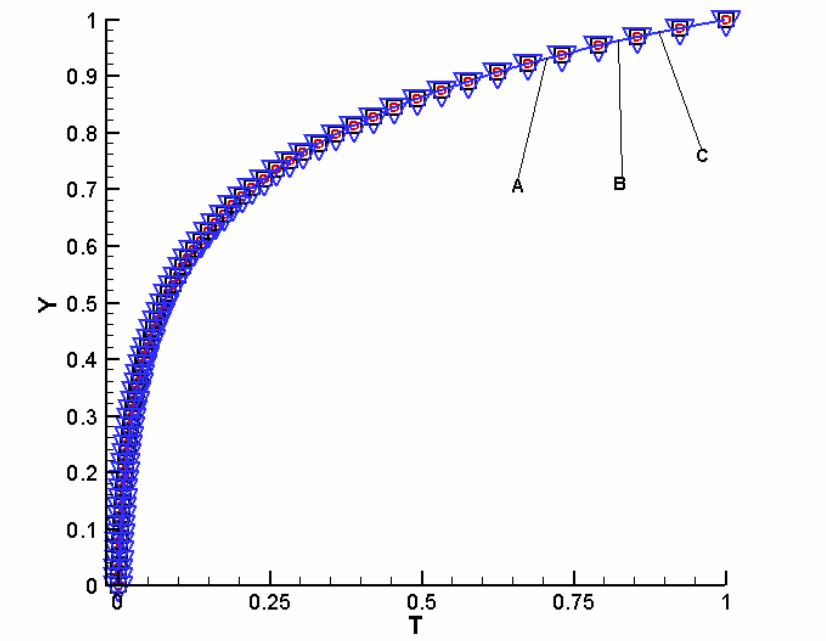

Figure 4.19 Temperature profile in channel with porous medium for Re = 5.0, ε = 0.7 and Ra = 100.0 at different Da. Solid lines: DDF LBM. Symbols: analytical simulations. A, ∇ : Da = 10^{-3}; B, $\square$: Da = 10^{-2}; and C, $\bigcirc$: Da = 0.1.

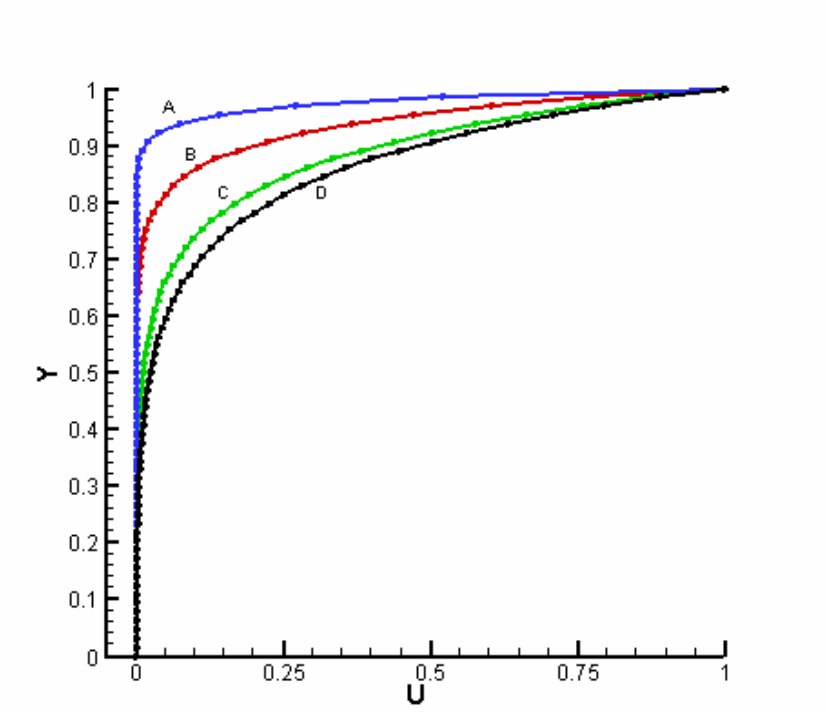

Figure 4.20 Velocity profile in channel with porous medium for Re = 5.0, ε = 0.7 and Ra = 100.0 at different Da. Solid lines: DDF LBM. Symbols: analytical simulations. A: Da = 10^{-3}, B: Da = 10^{-2}, C: Da = 0.1, and D: Da = 1.0.

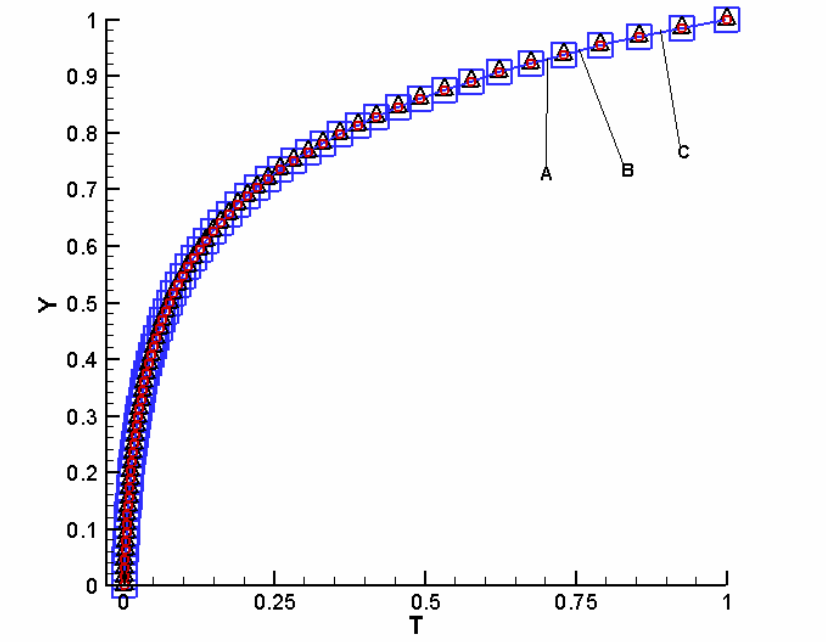

Figure 4.21 Temperature profile in channel with porous medium for Re = 5.0, Da = 0.01 and Ra = 100.0 at different ε. Solid lines: DDF LBM. Symbols: analytical simulations. A, △ : ε = 0.1; B, □ : ε = 0.5; and C, ○ : ε = 0.99.

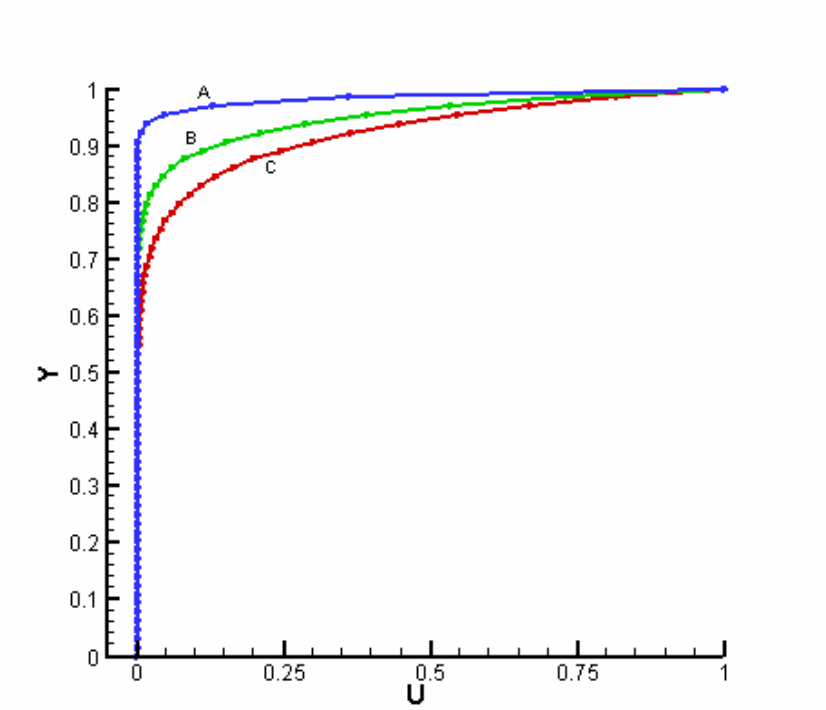

Figure 4.22 Velocity profile in channel with porous medium for Re = 5.0, Da = 0.01 and Ra = 100.0 at different ε. Solid lines: DDF LBM. Symbols: analytical simulations. A: ε = 0.1, B: ε = 0.5, and C: ε = 0.99.

4.2.2 Channel with Fixed Walls

a. Full Porous Medium

Another practical application of DDF LBM is discussed in the forced convection of channel. The fluid flow system consists of a two dimensional channel of length L and width H filled with a porous medium with porosity ε. A constant force G along the channel direction drives the fluid flow, which is fully developed along the channel. The inlet is hot (with temperature T_h). There is the heat dispersion $\frac{\partial T}{\partial y}$ at the bottom plate and adiabatic on the upper plate while the outlet has no constraint.

The non-equilibrium extrapolation boundary condition of Equation (3.52) is implemented for velocity boundary conditions of all boundaries except the outlet; Equation (3.54) is used for the temperature boundary of the inlet; and Equation (3.55) is applied for upper and bottom plates boundaries. For initial conditions, the velocity field is set to be zero at each lattice. The flow density is set as a constant $\rho = 1.0$ at the beginning. The density distribution function f_i is set to be equal to its equilibrium $f^{(eq)}$ and the temperature distribution T_i is set to be equal to the equilibrium $T^{(eq)}$ at t = 0.

The DDF LBM is used for the current problem at different Peclet Numer Pe. The capacity ratio σ, the effective thermal diffusivity σ_m and viscosity ratio Je are set to be 1.0; Da is 10^{-2}; Pr is set as 0.7; Ra is 0 with Pe varies from 1.0 to 100.0; $\frac{\partial T}{\partial y}$ changes from 1.0 to 0.1; and porosity ε varies from 0.8 to 0.01. The simulation is based on a lattice of size 32 x 32 and the relaxation time τ and τ' both are set to be 0.503.

The temperature profiles along the bottom and vertical midline of the channel are presented in Figure 4.23 to 4.26. All results here are non-dimensional and defined as $X = \frac{x}{H}$, $Y = \frac{y}{H}$ and $T = \frac{T(x,y)}{T_h}$. Figure 4.23 and Figure 4.24 shows the temperature profiles when dissipation rate $\frac{\partial T}{\partial y}$ is 1.0. Both show that when Pe decreases, the temperature magnitudes along channel bottom decrease. This is because when Pe decreases, the flow is weaker; and heat convection is weaker, which makes the temperature lower.

Figure 4.25 and Figure 4.26 shows the results with $\frac{\partial T}{\partial y}$ as 0.1. They show the temperature magnitudes along the vertical midline of the channel also decrease when Pe decreases. This is also because when Pe decreases, the flow is weaker, and heat convection in the channel is weaker, which makes the temperature of low Pe lower than the temperature of high Pe. But the temperature for small $\frac{\partial T}{\partial y}$ (i.e. 0.1 of Figure 4.25 and 4.26) is higher than that for large $\frac{\partial T}{\partial y}$ (i.e. 1.0 of Figure 4.23 and 4. 24), even though the Da and ε are smaller in Figure 4.25 and 4. 26. This is because when $\frac{\partial T}{\partial y}$ is large, the heat flux is stronger; and more heat would lost from the channel bottom through the porous medium.

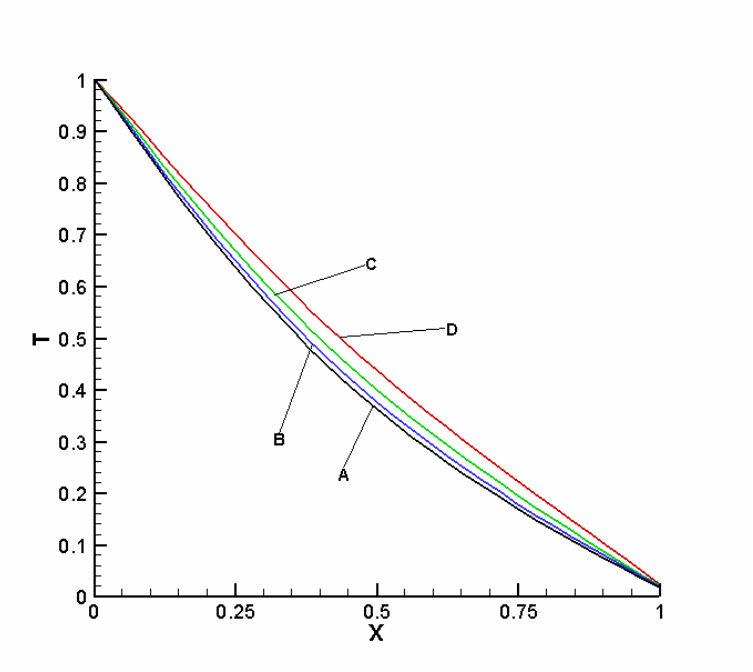

Figure 4.23 Temperature profiles along bottom of the channel with porous medium for Da = 10^{-2} , ε = 0.8, and $\frac{\partial T}{\partial y}$ = 1.0 at different Pe. A: Pe = 1.0; B: Pe = 20.0; C: Pe = 50.0; and D: Pe = 100.0.

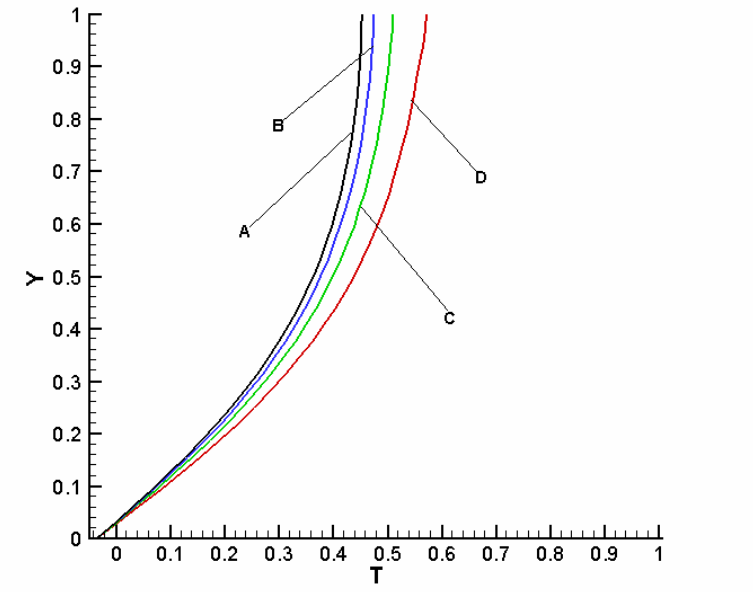

Figure 4.24 Temperature profiles along the vertical midline of the channel with porous medium for Da = 10^{-2}, ε = 0.8 and $\frac{\partial T}{\partial y}$ = 1.0 at different Pe. A: Pe = 1.0; B: Pe = 20.0; C: Pe = 50.0; and D: Pe = 100.0.

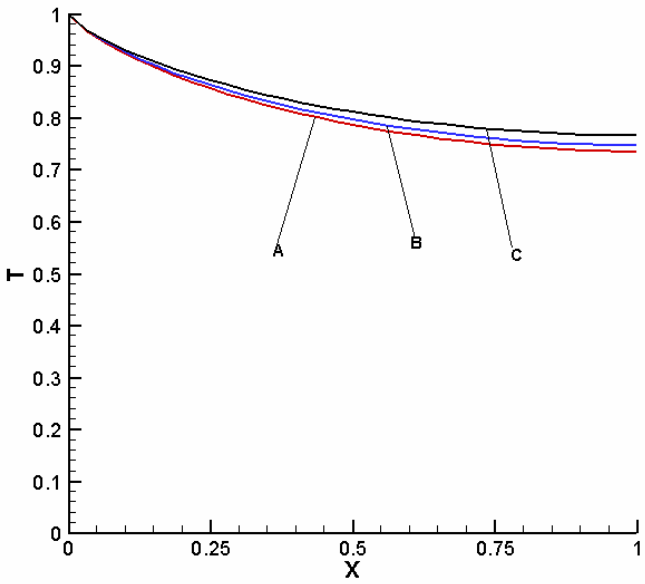

Figure 4.25 Temperature profiles along bottom of the channel with porous medium for Da = 10^{-4}, ε = 10^{-2} and $\frac{\partial T}{\partial y}$ = 0.1 at different Pe. A: Pe = 1.0; B: Pe = 20.0; and C: Pe = 40.0.

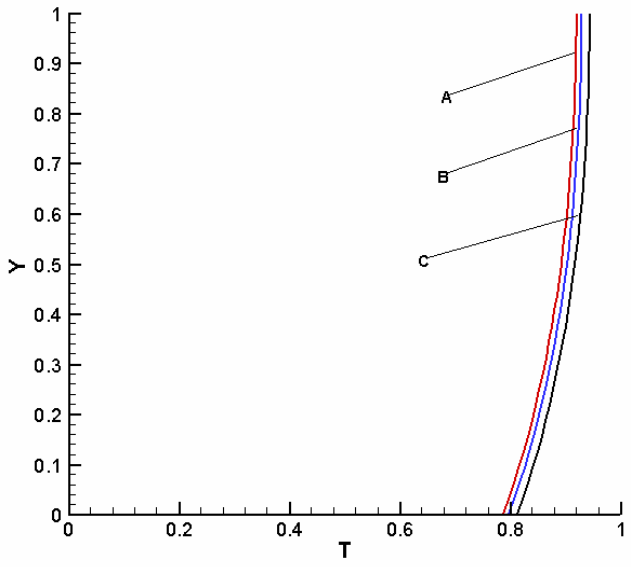

Figure 4.26 Temperature profiles along the vertical midline of channel with porous medium for Da = 10^{-4}, ε = 10^{-2}, and $\frac{\partial T}{\partial y}$ = 0.1 at different Pe. A: Pe = 1.0; B: Pe = 20.0; and C: Pe = 40.0.

b. Partial Porous Medium

The DDF LBM can also be used to simulate a two dimensional channel partially filled with porous medium. It is a channel with length L and width H partially filled with porous media with porosity ε. The porous medium lies in the channel such that there is a fluid region domain between the porous medium and the upper plate. A constant force G along the channel direction drives the fluid flow, which is fully developed along the channel. The inlet is hot (with temperature T_h). There is the heat dispersion $\frac{\partial T}{\partial y}$ at the bottom plate and adiabatic on the upper plate while the outlet has no constraint.

The non-equilibrium extrapolation boundary condition of Equation (3.52) is implemented for all velocity boundaries except the outlet; Equation (3.54) is used for the temperature boundary conditions of the inlet, and Equation (3.55) is applied for upper and bottom plates boundaries. For initial conditions, the velocity field is set to be zero at each lattice. The flow density is set as a constant $\rho = 1.0$ at the beginning. The density distribution function f_i is set to be equal to its equilibrium $f^{(eq)}$, the temperature distribution T_i is set to be equal to the equilibrium $T^{(eq)}$ at t =0.

The DDF LBM is used for the current problem at different Pe from 10.0 to 50.0. In the simulation, Ra is set to be 0; σ is 1.0; σ_m is 1.0; Da is 10^{-2}; Je is 1.0; Pr is 0.7; $\frac{\partial T}{\partial y}$ is 0.1, and viscosity ε is set to be 10^{-2}. The relaxation time τ and τ' are both set to be 0.503 in the simulation with 32 x 32 lattice nodes.

All results in this section are non-dimensional, which are defined as $X = \frac{x}{L}$, $Y = \frac{y}{H}$ and $T = \frac{T(x,y)}{T_h}$. The temperature profiles along the bottom and the vertical midline of the channel with partial porous medium are presented in Figure 4.27 and 4.28. Figure 4.27 shows when Pe decreases, the temperature magnitude along the channel bottom decreases slightly. Figure 4.28 shows the temperature magnitude along the vertical midline of the channel height also decreases slightly when Pe decreases. Both are because when Pe decreases, the flow is slightly weaker, and heat convection in the channel is weaker, which makes the temperature slightly lower.

Comparisons of the channels filled with full and partial porous medium are shown in Figure 4.29 and 4.30. Results show that the difference of temperature profiles between the channel with partial and full porous medium is not obvious at different Pe. This is because the definition of Pe is based on the flow through porous medium. And the heat flux is through the porous medium in both the channels filled with partial and full porous medium. Only when Pe is very large (i.e. Pe=50), the temperature of channel partially filled with porous medium is a little bit lower than the one with full porous medium. This is because when Pe is very large; there is more heat being taken away from outlet in the fluid region. Therefore, when Pe is very large, the temperature of the channel filled with partial porous medium is a little bit lower than that of full porous medium. However the effect is not significant; this is because the heat dissipation rate from the bottom wall is not large.

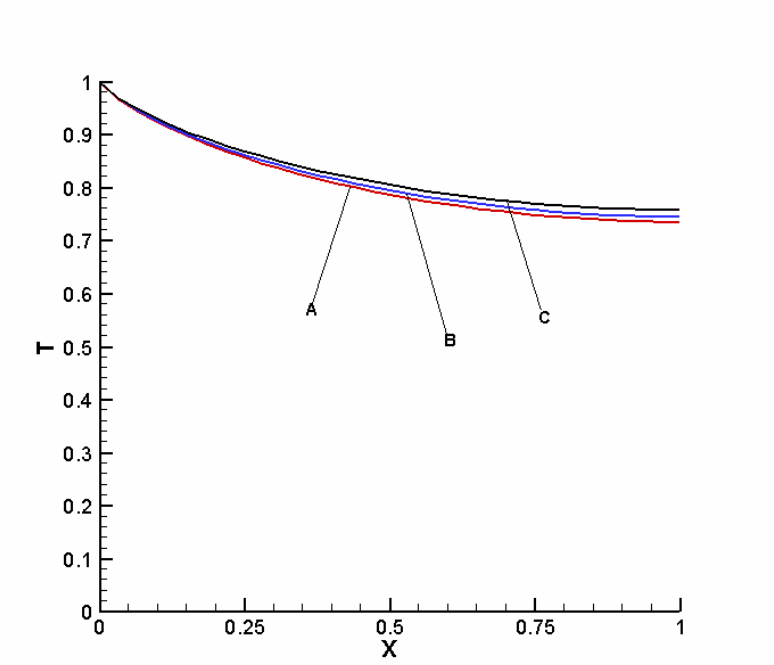

Figure 4.27 Temperature profiles along the bottom of channel with partial porous medium for Da = 10^{-4} , ε = 10^{-2} and $\frac{\partial T}{\partial y}$ = 0.1 at different Pe. A: Pe = 1.0; B: Pe = 20.0 and C: Pe = 40.0.

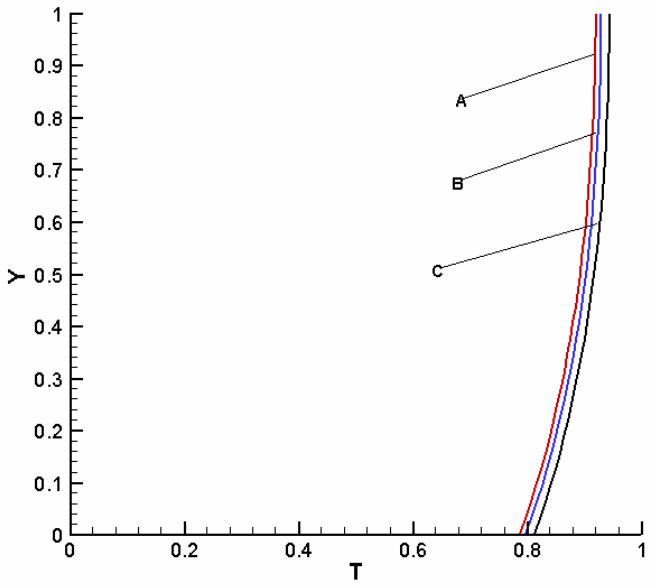

Figure 4.28 Temperature profiles along the vertical midline of channel with partial porous medium for Da = 10^{-4}, ε = 10^{-2} and $\frac{\partial T}{\partial y}$ = 0.1 at different Pe. A: Pe = 1.0; B: Pe = 20.0 and C: Pe = 40.0.

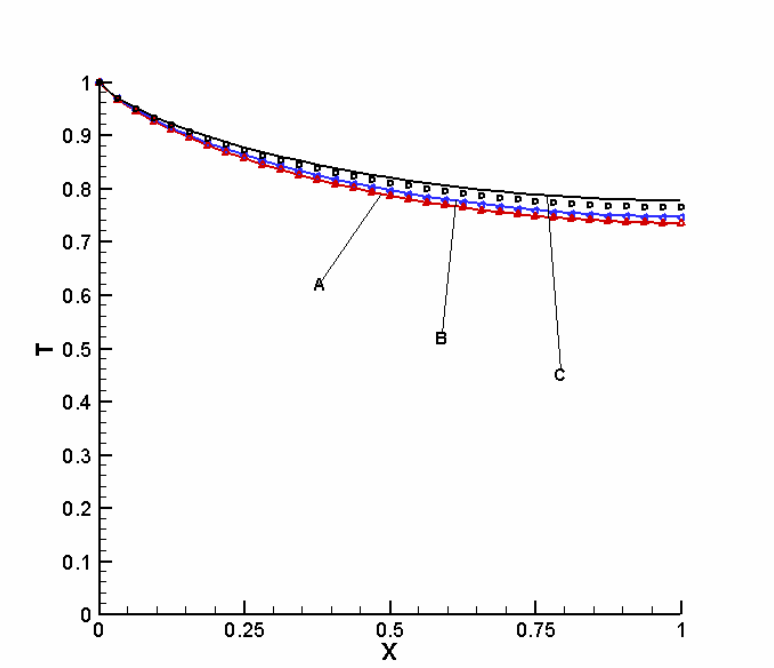

Figure 4.29 Temperature profiles along channel bottom with Da = 10^{-4}, ε = 10^{-2} and $\frac{\partial T}{\partial y}$ = 0.1 at different Pe. Solid line: Full porous medium. Symbols: Partial porous medium. A: Pe = 1.0; B: Pe = 20.0 and C: Pe = 50.0.

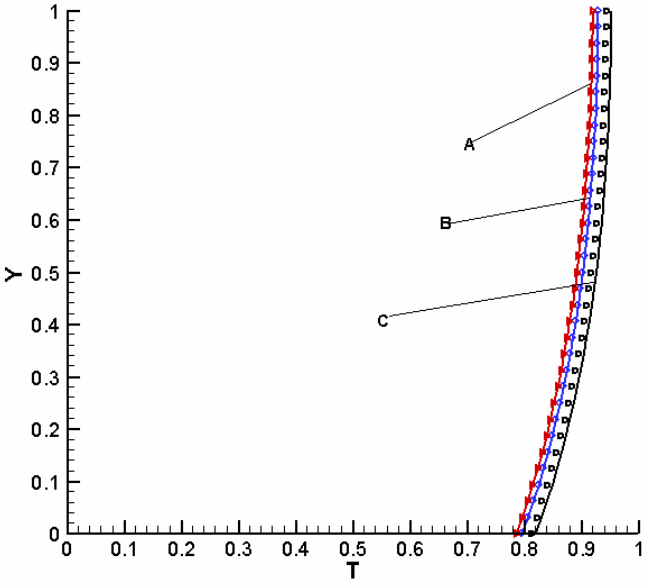

Figure 4.30 Temperature profiles along midline of channel height with Da = 10^{-4}, ε = 10^{-2} and $\frac{\partial T}{\partial y}$ = 0.1 at different Pe. Solid line: Full porous medium. Symbols: Partial porous medium. A: Pe = 1.0; B: Pe = 20.0; and C: Pe = 50.0.

CHAPTER 5

CONCLUSIONS AND RECOMMENDATIONS

5.1 Conclusions

In this thesis a Lattice Boltzmann Method, with double distribution function, is used to simulate fluid flow and heat transfer in porous media. In addition to the usual density distribution function in the lattice Boltzmann Equation to obtain the velocity field, a temperature distribution function is included for the temperature field and a force term for the drag effect of the porous media. Some two dimensional flows, with full and/or partial porous media, have been investigated: channel with fixed walls, channel with a moving wall, and cavity with a moving wall. The effects of different Reynolds and Darcy numbers were considered. Also studied was the effect of different porosity.

The present investigation on isothermal flow with partial porous media continues a previous work by Guo and Zhao (2002d) who studied a channel with a moving wall, also based on GLBE. The forced convection in channel with moving wall filled with full porous media has been studied previously, based on DDF LBM, by Guo and Zhao (2005a); and this thesis extends it to investigate effect of different Reynolds number, Darcy number, porosity. A partial porous media was also considered for a channel with fixed wall, which include effect of Peclet number and heat flux.

The LBM results are compared with analytical or finite difference solutions, and the good agreement validates the accuracy and reliability of the present DDF LBM. It was found that when the Reynolds number, Darcy number and porosity increase, the velocity in the full porous medium will increase; and the velocity gradient discontinuity at the interface of the partial porous medium will be less abrupt. The results show that

when Peclet decreases, the temperature decreases slightly both in the channels filled with full and partial porous media. It was found that the difference of temperature between partial and full porous media is not significant in the channel with fixed walls.

5.2 Recommendation for Further Studies

For efficiency reasons, it is always necessary to set the flow as the local equilibrium distribution function. However, more work is necessary to obtain a better condition which properly and sets a flow with appropriate density, velocity and temperature profiles. Another suggestion for future work is to use the very high Reynolds number flow in the porous medium flow, which could produce turbulence flow. The variable viscosity ratio was not investigated in this thesis, which is also important for the velocity and temperature profile and could be further discussed. By deducing the effect of the porous medium from the boundary conditions which is used at pore scale, the direct connection could be built between the LBM at pore scale and REV scale in the future. This needs further study in the future.

REFERENCE

Abraham F., Brodbeck D., Rafey R. and Rudge W., “Instability dynamics of fracture: a computer simulation investigation”, Physical Review Letters, **73**, p272-275 (1994).

Adrover A. and Giona M., "Analysis of Linear Transport Phenomena on Fractals." The Chemical Engineering Journal and The Biochemical Engineering Journal, **64**, p45-61 (1996).

Alexander F. J., Chen S., and Sterling J. D., “Lattice Boltzmann Thermohydrodynamics”, Physical Review E, **47**, p2249-2252 (1993).

Amiri A., “Analysis of momentum and energy transfer in a lid-driven cavity filled with a porous medium”, International Journal of Heat and Mass Transfer, **43**, p3513-3527 (2000).

Balasubramanian H., Hayot F. and Saam W. F., “Darcy’s Law from Lattice-Gas Hydrodynamics”, Physical Review A, **36**, p2248-2253 (1987).

Bartoloni A. and Battista C., “LBE Simulations of Rayleigh-Be′nard Convection on the APE100 Parallel Processor”, International Journal of Modern Physics C, **4**, p993-1006 (1993).

Bathnagar P., Gross E.P. and Krook M.K., “A model for collision processes in gases, I: small amplitude processes in charged and neutral one-dimensional system”, Physical Review, **94**, p511-525 (1954).

Beavers G.S. and Joseph D.D., “Boundary conditions at a naturally permeable wall”, The Journal of Fluid Mechanics, **30**, p197-207 (1967).

Benzi R., Succi S. and Vergassola M., “The lattice Boltzmann equation: theory and applications”, Physics Report, **222**, p145-197 (1992).

Bernsdorf J., Bernner G. and Durst F., “Numerical analysis of the pressure drop in porous media flow with lattice Boltzmann (BGK) automata”, Computer physics communications, **129**, p247-255 (2000).

Boon J.P., editor, “Advanced Research Workshop on Lattice Gas Automata Theory, Implementations, and Simulation”, Journal of Statistical Physics, **68**, p3-4 (1992).

Boussinesq J., “Essai sur la the'orie des eaux courantes”, Me'm. pre's. par div. savants a' l'Acad. Sci, **23**, p1-680 (1877).

Chapman S. and Cowling T.G., “The mathematical theory of non-uniform gases”, 3rd. edn.,Cambridge University Press (1990).

Chen H.D., Chen S.Y. and Matthaeus W.H., "Recovery of navier-stokes equations using a lattice-gas boltzmann method", Physical Review A, **45**, pR5339-42 (1992).

Chen H., Chen S. and Matthaeus W.H. , "Recovery of the navier-stokes equations using a lattice gas boltzmann method", Los Alamos Nat.Lab archives (1994).

Chen S., Chen H. Martnez D. and Mathaeus W., "Lattice Boltzmann model for simulation of magnetohydrodynamics", Physical Review Letters, **67**, p3776-3779 (1991).

Chen S. and Doolen G.D., "Lattice Boltzmann methods for fluid flows", Annual Review of Fluid Mechanics, **30**, p329-364 (1998).

Chen S., Martinez D. and Mei R., "On boundary conditions in lattice Boltzmann methods", Physics of Fluids, **8**, p2527-2536 (1996).

Chopard B and Droz M., "Cellular Automata Modeling of Physical Systems", Cambridge University Press (1998).

Chopard B., Luthi P. and Masselot A., "Cellular automata and lattice Boltzmann techniques: An approach to model and simulate complex systems" (1998).

Cornubert R. et al. "A Knudsen layer theory for lattice gases". Physica D, **47**, p241-259 (1991).

Dardis O. and McCloskey J., "Lattice Boltzmann Scheme with Real Numbered Solid Density for the Simulation of Flow in Porous Media", Physical Review, **E**, **57**, p4834-4837 (1998).

D'Humieres, D. and Lallemand P., "Lattice gas models for 3d hydrodynamics", Europhys Letters, **2**, p291-297 (1986).

Drona Kandhai, "Large Scale Lattice-Boltzmann Simulations", PhD thesis, University of Amsterdam (1999).

Doolen G., editor, "Lattice Gas Method for Partial Differential Equations", Addison-Wesley (1990).

Donald Z., "Boundary conditions for lattice Boltzmann simulations", Journal of Statistical Physics, **71**(5/6), p1171-1177 (1993).

Dupuis A. and Chopard B., "Cellular Automata of traffic: a model for the city of Geneva", Network and Spatial Economics (2001).

Dupuis A. , "From a lattice Boltzmann model to a parallel and reusable implementation of a virtual river", PhD thesis, Geneva, Switzerland (2002).

Ergun S., “Fluid Flow through Packed Column”, Chemical Engineering Progress, **48**, p89-94 (1952).

Filippova O. and Hänel D., “Grid refinement for lattice-BGK models”, Journal of Computational Physics, **147**, p219-228 (1998a).

Filippova O. and Hänel D., “Boundary-Fitting and Local Grid Refinement for Lattice-BGK Models”, International Journal of Modern Physics C, **9**, p1271-1279 (1998b).

Filippova O. and Succi S., “Multiscale latticeBoltzmann schemes with turbulence modeling”, Journal of Computational Physics, **170**, p812-829 (2001).

Freed D. M., “Lattice-Boltzmann Method for Macroscopic Porous Media Modeling”, International Journal of Modern Physics C, **9**, p1491-1503 (1998).

Frisch U., Hasslacher B. and Pomeau Y., “Lattice-gas automata for the Navier-Stokes equation”, Physical Review Letters, **56**, p1505-1508 (1986).

Frisch U., d'Humiéres D. and Hasslacher B., “Latticegas hydrodynamics in two and three dimensions”, Complex Systems, **1**, p649-707 (1987).

Gartling D.K., Hickox C.E. and Givler R.C., “Simulation of coupled viscous and porous flow problems”, Theoretical and Computational Fluid Dynamics, **7**, p23-48 (1996).

Goyeau B. et al., “Momentum transport at a fluid–porous interface”, International Journal of Heat and Mass Transfer, **46**, p4071-4081 (2003).

Guo Z., Shi B. and Zheng C., “A Coupled Lattice BGK Model for the Boussinesq Equations”, International Journal for Numerical Methods in Fluids, **39**, p325-342 (2002a).

Guo Z., Zheng C. and Shi B., “An Extrapolation Method for Boundary Conditions in Lattice Boltzmann Method”, Physics of Fluids, **14**, p2007-2010 (2002b).

Guo Z., Zheng C. and Shi B., Physical Review E, **65**, 046308 (2002c).

Guo Z. and Zhao T. S., “Lattice Boltzmann Model for Incompressible Flows through Porous Media”, Physical Review E, **66**, p0363041-0363049 (2002d).

Guo Z. and Zhao T. S., “A Lattice Boltzmann Model for Convection Heat Transfer in Porous Media”, Numerical Heat Transfer, Part B, **47**, p157-177 (2005a).

Guo Z. and Zhao T. S., “Lattice Boltzmann Simulation of Natural Convection with Temperature Dependent Viscosity in a Porous Cavity”, Progress in Computational Fluid Dynamics, **47**, Nos.1/2, p110-117 (2005b).

Hardy J., Pomeau Y. and de Pazzis O., “Time evolution of a two-dimensional classical

lattice system", Physical Review Letters , **31**, p276-279 (1973).

He H. and Zou Q., "Analysis and boundary condition of the lattice Boltzmann BGK model with two velocity components", Technical Report LAUR-95-2293, Los Alamos National Laboratory (1995).

He X. and Luo L.S., "Theory of the lattice Boltzmann method: From the Boltzmann equation to the lattice Boltzmann equation", Physical Review E, **56**, p6811-6817 (1997a).

He X. and Luo L.S., "Lattice Boltzmann model for the incompressible Navier-Stokes Equation". Journal of Statistical Physics, **88**, p927-944 (1997b).

He X. Y., Chen S. Y. and Doolen G., "A Novel Thermal Model for the Lattice Boltzmann Method in Incompressible Limit", Journal of Computational Physics, **146**, p282-300 (1998).

Hickox C.E. and Gartling D.K., "A numerical study of natural convection in a vertical, annular, porous layer", International Journal of Heat and Mass Transfer, **28**, p720-723 (1985).

Higuera F., Jimenez J. and Succi S., "Boltzmann approach to lattice gas simulations". Europhysics Letters, **9**, p663-668 (1989a)

Higuera F., Jimenez J. and Succi S., "Lattice gas dynamics with enhanced collision". Europhysics Letters, **9**, p345-349 (1989b).

Hortmann M., Peri'c M. and Scheuerer G., "Finite volume multigrid prediction of laminar natural convection: bench-mark solutions", International Journal for Numerical Methods in Fluids, **11**, p189–207 (1990).

Hou S., Zou Q. and Chen S., "Simulation of cavity flow by the lattice Boltzmann method", Journal of Computational Physics, **118**, p329-347 (1995).

Hsu C.T. and Cheng P., "Thermal dispersion in a porous medium", International Journal of Heat and Mass Transfer, **33**, p1587-1597 (1990).

Jeffreys H., "Cartesian Tensors", Cambridge University Press (1965).

Kang Q., Zhang D. and Chen S., "Unified Lattice Boltzmann Method for Flow in Multiscale Porous Media", Physical Review E, **66**, p0563071-05630711 (2002).

Kaviany M., "Principles of Heat Transfer in Porous Media", 2nd ed., Springer-Verlag, New York (1995).

Kim J., Lee J. and Lee K.C., "Nonlinear correction to Darcy's law for a flow through periodic arrays of elliptic cylinders", Physica A, **293**, p13-20 (2001).

Koelman J., “A simple lattice Boltzmann scheme for Navier-Stokes fluid flow”, Europhysics Letters, **15**, p603-607 (1991).

Koponen, A., Kataja, M. and Timonen, J., “Simulations of Single-Fluid Flow in Porous Media”, International Journal of Modern Physics C, **9**, p1505-1521 (1998).

Krafczyk M., Tölke J. and Luo L.S., “Large-eddy simulations with a multiple-relaxation-time LBE model”, International Journal of Modern Physics B **17**, p33-39 (2003).

Lallemand P. and Luo L.S., “Theory of Lattice Boltzmann Method: Acoustic and Thermal Properties in Two and Three Dimensions”, Physical Review E, **68**, p0367061-03670625 (2003).

Landau L.D. and Lifshitz E.M., “Fluid mechanics”, Pergamon Press, London (1963).

Langaas K. and Grubert D., “Lattice Boltzmann simulations of wetting and its application to disproportionate permeability reducing gel ”, Journal of Petroleum Science and Engineering, **24**, p199-211 (1999).

Le H., Moin P. and Kim J., “Direct numerical simulation of turbulent flow over a backward-facing step”, Journal of Fluid Mechanics, **330**, p349-374 (1997).

Luo L. S., “Unified theory of the lattice Boltzmann models for nonideal gases”, Physical Review Letters, **81**(8), p1618-1621 (1998).

Martys N. S., “Improved Approximation of the Brinkman Equation Using a Lattice Boltzmann Method”, Physics of Fluids, **6**, p1807-1810 (2001).

Martys N. S., Bentz D.B. and Garboczi. E.J., “Computer simulation study of the effective viscosity in Brinkman's equation”, Physics of Fluids, **6**, p1434-1439 (1994).

Martys N.S., Shan X. and Chen H., “Evaluation of the external force term in the discrete Boltzmann equation”, Physical Review E, **58**, p6855-6857 (1998).

Mei R.W., Luo, L.S. and Wei S., “An accurate curved boundary treatment in the lattice Boltzmann method”, Journal of Computational Physics, **155**, p307-330 (1999).

Neale G. and Nader, W., “Practical significance of Brinkman's extension of Darcy's law: coupled parallel flows within a channel and a bounding porous medium”, The Canadian Journal of Chemical Engineering, **52**, p475-478 (1974).

Nield D. A. and Bejan A., “Convection in Porous Media”, 2nd ed., Springer-Verlag, New York (1992).

Nield D.A. and Bejan A., "Convection in Porous Media", Springer-Verlag, New York (1998).

Nishimura T. et al., "Numerical analysis of natural convection in a rectangular enclosure horizontally divided into fluid and porous regions", International Journal of Heat and Mass Transfer, **29**, p889-898 (1986).

Nithiarasu P., Seetharamu K. N. and Sundararajan T., "Natural Convection Heat Transfer in a Fluid Saturated Variable Porosity Medium", International Journal of Heat and Mass Transfer, **40**, p3955-3967 (1997).

Nithiarasu P. and Ravindran K., "A New Semi-implicit Time Stepping Procedure for Buoyancy Driven Flow in a Fluid Saturated Porous Medium", Computer Methods in Applied Mechanics and Engineering, **165**, p147-154 (1998).

Noble DR. and Chen S., "A consistent hydrodynamic boundary condition for the lattice Boltzmann method", Physics of Fluids, **7**, p203-209 (1995).

Pavlo P., Vahala G. and Vahala L., "Higher-order isotropic velocity grids in lattice Methods", Physical Review Letters, **80** (18), p3960-3963 (1998).

Pierre L. and Luo L.S., "Theory of the lattice Boltzmann method dispersion, dissipation, isotropy, Galilean invariance, and stability", Technical Report TR-2000-17, ICASE, Nasa Research Center (2000).

Pope S. B., "Turbulent flows", Cambridge University Press (2000).

Qian Y.H., d'Humières D and Lallemand P, "Lattice BGK models Navier-Stokes equation", Europhysics Letters, **17**, p479-484 (1992).

Qian Y., "Simulating Thermohydrodynamics with Lattice BGK Models", Journal of Scientific Computing, **8**, p231-242 (1993).

Qian Y.H., Succi S. and Orszag S.A., "Recent advances in lattice Boltzmann computing". Annual Reviews of Computational Physics III, p195-242, World Scientific (1996).

Robert Maier, Robert Bernard and Daryl Grunau, "Boundary conditions for the lattice Boltzmann method", Physics of Fluids, **8**, p1788-1801 (1996).

Rothman D.H., "Cellular-Automation Fluids: A Model for Flow in Porous Media", Geophysics, **53**, p509-518 (1988).

Rothman D.H. and Zaleski S., "Lattice-gas models of phase separation: interface, phase transition and multiphase flows", Reviews of Modern Physics, **66**, p1417-1479 (1994).

Shan X. and Chen H., "Lattice Boltzmann model for simulating flows with multiple phases and components", Physical Review E, **47**, p1815-1819 (1993).

Shan X., "Simulation of Rayleigh- Be′nard Convection Using a Lattice-Boltzmann Method", Physical Review E, **55**, p2780-2788 (1997).

Shu C., Lecture Notes of Advanced Computational Fluid Dynamics, Part 2 (2004).

Shyy W., Liu J. and Wright J. "Pressure-Based Viscous Flow Computation Using Multi-Block Overlapped Curvilinear Grids," Numerical Heat Transfer, Part B, **25**, p39-59 (1994).

Singh M. and Mohanty K.K., "Permeability of spatially correlated porous media", Chemical Engineering Science, **55**, p5393-5403 (2000).

Skordos P., "Initial and boundary conditions for the lattice Boltzmann method", Physical Review E, **48**, p4823-4842 (1993).

Smits A. J., "A Physical Introduction to Fluid Mechanics". John Wiley & Sons, inc., (2000).

Satofuka N. and Nishioka T., "Parallelization of lattice Boltzmann method for incompressible flow computations",Computational Mechanics **23**,164 - 171(1999)

Spaid M. A. A. and Phelan F. R., "Lattice Boltzmann Methods for Modeling Microscale Flow in Fibrous Porous Media", Physics of Fluids, **9**, p2468-2474 (1997).

Spaid M. A. A. and Phelan F. R., "Modeling Void Formation Dynamics in Fibrous Porous Media with the Lattice Boltzmann Method", Composites A, **29**, p749-755 (1998).

Sterling J. and Chen S., "Stability analysis of Lattice Boltzmann methods", Journal of Computational Physics, **123**, p196-206 (1994).

Succi S., Foti E. and Higuera F., "Three-Dimensional Flows in Complex Geometries with the Lattice Boltzmann Method", Europhysics Letters, **10**, p433-438 (1989).

Succi S., "The Lattice Boltzmann Equation for Fluid Dynamics and Beyond", Clarendon Press, Oxford University Press, UK (2001).

Takaji I., Masato Y. and Fumimaru O., "A non-slip boundary condition for lattice Boltzmann simulations", Physics of Fluids, **7**, p2928-2930 (1995).

Tien C.L. and Vafai K., "Convective and Radiative Heat Transfer in Porous Media", Advances in Applied Mechanics, **27**, p225-282 (1990).

Tritton D.J., "Physical fluid dynamics", Clarendon Press (1988).

Van Dyke M., "An Album of Fluid Motion", The Parabolic Press, Standford, CA (1982).

Vafai K., "Convective Flow and Heat Transfer in Variable-Porosity Media", Journal of Fluid Mechanics, **147**, p233-259 (1984).

Vafai K. and Kim S.J., "On the limitations of the Brinkman-Forchheimer-extended Darcy equation ", International Journal of Heat and Fluid Flow, **16**, p11-15 (1995).

Vafai K. and Tien C. L., "Boundary and Inertia Effects on Flow and Heat Transfer in Porous Media", International Journal of Heat and Mass Transfer, **24**, p195-203 (1981).

Wolf-Gladrow D. A., "Lattice-Gas Cellular Automata and Lattice Boltzmann Models: An Introduction", Lecture Notes in Mathematics 1725, Springer-Verlag, Germany (2000).

Wolfram S., "Cellular automaton fluids. 1: Basic theory", Journal of Statistical Physics, **45**, p471-526 (1986).

Xu K. and Prendergast K.H., "Numerical Navier-Stokes Solutions from Gas Kinetic Theory ", Journal of Computational Physics, **114**, p9-117 (1994).

Zanetti G., "Hydrodynamics of lattice-gas automata", Physical Review A, **40**, p1539-1548 (1989).

Zhou Qisu and He Xiaoyi, "On pressure and velocity boundary conditions for the Boltzmann BGK model", Physics of Fluids 9 (6), June 1997.